The Pennsylvania State University
The Graduate School
College of Engineering

REAL-TIME SENSING OF FATIGUE CRACK DAMAGE FOR INFORMATION-BASED DECISION AND CONTROL

A Thesis in
Mechanical Engineering
by
Eric Keller

Submitted in Partial Fulfillment
of the Requirements
for the Degree of

Doctor of Philosophy

May 2001

We approve the thesis of Eric E. Keller.

Date of Signature

Asok Ray Professor of Mechanical Engineering Thesis Advisor Chair of Committee	
Marc Carpino Professor of Mechanical Engineering	
Eric R. Marsh Associate Professor of Mechanical Engineering	
Donald A. Koss Professor of Materials Science and Engineering	
Shashi Phoha Professor of Electrical and Computer Engineering	
Richard C. Benson Professor of Mechanical Engineering Head of the Department of Mechanical and Nuclear Engineering	

Abstract

Information-based decision and control for structures that are subject to failure by fatigue cracking is based on the following notion: Maintenance, usage scheduling, and control parameter tuning can be optimized through real time knowledge of the current state of fatigue crack damage. Additionally, if the material properties of a mechanical structure can be identified within a smaller range, then the remaining life prediction of that structure will be substantially more accurate. Typically, neither the damage state nor the material properties are known precisely for any given structure. Decision systems for maintenance and usage scheduling are often based on analytically derived reliability and anticipated usage patterns. At best, if the anticipated and actual usages are approximately the same, these systems can only project worst-case remaining life that is considerably worse than the average case. Thus almost all structures must be inspected and repaired on a schedule that is more conservative than is required for a given margin of safety. However, in a very common scenario, usage is considerably more demanding than the design usage, and thus the systems are not conservative enough, leading to unexpected failures and safety concerns. Information-based decision systems can rely on physical models, estimation of material properties, exact knowledge of usage history, and sensor data to synthesize an accurate snapshot of the current state of damage and the likely remaining life of a structure under given assumed loading. Thus the future usage can be modified, either through mission planning or through damage mitigating control in order to optimally use the remaining life of a structure.

The work outlined in this dissertation is structured to enhance the development of information-based decision and control systems. This is achieved by constructing a test facility for laboratory experiments on real-time damage sensing. This test facility makes use of a technique that has been formulated for fatigue crack model parameter estimation to significantly improve the quality of remaining life prediction. Specifically, the dissertation focuses on development of an on-line fatigue crack damage sensing and life prediction system that is built upon the disciplines of *Systems Sciences* and *Mechanics of Materials*. A major part of the research effort has been expended to design and fabricate a test apparatus which allows: (i) measurement and recording of statistical data for

fatigue crack growth in ductile alloys via different sensing techniques; and (ii) identification of stochastic model parameters for prediction of fatigue crack damage. To this end, this dissertation describes the test apparatus and the associated instrumentation based on four different sensing techniques, namely, traveling optical microscopy, ultrasonic flaw detection, Alternating Current Potential Drop (ACPD), and fiber-optic extensometry-based compliance, for crack length measurements.

Table of Contents

List of Figures

Acknowledgements

I would like to take this opportunity to thank the people and organizations that helped me undertake and complete this research. Particularly Dr. Asok Ray for being a friend and advisor who's scholarship and generosity I can only dream of emulating. Dr. Marc Carpino for his advice, encouragement, and support. I would like to acknowledge Dr. Donald Koss for generously providing me with expert advice. I would also like to thank Dr. Eric Marsh and Dr. Shashi Phoha for being on my committee and the time and energy they spent helping me.

The research work reported in this dissertation has been supported in part by:

Office of Naval Research Grant No. N0014-97-1-0786.
National Science Foundation under Grant No. CMS-9819074.
NASA Glenn Research Center under Grant No. NAG3-2448
ARINC Corporation under NASA Langley Research Center Cooperative Agreement No. NCC1-333.
Army Research Office under Grant No. DAAH04-95-1-0446

I would really like to thank all of the students and staff of the Penn State Department of Mechanical Engineering that have helped me while I have been here. I would like to thank Dr. Keith Hurley for helping me setting up the laboratory apparatus. I owe a lot to Peter Lee. His help when things looked impossible kept me from giving up more than once.

I thank Mr. Thomas Munns of ARINC Corporation for providing valuable suggestions for interpretation experimental results. I also thank Dr. James N. Rozak of Sikorsky Aircraft Corporation for providing me with test specimens.

I would like to thank my kids Roxanne and Jacob – their love has kept me going. Finally I would like to thank my wife, Vicky, for her patience, love and support through this almost never-ending process.

Chapter 1

Introduction

Due to the nonstationary random nature of fatigue crack propagation in mechanical structures, it is often very difficult to determine the current damage state and remaining service life of operating machinery. For structures where failures have grave consequences, current practice is either conservative estimations of service life, or frequent expensive and time-consuming inspections, or both. On-line sensing of damage would allow constant re-evaluation and extension of service life and inherent protection against unforeseen early failure. Figure 1.1 shows an example of the random nature of crack growth under constant amplitude loading in a controlled laboratory environment (Virkler, et. al., 1979). If no inspection or on-line prediction of damage is available, it is prudent to retire or repair the structure when the worst possible crack trajectory reaches some critical length reduced by a (possibly over-conservative) safety margin. This worst possible trajectory should be determined for an acceptable risk level from the observed statistics; however, this is not commonly done due to the lack of an appropriate stochastic model of crack propagation. There is a need for development of an operational methodology that will extend the service life of mechanical structures while fulfilling the mission objectives. That is, a trade-off must be achieved between the operational performance and service life (Ray et al., 1994a). The current state of the art attempts to achieve these objectives by inspections and maintenance actions based on fixed usage intervals. On-line sensing of the damage state and prediction of remaining service life will reduce the frequency of inspections and increase the mean time between major maintenance actions on serviceable structures.

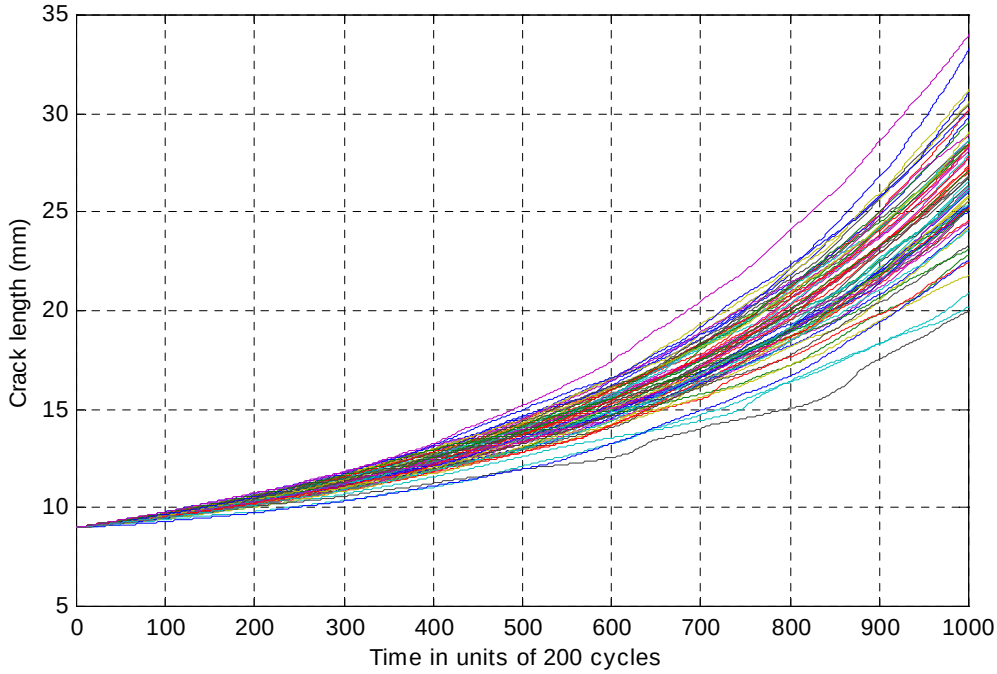

Figure 1-1 Fatigue Crack Propagation Trajectories for 2024-T3 Aluminum

The development of reasonably accurate on-line life prediction methodologies is difficult as very little statistical data of fatigue crack growth is available. A survey of the literature shows that researchers choose to rid their collected data of variability as best they can. For example, in ASTM E-647, which details accepted crack growth rate testing and data reduction procedures, the derivative is calculated from a number of data points, which removes noise from the data in order to get useful estimates of the growth rate. However, the process of smoothing also disposes of the information about material variability. Engineering materials can have large variability in material properties, and this variability is only increased during fabrication into a structure. Thus, it is likely that the variability researchers have encountered in materials testing is not predominantly related to errors in the test regime. The crack growth data shown in Figure 1.1 that were collected under tightly controlled conditions exhibit considerable variability. One of the major goals of the test apparatus developed in this research is the collection of information about fatigue crack growth statistics in different materials under a variety of loading conditions.

Complex structures such as aircraft often have widely varying usage patterns. Due to the difficulty and expense of implementing any other schemes, usage is often measured by a simple quantity such as flight hours for aircraft, years for bridges and roads, and number of starts for diesel engines [Bolotin, 1989]. Then, the state of damage in the structure is assumed to be correlated to the amount of usage. However, one structure may be used in a benign manner and another may be used in a manner that causes a drastic reduction of service life; for example, engines are more highly stressed in aircraft used for pilot training [Mattingly et. al. 1987]. This causes difficulty and expense in maintenance and logistics efforts due to the fact that maintenance actions and logistics planning are based on aggregate usage, and thus, as failures are experienced over time, premature replacements of parts and periodic maintenance become more frequent to maintain the safety of the most heavily used structure. However, in general, both safety and economics suffer as no good compromise can be achieved without a systematic analytical procedure. This problem motivates the research, since one of the most fundamental solutions to this problem is on-line failure diagnosis as well as on-line prognosis that allows remaining life prediction for the critical structural components of operating machinery, under anticipated load profiles.

On-line failure prognosis is also critical for advances in the field of life extending (or damage mitigating) control. The idea of damage mitigating control is that control policies can be modified so that large increases in service life can be realized with no significant loss of performance. The concept of the life extending control of a reusable rocket engines has been introduced by Lorenzo and Merril (1990). Trading performance for service life in a control policy can be considered as a constrained optimization problem. Ray et al. (1994b, 1994c) developed a damage prediction system for the turbine blades of a reusable rocket engine. Dai and Ray (1995, 1996a, 1996b) developed a damage mitigating control system that used a computationally efficient model of the coolant channel ligament of a reusable rocket engine. Kallapa et. al. (1997) have demonstrated by simulation the benefits of an optimal open loop control policy for life extension and high performance in electric power plant operations. Zhang and Ray (1999) have demonstrated through experiment a robust damage mitigating control scheme for fatigue cracks. Central to all of these efforts has been the ability to model

damage and conduct off-line optimization of damage and performance for specified trajectories. A requirement for advancement in the field of damage mitigating control is the ability to make on-line damage measurements and life prediction for anticipated trajectories that are not necessarily known much ahead of time.

Ray and Tangirala [1996a, 1996b] have showed significant progress towards an on-line damage prediction system. The authors adapted the (deterministic) short crack model (Newman, 1983; Newman et al., 1986) to develop two damage models in the stochastic setting that models adequately predicted the crack growth statistics based on the available data (Virkler et al., 1979; Ghonem and Dore, 1987). The two stochastic models used lognormal distributed crack growth rate and lognormal distributed crack length models where the growth rate or the crack length are assumed to have lognormal distribution, respectively. The authors validate an Extended Kalman Filter (EKF) incorporating the lognormal distributed crack growth rate model. Ray and Patankar[1999] have developed a deterministic state space model of fatigue crack growth under variable amplitude loading that has both crack length and crack opening stress as states. Ray [1999] has presented a stochastic model of fatigue crack growth under constant amplitude stress that allows the probability distribution function of fatigue crack growth to be derived in closed form. This avoids the computationally intensive task of solving non-linear stochastic differential equations in the Wiener integral or Ito integral setting. Ray and Patanker (1999) have developed a stochastic model of fatigue crack growth under variable amplitude loading by treating parameters of the state space model as random variables. This work incorporates these modeling developments into a crack length estimator using recursive least squares. The main work within the estimator structure is to characterize the noise statistics of the measurements.

Figure 1-2 shows a cracked specimen typical of those used in this work. The detail in the Figure shows the machined notch with cracks. The next section discusses the progression of fatigue crack growth in the context of the study outlined in this dissertation. This is done to provide context for the discussion of crack modeling, crack size instrumentation, and experimental results that follows.

1.1 Progression of crack growth observed in these tests

The purpose of this section is to discuss the progression of crack growth as observed in the specimens designed for this study. The specimens are typical hourglass shaped flat plates that have a machined notch with smooth ends for a stress riser to guarantee a center crack configuration. The design of the notch is well within typical engineering design practice for such a structure that needs a small notch in the middle, and thus the cracks generated from the notch are typical of those seen in an actual structure. Experiments were conducted with uncracked specimens. Although it may seem formulistic for practitioners in fracture mechanics, for the purposes of this study, there are six stages of crack growth. The first is crack initiation. The second stage is two-dimensional (2D) crack growth under plane strain. The next stage is the propagation of a through crack under plane strain. The fourth stage of fatigue growth is a transition from plane strain to plane stress crack growth. The fifth stage of fatigue growth is pure plane stress crack growth. The final stage is rupture, where there is so little residual strength left that the remaining ligament fails in one stress cycle. These stages of crack growth are notated on the image in Figure 1-3. The reason for differentiating between crack growth in plane strain and plane stress conditions is that this information is used in the crack growth model to influence the calculation of the crack growth increment. In the transition between plane stress and plane strain, an average of the plane strain and plane stress parameters is used in the calculation.

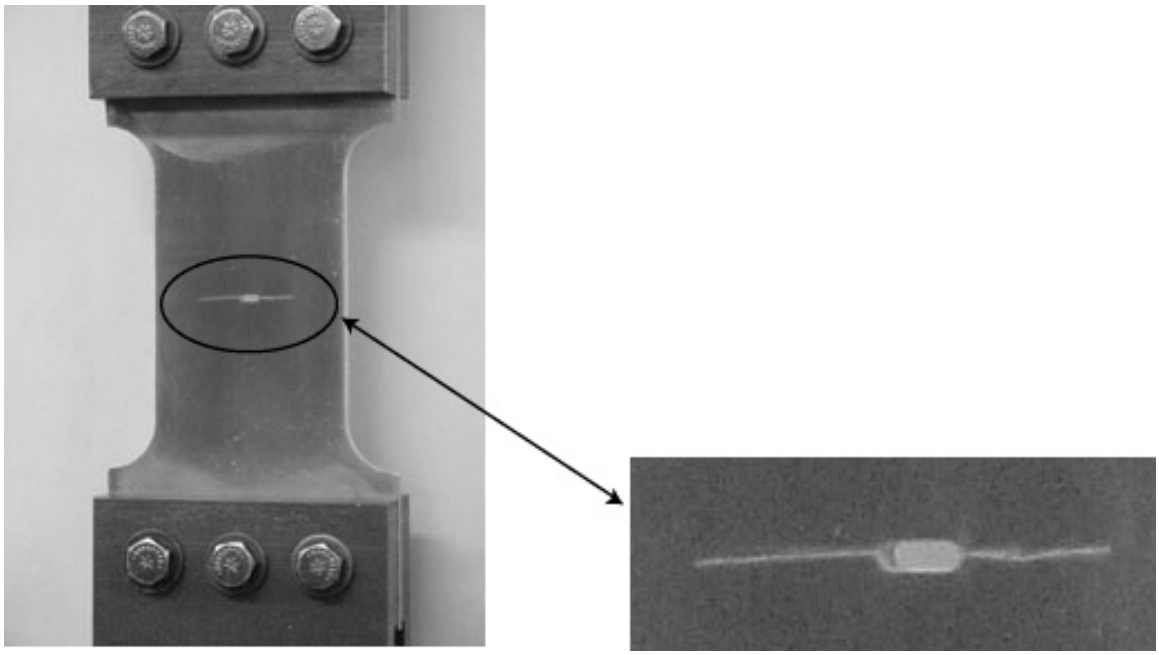

Figure 1-2 Typical specimen with fatigue crack. Detail shows machined notch and fatigue cracks

The crack initiation stage occurs prior to the formation of a well defined crack and involves mechanisms at a microstructural level that are beyond the scope of this study due to the following reasons. Most importantly, optical microscopy does not adequately resolve the features of this stage of crack formation, most of which are too small and are not clearly observable on the surface of the metallic specimen. Thus there is no way to correlate the progression of crack initiation with measurements from other instruments. The other problem is a lack of usable models. Strain-Life is commonly used to model initiation. Although strain-life models essentially allocate the observed period of initiation in a fixed pattern. Initiation is highly uncertain, even in low cycle fatigue. Thus, however good an analytical model is, it will not be adequate to predict the crack initiation behavior of any given specimen.

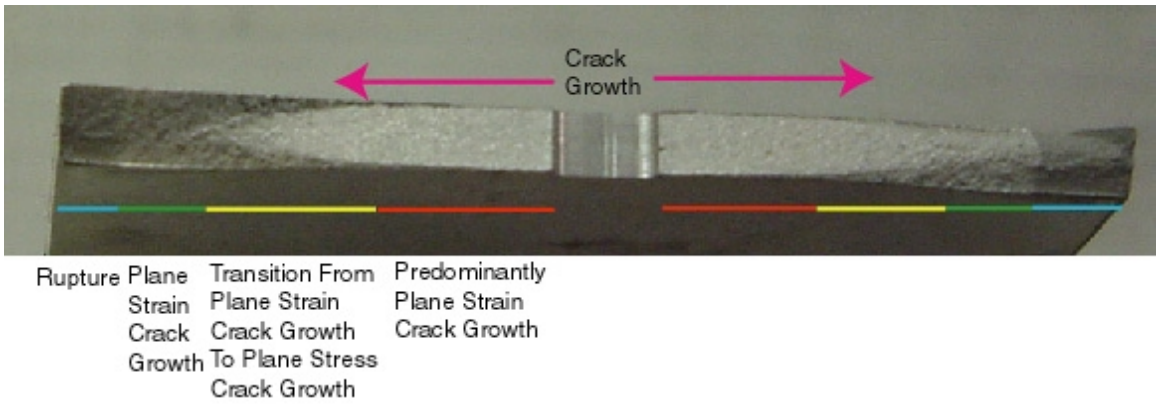

Figure 1-3 Crack Surface Showing the Macro-Stages of Crack Growth (7075-T6)

Finally, in commercial aluminum alloys, it is generally considered that cracks initiate from relatively large inclusions that are a byproduct of the alloying process [Suresh,99]. Thus, it may well be the case that there are always cracks present in the specimens used for this study. Since inclusion and flaws are randomly distributed throughout the material, small cracks that form at these defects propagate and join on the machined surface of the notch for a considerable number of cycles before even microscopically small cracks appear on the surface. Although experiments with low quality 6061-T6 aluminum had indicated that some of the effects of initiation mechanisms were being captured using ultrasonic methods, this was not confirmed in 2024-T3 or 7075-T6. Since no effort was made to monitor the condition of the machined notch surface, it is difficult to ascertain if the effects seen in the 6061 were a result of initiation or very small macro-crack growth. The goal of this study as pertains to initiation is thus best described as the prediction of microscopically small (20-50 microns long) crack formation on the surface of the specimen, which is well into the regime of 2D crack growth. However, as documented in Chapter 3, considerable progress towards this goal has been achieved.

The 2D stage of crack growth is the first stage that was considered in detail for this study, although a considerable amount of work remains to be accomplished. This stage is important for a number of reasons as it is a large source of variability in the life of a structure. More importantly, in low cycle fatigue, the 2D stage constitutes a large portion of the life of the structure. Considering that, roughly speaking, 2D cracks have equal length through the thickness and along the width of the specimen. Thus, it is likely

that the 2D stage will last until the surface crack length is in the range of ½-1 times the thickness of the specimen. Since this crack size is visible to the naked eye, this would be cause for retirement or repair of almost any structure. While, unfortunately, modeling of 2D crack growth in a stochastic setting is only at the earliest stages, the longer 2D cracks have been modeled successfully as 1D cracks for the purposes of this work, particularly when combined with measurements.

There are three major scenarios for the 2D crack progression on a given side of the notch. The first scenario is that a corner crack forms on both corners of the notch at approximately the same time. These cracks grow independently in roughly semicircular shape until they join in the middle. The relatively small ligament left between the cracks cracks very quickly, and form a through crack. This is ideal because the visible portion of the crack on either surface of the specimen is a very good measure of the progress of crack growth for the entire test.

A somewhat less likely scenario is that a penny shaped crack forms in the center of the notch and grows outwards to the edge of the specimen. This can result in fairly large crack growth in the center of the specimen before it propagates outward to the surface. In practice it is very likely that surface cracks will form and join the interior crack before the interior crack can propagate to the surface.

The most problematic scenario is that a corner crack forms on one surface and propagates through to the other side of the specimen. This results in a crack that is longer on one surface than the other for most of the test. A specimen that cracked in this configuration would require post processing of the optical measurements.

In any given test, some mixture of these scenarios will undoubtedly occur. The 2D stage of crack growth is of great interest not only because it is a critical stage of crack growth, but also because it is easily detectable using ultrasonic equipment. However since this stage is so random, many challenges remain before it can be fully characterized in real time.

Once one side of the specimen has cracked through from one surface to another the third stage of crack growth is started. Unfortunately, it is extremely unlikely that the crack on one side of the notch will form a through crack at the same time as the other side of the notch. For this portion of the testing, the through crack progresses independently

of any 2D cracking on the other side of the notch. The 2D crack growth is accelerated because of the larger localized displacement. When the cracking of both sides of the notch has formed a through crack, the total crack length has been observed to grow as a center cracked specimen. On most specimens when the second through crack is formed it will grow much more quickly than the other side.

Assuming reasonable stress levels, the bulk of the specimen is in a state of plane strain through the stage where a through center-crack has formed, and for a considerable portion of the propagation afterwards. The material at the surfaces of the specimen is always in plane stress since it is not constrained in the through-thickness direction. For the purposes of modeling macro-crack behavior this is of little consequence, since this area is so small. For this stage of crack growth, any plasticity in the bulk of the material is constant through the thickness of the specimen as the material is constrained by the material around it. As the localized stress becomes high enough, the stress state of the specimen undergoes a transition from plane strain to plane stress. This is evidenced by the formation of angled area on the surface of the specimen. This transition can be viewed in Figure 1-3. As this stage progresses, the angled areas grow larger, and the area in the center of the specimen that is still in plane strain gets smaller and eventually disappears. This transition is observable on the surface, since the crack grows in a reasonable facsimile to a straight line when it is in plane strain. Observing the specimen after it has failed all the way through, it can be seen that the plane strain area in the center of the transition from plane strain to plane stress remains in plane with the crack that formed fully in plane strain. Thus, when the transition from plane strain to plane stress occurs, the crack on the surface starts to move up or down on the surface of the specimen, which is visible on the specimen in Figure 1-2. As indicated in Figure 1-3, the final stage of crack growth is rupture, which is a failure of the remaining ligament in one cycle. As one can see from the right side of the specimen shown in Figure 1-3, this area is darker than the area caused by fatigue in the case of 7075-T6 aluminum.

1.2 Contributions of the Research

The research reported in this dissertation involves design and construction of a special purpose test facility and its instrumentation & control system that allows real-time

sensing and analytical prediction of fatigue crack damage for information-based decision and control. The test facility provides a unique framework for integration of multiple crack length measurements into a robust, flexible, and extendable instrumentation and control system. The system also demonstrates a novel approach to on-line estimation of crack damage model parameter(s), which results in significant reduction in the variability inherent in remaining life prediction. Other contributions of the research are:

- Demonstration of real-time damage sensing and life prediction in the laboratory environment which is a significant step towards application on actual structures.
- Identification of the sources of uncertainty in the fatigue crack growth process and crack length measurements, and the use of statistically optimal (or best possible sub-optimal) methods of combining measurements and damage model predictions to generate the (nonstationary) statistical distribution of the crack damage.
- Application of the data fusion concept for damage estimation by including a stochastic model of fatigue crack growth, real-time measurement data, and the use of recursive least-squares estimation in damage monitoring.
- Construction of the test facility which will be available for future research on fatigue crack damage under different operating environments such as (e.g., high temperature and corrosive atmosphere) as well as on damage mitigating control.
- Novel application and analysis of ultrasonic flaw detection systems for real-time damage sensing for detection of very small cracks and quantification of the associated damage.
- Generation of stochastic databases for future research in damage mitigating control, on-line damage prediction, and information-based maintenance.
- Development of real-time software packages: Sensor data collection software package, Load frame control software package, Optical microscopy crack measurement package. Additional software packages have been written for driving two different ultrasonic flaw detection systems, ACPD system, and the Fiber-optic strain gage system.

1.3 Organization of the Dissertation

This section outlines the organization of the remainder of the dissertation. Chapter 2 contains a discussion of the experimental apparatus. Chapter 3 discusses the measurements made with ultrasonic flaw detection systems. Chapter 4 discusses a method for on-line parameter estimation for fatigue crack growth. Chapter 5 presents a summary, conclusions and recommendations for further work.

Chapter 2

Design of The Test Apparatus

This chapter covers the design and construction of the test apparatus used in this research. From a research perspective, this chapter describes the results of a solid engineering development effort, that is a prerequisite to the research work reported in later chapters. As such, the material presented here represents an essential part of the reported research, and the apparatus it describes is unique and its analog is not commercially available. There are 5 main topics in this chapter. They are the mechanical design of the load frame, the design of the control system for the load frame, the test schedule/load frame control software, the sensors, and the sensor integration software.

2.1 Design Goals

The primary purpose of the apparatus is to demonstrate on-line damage sensing and prediction, which for the purposes of this research means that the test apparatus will be able to provide an accurate assessment of fatigue crack length. In order to accomplish this the apparatus must have the capability to accurately control the load on the specimen over a large number of cycles. The apparatus must be flexible enough to perform various test schedules without extensive programming efforts for each new type of test. There must be damage sensors that provide accurate and reasonably simple methods of calibrating new sensors. The damage sensing system must be tightly integrated with the loading system.

2.2 Load Frame Apparatus

The first part of this section discusses the hydraulic power system, and the second half of the section discusses the design of the load control system. The load control system discussion is further broken down into a discussion of system identification experiments and analysis, controller synthesis, and finally a discussion of the experiment sequencing and controller software.

2.2.1Equipment

Two fatigue testing machines have been built for load control or strain control on the frame of existing machines provided by the NASA Lewis Research Center (Hirschberg, 1970). The first machine is capable of low cycle speeds (less than 2Hz). The second machine is capable of speeds up to 12 Hz under normal fatigue cycling, and has been used as the test apparatus in Figure 4-1 for this research. The specimen is loaded by a hydraulic cylinder, which is driven by hydraulic pressure controlled by an electronic-hydraulic servo valve. The servo valve is fed with high-pressure hydraulic fluid from a pump driven by a 10hp electric motor. The servo valve is controlled from a personal computer. The feedback signals are generated by a load cell and read by the computer. Thus the computer performs all closed-loop control operations. The design of the digital control system is presented in later sections.

2.2.1.1 Safety Measures

The system at full pressure is capable of generating 90000 lb., and in the currently configured state is capable of generating 70,000 lb. Thus, although it is unlikely, it is possible for the machine to be considerably damaged if not properly controlled. There are three kinds of interlock that can shut down the machines: human, mechanical, and software. The effect of an interlock actuation is that the electric motors are stopped by the control relay in the motor starters, and the hydraulic pressure is dumped to tank by solenoid valves. All solenoid valves and control relays are of the proper logic such that the unpowered state is “safe”. This means that the motor cannot run and system pressure is at tank (atmospheric) pressure. The mechanical interlocks are switches that open a circuit if the position of the actuator is out of limits. The human operator has the option of pushing an emergency switch to stop the machine at any time. The computer controls solid state relays that can remove the signal to the solenoids and relays in the event that the code detects a problem such as the load or position exceeding preset limits. These safeguards have been extensively tested primarily through long, sad experience.

2.2.1.2 Hydraulic System Design

The main hydraulic system elements are the pump, the supply manifold, and the cylinder. A schematic of the hydraulic system is shown in Figure 4-2. The pump is a pressure regulated variable displacement piston pump.

The purpose of the supply manifold is to properly sequence the system pressure and to accommodate the accumulators. The accumulators help the performance of the system by maintaining the system pressure when the instantaneous demand from the servo valve/cylinder is higher than the flow rate available from the pump. This allows a smaller pump to be used than if the accumulators were not in the system. The disadvantage posed by the accumulators is the stored energy that must be dissipated while the system is shut down. A small solenoid valve is used under most shutdown conditions to bleed the accumulator pressure slowly. This prevents a high-pressure spike from causing the return filters to fail. Under emergency shutdown conditions, a large pressure relief valve bypasses the filter and heat exchanger. The pressure relief valve has a 100psi cracking pressure, thus making it extremely unlikely that the 300psi. limit of the return filter is exceeded. The two pressure dump valves allow for proper sequencing of pressures under startup and shutdown operations, and are also required to preclude dangerous pressures remaining in the accumulators when the system is unpowered. The schematic shows the system in the unpowered state. Under operation the dump valves would be closed and the shutoff valve would be open.

The cylinder has a 6” bore and a 2.5” rod, and is double ended (the rod extends through seals at both ends of the cylinder). Moog Inc recommends that 2/3 of the available pressure drop should be available to the servo valve and 1/3 used for the load. Following this recommendation, 5000-10000lbf is available for applying stress on the load. A lumped parameter nonlinear dynamic model of the hydraulic system is given in an appendix.

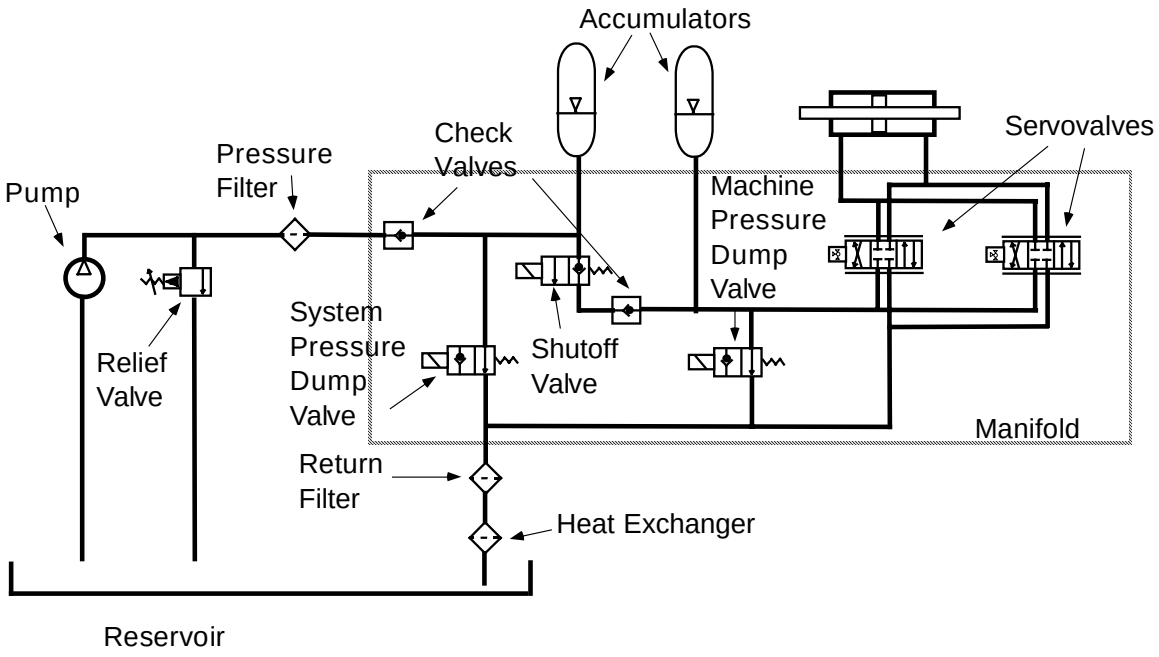

Figure 2-1 Hydraulic System Schematic

2.2.1.3 Load Sensing

The Load frame is equipped with a 10,000 lbf load cell for performing load controlled testing. The output of the load cell is conditioned internally and output to the Analog to Digital (A/D) converter in the computer. The computer uses this signal to generate an analog control signal, which is amplified and drives the hydraulic servo valve. If strain control is desired, an extensometer can be used in an exactly analogous manner to the load cell. It is also possible to infer crack length from the extensometer output when the specimen is under load control as shown in a later section. The position of the cylinder is sensed using an LVDT that is used for position control and position limit detection.

2.2.1.4 Pressure Sequencing

The dump and shutoff valves must be sequenced properly in order to control system pressure and avoid unwanted load excursions. Prior to energizing the motor starter relay, the control loop is started so that the servo valve can counteract any transients that may occur on startup. After the pump motor is started, all valves but the

small dump valve are energized to the high pressure/high flow position. The operator chooses when to close the small dump valve, thus building pressure. When the pump has recovered from the high flow demand, the operator starts the test. When the test is over, the small dump valve opens for a long enough period to allow the pressure to bleed from the accumulators. Then the motors are turned off and all valves are de-energized which is the no flow/low pressure position.

2.2.2 Control System Design

Since fatigue crack growth rate and crack length can be affected considerably by small variations in load, good load regulation is critical to this project. Load control using hydraulic power presents 2 major problems – the system is unstable and non-linear. The system is unstable because the hydraulic cylinder acts as an integrator – the position of the cylinder is a function of the integral of the flow rate of fluid into the cylinder. This could be called marginally stable, however in practice there are always biases in the system that cause the cylinder to move when the system is under pressure but uncontrolled. Fortunately this instability is easily counteracted by closed loop control, but it does complicate the design process considerably. This section discusses the load control system design process.

Prior to the availability of the hardware, simulations were run using a nonlinear system model of the hydraulic system (the system equations are given in the appendix). With this experience a simple proportional gain controller was implemented in order to operate the hydraulic system. This controller stabilized the system, but it had low performance and was not capable of disturbance rejection. It was desired to develop a linear model (or multiple models) of the system in order to use robust control methods. Further development required system identification over the full range of system dynamics and development of a robust controller. The next section discusses system identification and is followed by a discussion of the control system design followed by a discussion of the control system software.

2.2.2.1 System Identification

As discussed in Ljung (1999), open loop system identification is superior to closed loop identification due to the feedback of output noise through the system.

However, as previously discussed, this system is unstable in the open loop. An attempt was made to perform open loop identification by using a bang-bang controller that only interacts with the system when the load goes above or below a preset limit, but the results were unusable. Thus, it became obvious that some form of closed loop identification was required.

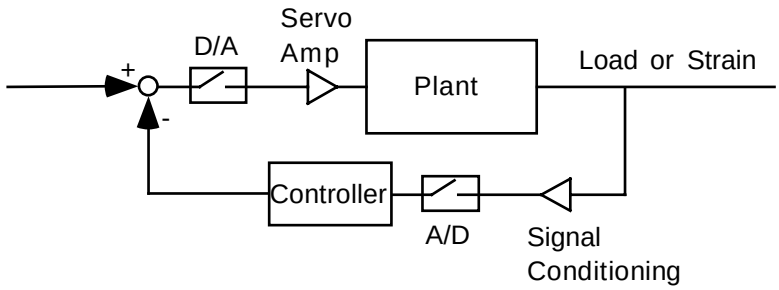

Figure 2-2 Control System Schematic

The control software written for normal operation of the machine was modified considerably for system identification testing. Since it is desired to have uncertainty models in the frequency domain, it is natural to perform frequency domain system identification. The input chosen was a sine wave with a Schroder Multisine superimposed on it. To avoid transients, multiple cycles of the base sine wave precede each experiment. Given the correct parameters, the Schroder Multisine has equal amplitudes at each frequency in the frequency band of interest, and in the time domain it has minimum variations in amplitude due to the phase relationships between the sine waves that make up the signal[Ljung, 1999]. The input signal is formulated on the following principle: The base sine wave is varied in frequency at approximately the same amplitude so as to explore the system dynamics at various slew rates of the cylinder. The major non-linearity in the system is related to hydraulic fluid flow, and thus slew rate of the cylinder is a major determinant of the linearized dynamics. The experiment was run at various proportional gains. The extremes of the dynamics were realized with the highest gain used.

The data from an experiment with low frequency nominal trajectory is shown in Figure 2.3. Sections of the system response are shown in Figure 2.4 and Figure 2.5. The

data from an experiment with high frequency nominal trajectory is shown in Figure 2.6. Comparing the data from Figure 2.5 and Figure 2.7, it is possible to note that the system does not track the Multisine data as well (i.e. the system is less responsive) when the nominal trajectory is of high frequency.

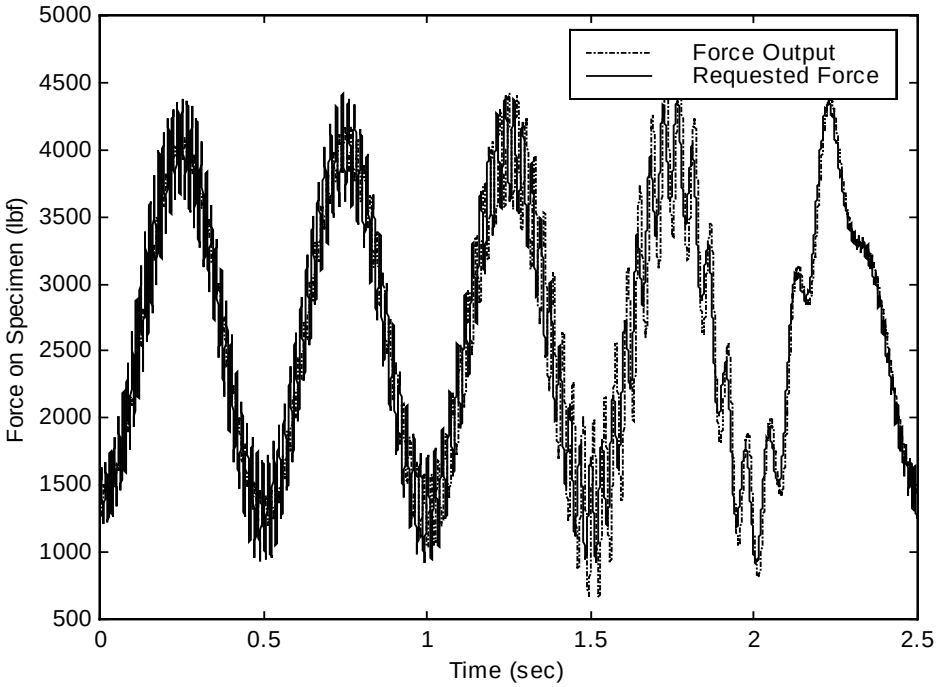

Figure 2-3 Typical System Identification Experiment With Low Frequency Nominal Trajectory

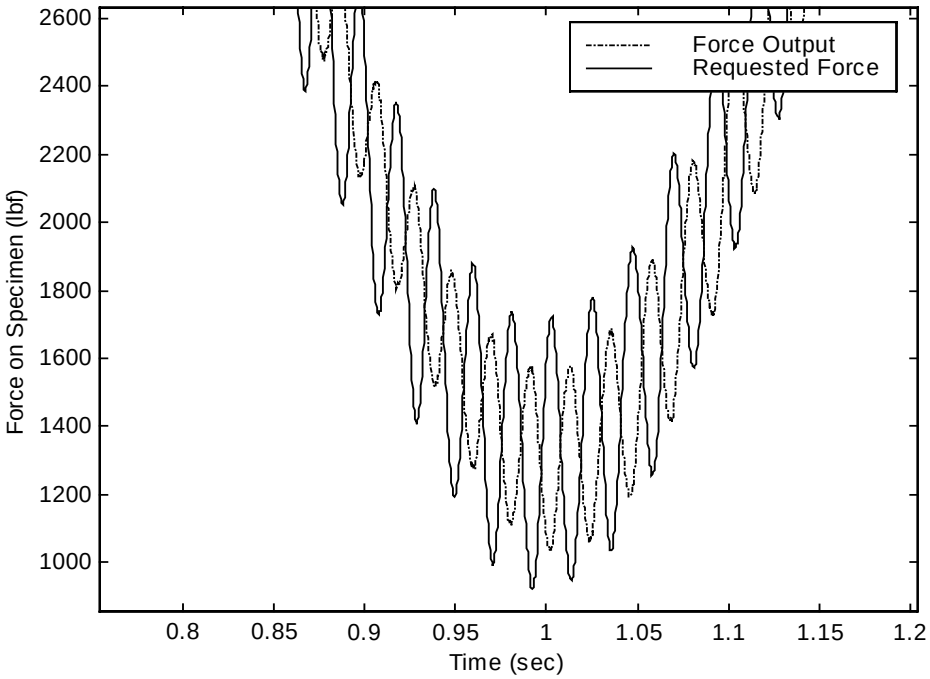

Figure 2-4 Close up of data in Figure 2-3

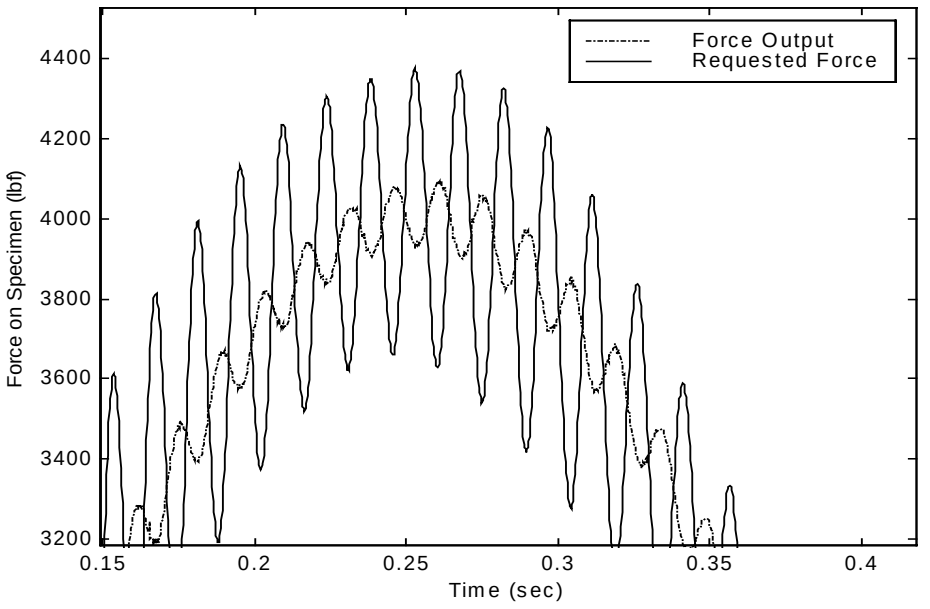

Figure 2-5 Same Experiment as Figure 2-3 Showing High Frequency Response of System

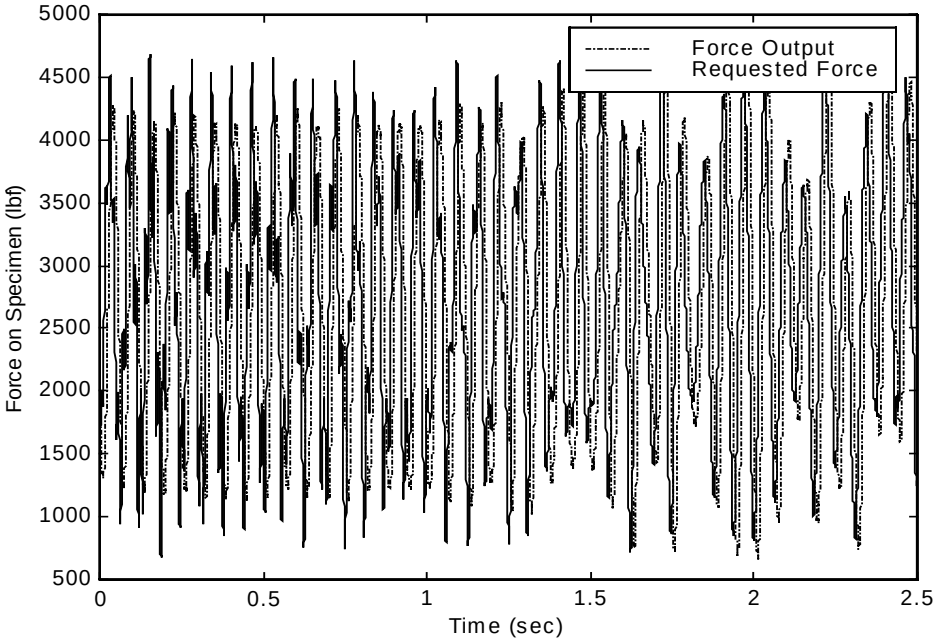

Figure 2-6 System Identification Experiment With High Frequency Nominal Trajectory

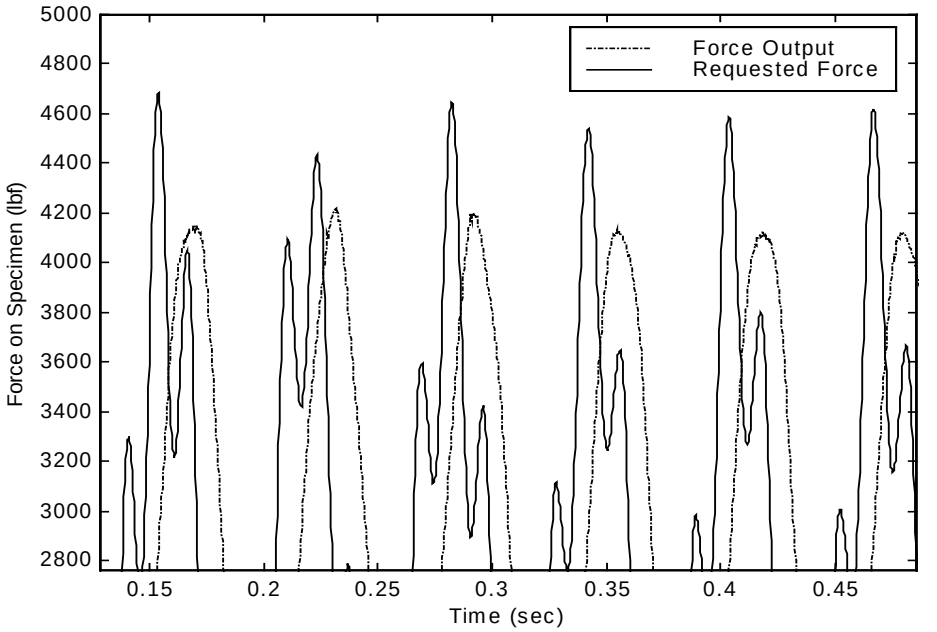

Figure 2-7 Close-up of Data in Figure 2-6

One limitation of the experiment is that the experiment length was limited to 2.5 seconds. This is due to the fact that using MS-DOS, a disk access can cause a large delay thus potentially leading to a failure of the control code. Thus disk accesses were avoided during dynamic portions of the testing. The upshot of this limitation is that the low frequency information is very noisy. This is unfortunate but is not insurmountable, since the low frequency dynamics consist of the well understood integral action of the hydraulic cylinder. Additionally, it should be noted that the low frequency response of an integrator is difficult to measure since the system has a large output even for very small inputs. Since the input and output in this system are both limited to a 12 bit range, the low frequency open loop response easily exceeds the dynamic range of the system. As seen in the Figure 2.8, the low frequency information is very widely spaced, representing very few data points.

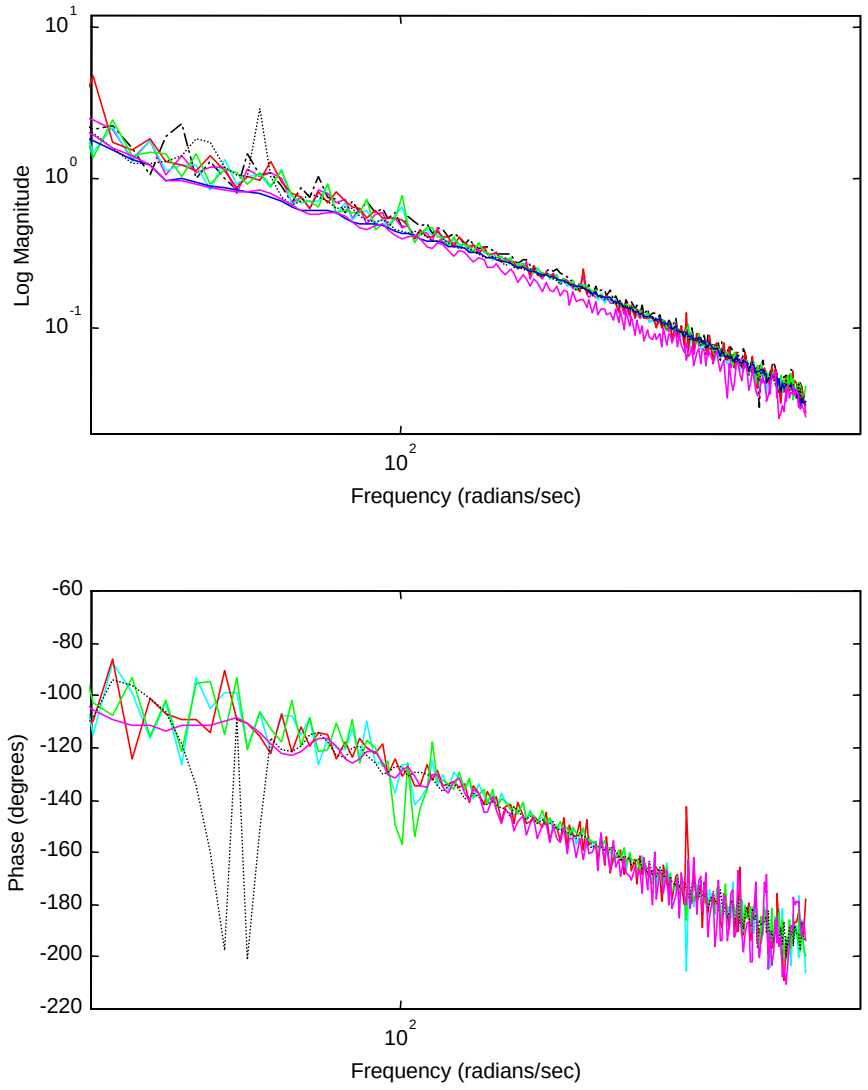

Figure 2-8 Open Loop Frequency Response Data

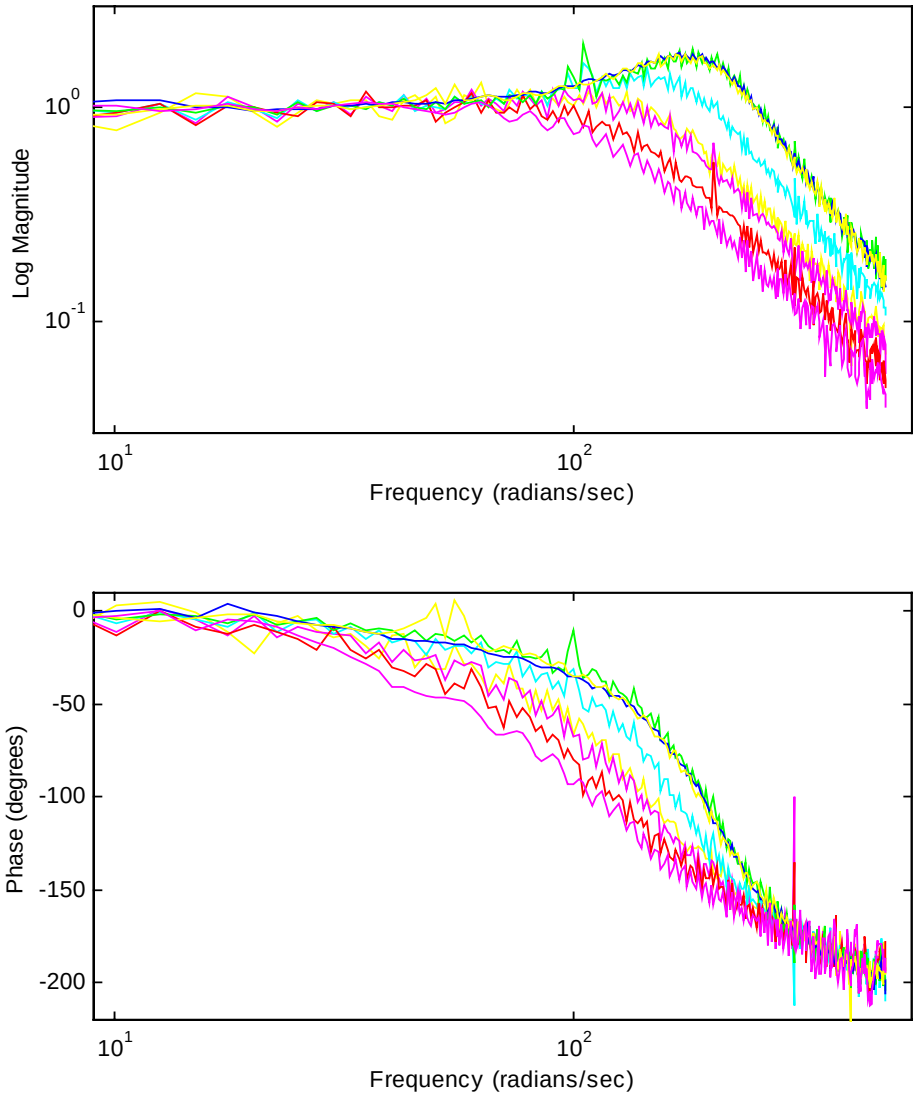

Figure 2-9 Closed Loop Frequency Response Data

The Matlab Frequency Domain System Identification Toolbox [Kollár 1994] was used to identify the system model from the experiment results. This toolbox allows the user to pick the order of the system dynamics and then calculates the most likely (in a mean square sense) matching model of that order. The best fit also was most internally consistent. The identification analysis resulted in the open loop model of the form:

$$\frac{d^2y}{dt^2} + c\frac{dy}{dt} = -a\frac{du}{dt} + bu \qquad (2.1)$$

where: y is the applied load

u is the control command.

The negative sign on the right hand side of the above equation is unusual in a physical system. It implies an active control system where energy is forced into the system as a result of the control command, as is clearly the case in this system. This non-minimum phase characteristic does moderately complicate the design of the control system since it is possible that a high-gain controller causes the system to be unstable. Plotting the map of possible closed loop eigenvalues of the above differential equation (with a proportional controller) results in the root locus plot shown in Figure 2.10. This figure shows that given high enough gain, the system will become unstable. In practice, the servovalve will become saturated at a gain that is lower than required by the linear model to become unstable, so high gains must be avoided in any case. Figure 2.11 shows a portion of the same plot focusing on the location of the closed loop eigenvalues, which were identified separately from the open loop eigenvalues. This plot shows that the closed loop and open loop identification results agree fairly well. Finally, Figure 2.12 shows the portion of the root locus that dominates the closed loop operation of the machine. The eigenvalues (shown by x's) on the real axis are from the open loop identification. Each model has 2 eigenvalues, one which is fixed at 0, and the other which falls in the range from 18-30 Hz. The eigenvalue at 18Hz was the result of an experiment with high slew rate demands and high gain, which resulted in a fairly noisy data set. However, from a design perspective, the objective of the identification step was to bound the possible system dynamics, and thus it was fairly successful, particularly

since the (independently) identified closed loop and open loop models are consistent for this experiment.

The final step in the system identification analysis is to pick a nominal system representation and to find a transfer function that bounds the differences between the nominal system model and all of the other identified system models. While it is appealing to try to pick the system model that matches the most likely operating point, the approach taken here was to pick a nominal system that results in the most desirable representation for the system uncertainty. The desirable characteristics in this case were low amplitude of the uncertainty model at low frequencies and higher uncertainty amplitude at high frequencies.

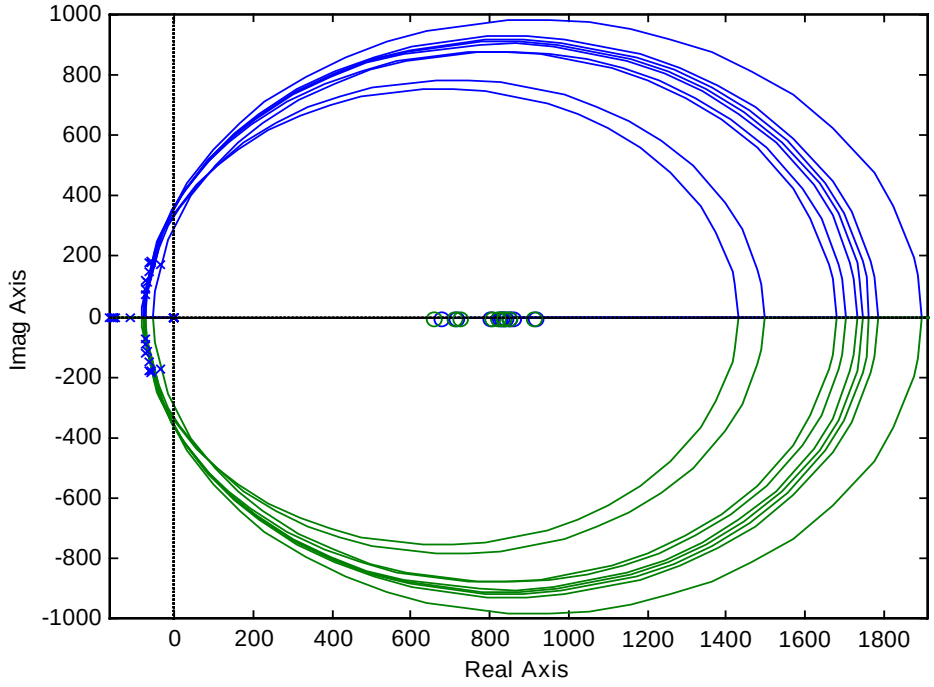

Figure 2-10 Possible closed loop eigenvalues under proportional control, all identification cases

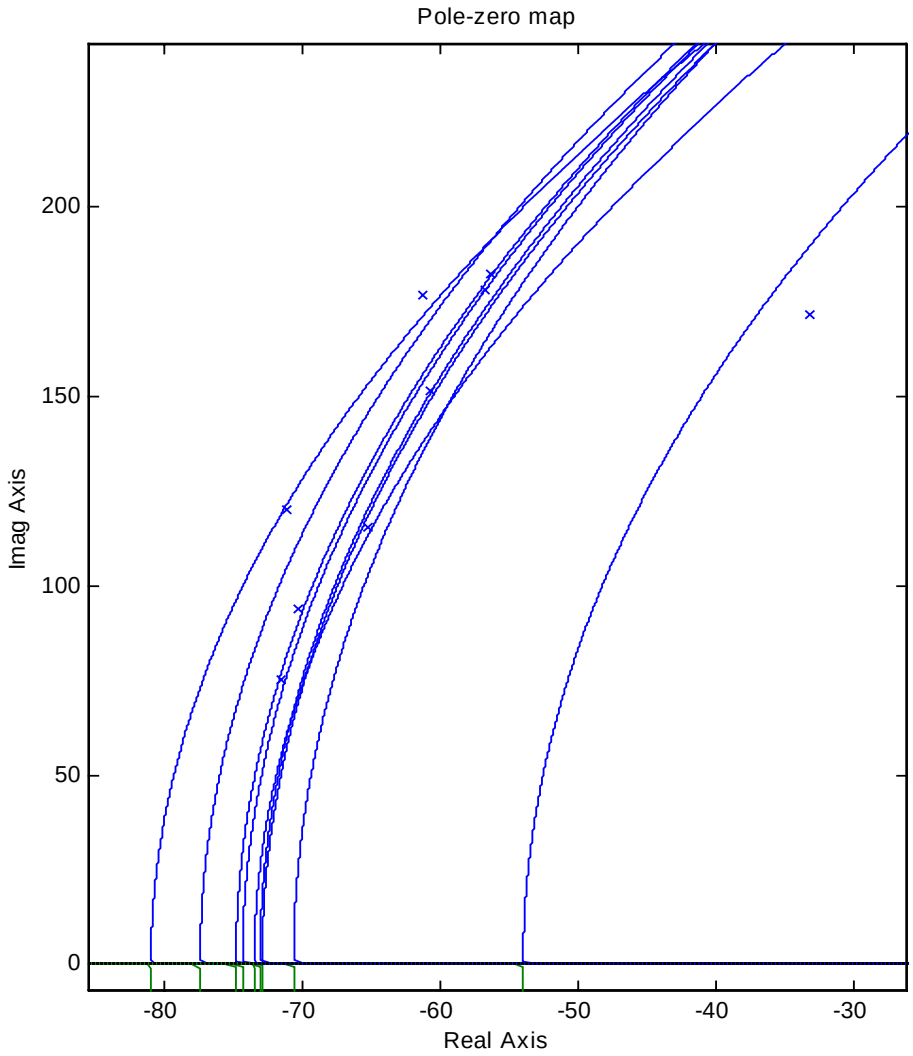

Figure 2-11 Same plot showing identified closed loop eigenvalues

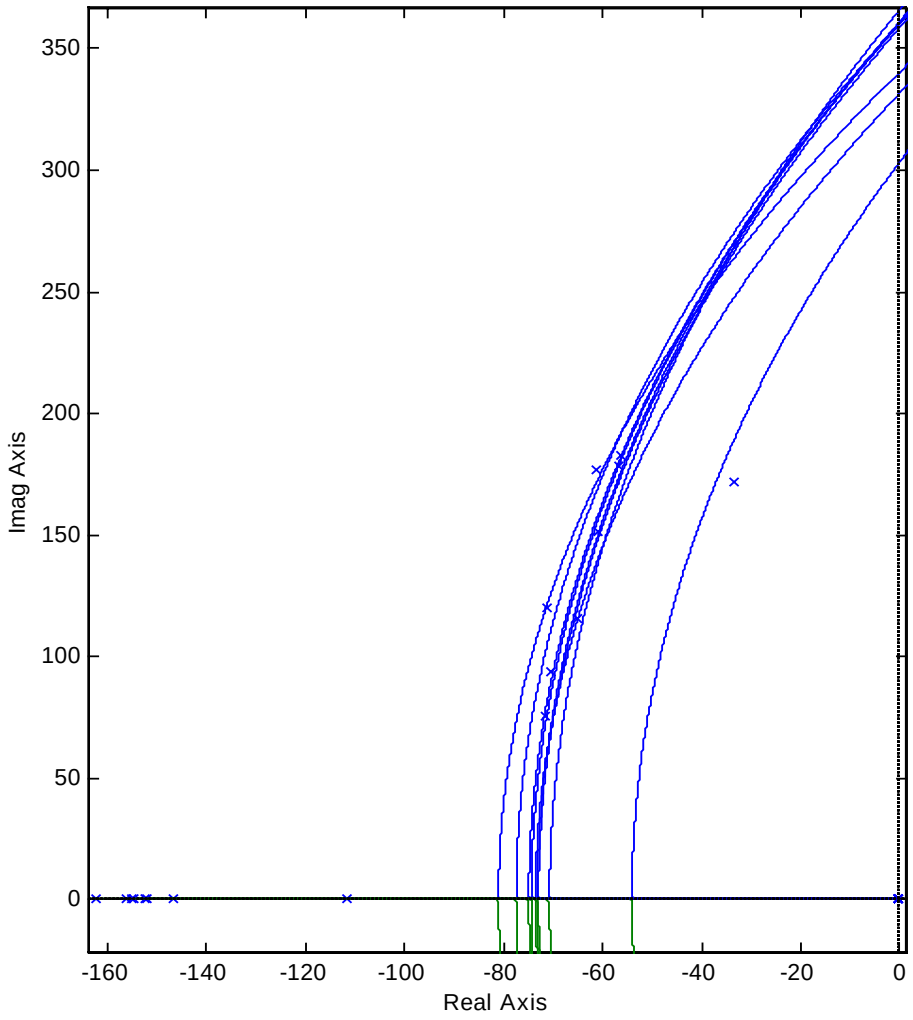

Figure 2-12 Showing the full range identified open loop eigenvalues

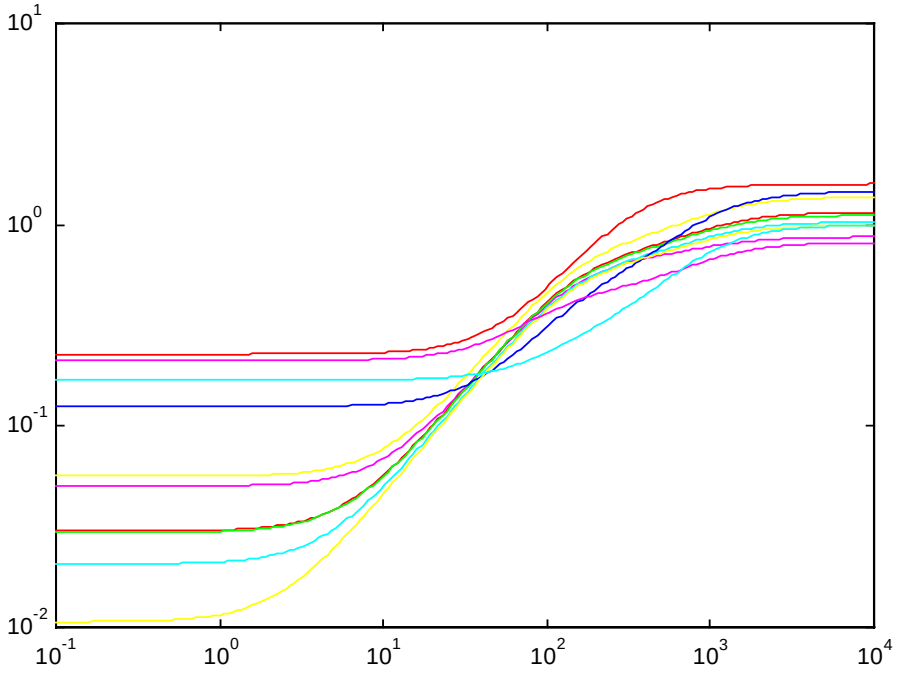

Figure 2-13 Multiplicative Uncertainty Model

2.2.2.2 H_∞ Controller Design

As shown in the identification experiments, a fairly simple controller can stabilize the system. However, this controller does not meet the performance requirements for this machine. Namely, it is very sensitive to disturbances, and it does not accurately control the amplitude of the load over a wide enough range of desired loading cases. Thus H_∞ controller design methods were chosen for a number of reasons [Balas, et. al. 1993]. Most importantly is the ability of such methods to accommodate uncertainty in the system model. Also important is the ability to relate performance measures with physical quantities. Furthermore, it is easy to change performance weights to adjust the controller scaling such that it fits within the available 12 bit dynamic range of the A/D and D/A hardware. If the nominal system in combination with the uncertainty model bound the actual range of system dynamics, then stability can be guaranteed and minimum performance measures can be met for that range of dynamics. This is why the system identification tried to excite the entire range of possible dynamics of the load frame.

In order to design an H_∞ control, the system as shown in the schematic in Figure 2.2 needs to be changed as shown below in Figure 2.14. The system is augmented with the system uncertainty model derived in the system identification step. Performance weighting transfer functions are added to the output and on the controller output. The performance weight on the output, W_{p1}, is used to force the H_∞ algorithm to produce control effort in the frequency band of interest. In the absence of this weighting function, no output would be produced except that required to stabilize the system. The performance weight on the control effort, W_{p2}, limits the magnitude of the control effort. In the design outlined here, this weight was essential to allow the controller dynamic range to be matched to the dynamic range available with the digital hardware. Otherwise, since these are linear techniques results in controller transfer functions that do not produce usable controllers, specifically the controller coefficients saturate the hardware, or produce very small outputs. The final weighting block in Figure 2.14 is the system uncertainty block, W_{del}. The system uncertainty block includes all known deviation from the nominal system model and directly uses the results of the system identification experiments outlined in the previous section.

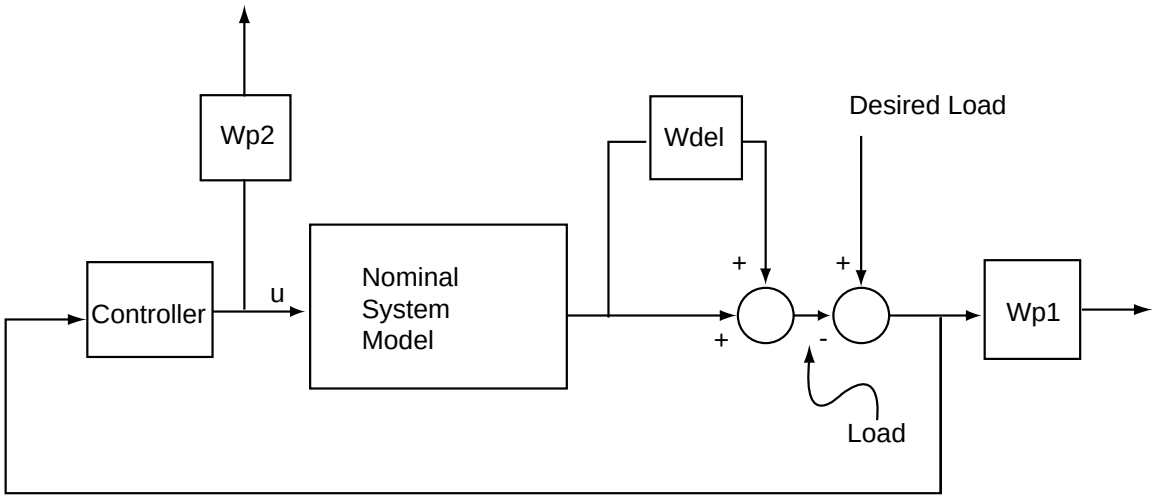

Figure 2-14 Block Diagram for H_∞ Control Design

2.2.3 The Control System Implementation

In addition to the requirement for accurate load application, the control system must be very reliable and capable of responding to failure conditions rapidly. These

requirements well served by using a computer for the controller. However it is imperative that the software be without flaws that are capable of causing system failures. In addition, the software must allow flexibility in test scheduling, and offer an acceptable operator interface. This section discusses the control system software design with these issues in mind.

2.2.3.1 System Organization

Specimen loading can be controlled from load or strain. For this work, testing was conducted under load control. However, in order to safely load specimens, a Linear Variable Displacement Transducer (LVDT) was used to control the position. The LVDT was also used for a crude (noisy) measure of the compliance of the specimen. The control system schematic is shown in Figure 2.15. All control logic is normally handled by software. Manual overrides can release the hydraulic pressure and stop the pump motor. The pump motor must be turned on by hand after the motor starter relay is enabled by software, and is normally turned off by software after the pressure is released from the system in order to avoid driving the pump backwards. The motor starter relay is only enabled after the control loop is started. The relays that are attached directly to the computer are all solid state and are rated for 1500 volts of isolation so that the computer does not suffer any ill effects from the voltage transients that occur when mechanical solenoids and relays are turned off.

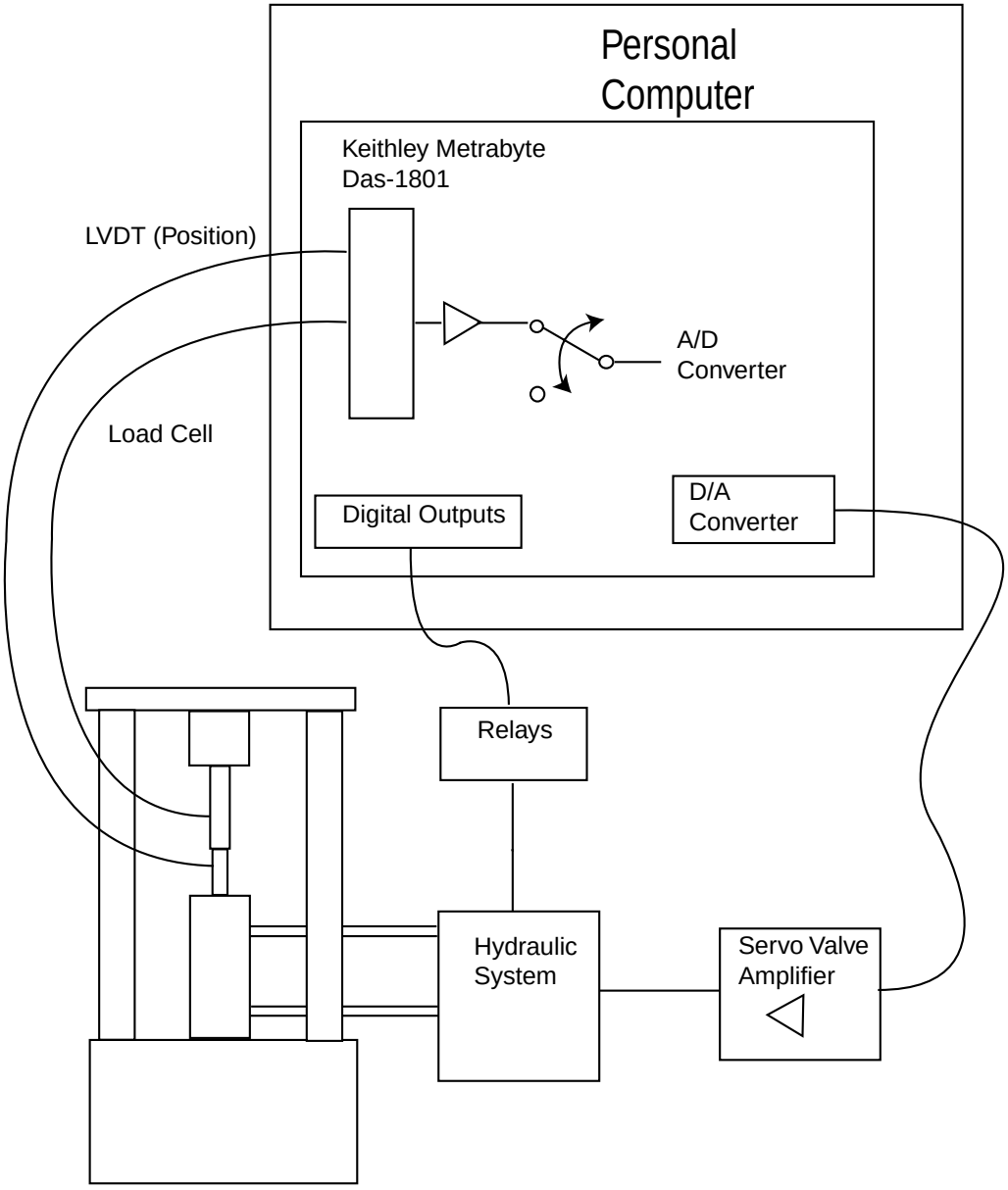

Figure 2-15 Control system schematic.

2.2.3.2 How The Test Was Run

This work was originally proposed to include only constant amplitude testing. However, it became clear during the software development that adding block loading and other types of loading cycles to the software was essential. Memory limitations imposed by the choice of MS-DOS as the control computer's operating system preclude fully random loading. However, it is possible to define piecewise constant amplitude tests that fully explore the issues that are poorly understood in variable amplitude fatigue crack growth. Thus the following cycles are defined in the software:

- Precracking cycle, which is simply a constant amplitude cycle of no fixed number of cycles for the first and last legs of the test. The test operator ends the precracking cycle manually.
- Crack Open Cycle and Single Overload Cycle, which are single sine wave cycles that are completed very slowly so that measurements can be taken multiple times during the cycle.
- Constant Amplitude Cycle, which has a fixed number of cycles.

The control software reads a test schedule file and stores the schedule internally. The tests are performed in the order which they are found in the file. For each test segment the file entry defines the type of cycle, the maximum and minimum load, the number of cycles which the segment will be run (if applicable). The operator can truncate any test (to an integral number of cycles). The operator can pause a test at the current cycle's minimum load or maximum load, or to zero load. Additionally, the operator can slow the test cycle frequency.

2.2.3.3 Failure Accommodation

The system has one clearly catastrophic failure mode, which is the hydraulic cylinder extending too far and possibly crushing the sensors, the specimen, and the load cell. The other extreme, the cylinder retracting fully, is of very little consequence, other than the loss of a specimen. The other major failure mode is of a loss of hydraulic fluid containment. This situation is potentially messy, but self-limiting, and the hydraulic fluid

poses little danger of fire and is non-toxic. However, the system is not operated at its rated pressure and the components are designed to have considerable safety margin, so this failure mode is of acceptable. Thus the failure of interest is an out of limits position or load. This condition has a number of potential causes. It should be noted here that if the pressure is dumped from the accumulators, no further damage will occur. The pressure can be dumped from the accumulators by three different valves that are designed such that they are forced open by hydraulic pressure when power is removed. The power can be removed quickly by software, manually or by the limit switches. Thus the software can accommodate (or at least limit the damage from) a mechanical problem, such as a stuck servo valve or a loss of pressure in one of the cylinder feed lines. A software bug has the potential to defeat almost any accommodation mechanism, but the design of the software has been carefully laid out to reduce most potential bugs to annoyances rather than major failures. This subject is discussed more fully in the next section.

The software primarily monitors load and strain for out of limit conditions. The possibility of both the LVDT and the load cell to have an in range failure simultaneously is remote. Additionally, the design of the A/D converter board is such that if a sensor is disconnected or not powered, it will read the maximum value. However, since it is possible for the single A/D converter to fail, limit switches are in place to turn off the system in the case that position limits are exceeded.

2.2.3.4 Software Organization

As discussed in the previous section, a major concern in the design of the control software architecture is that a software bug shall not cause the system to be uncontrolled or improperly controlled. Although this is clearly not possible with the system as designed, in practice the risk is reduced as much as possible. The control software was originally hosted on Microsoft Windows for Workgroups so that the same computer could be used for both sensing and machine control. However, some of the instruments were not able to work under this version of Windows, so the software was ported to Windows NT. While guaranteeing good average response under normal conditions, fairly regularly the system will not run the control software for periods up to the hundreds

of milliseconds. This neglect causes smashing and crushing of delicate machinery. This problem was insurmountable the control software was ported to MS-DOS. While MS-DOS lacks the services that are offered by Windows or Unix, it does no harm. In fact, in the program as it currently exists, MS-DOS is not called after the program enters closed loop control, and the only activity by MS-DOS is the time of day interrupt servicing 18 times per second. Thus all software failures are solely the responsibility of the author.

The software effectively has two threads of operation, the main program and the controller. A schematic depiction of the software is shown in Figure 2.16. The main program enforces the test sequence. The controller itself is implemented in an interrupt routine that is driven by the A/D board as discussed in a later section. The controller is timeless and modeless. It checks for out of limits conditions, calculates the control law and does real time communication tasks. It is deterministic and is reentrant. All data structures that affect the operation of the controller are only accessible through functions in the same module as the controller. A major problem with controllers such as this is mode switching between one control objective and the next, because the switch is an exception that tends to be difficult to test and thus is unreliable. This problem is addressed in this controller by having a mode switch at the end of each cycle. Each control objective is represented in software by a pointer to a structure with information about the cycle. At the end of each cycle the controller loads this pointer from a different pointer representing the next cycle. If the control objective is not changing, the pointers will be the same. However if the control objective is changing, it is a simple matter of a trusted routine changing the pointer that will be loaded at the end of the current cycle. The trusted routine checks the proposed reference structure to see if it exists, to see that all parameters are reasonable, and to see that the commanded loads are within limits.

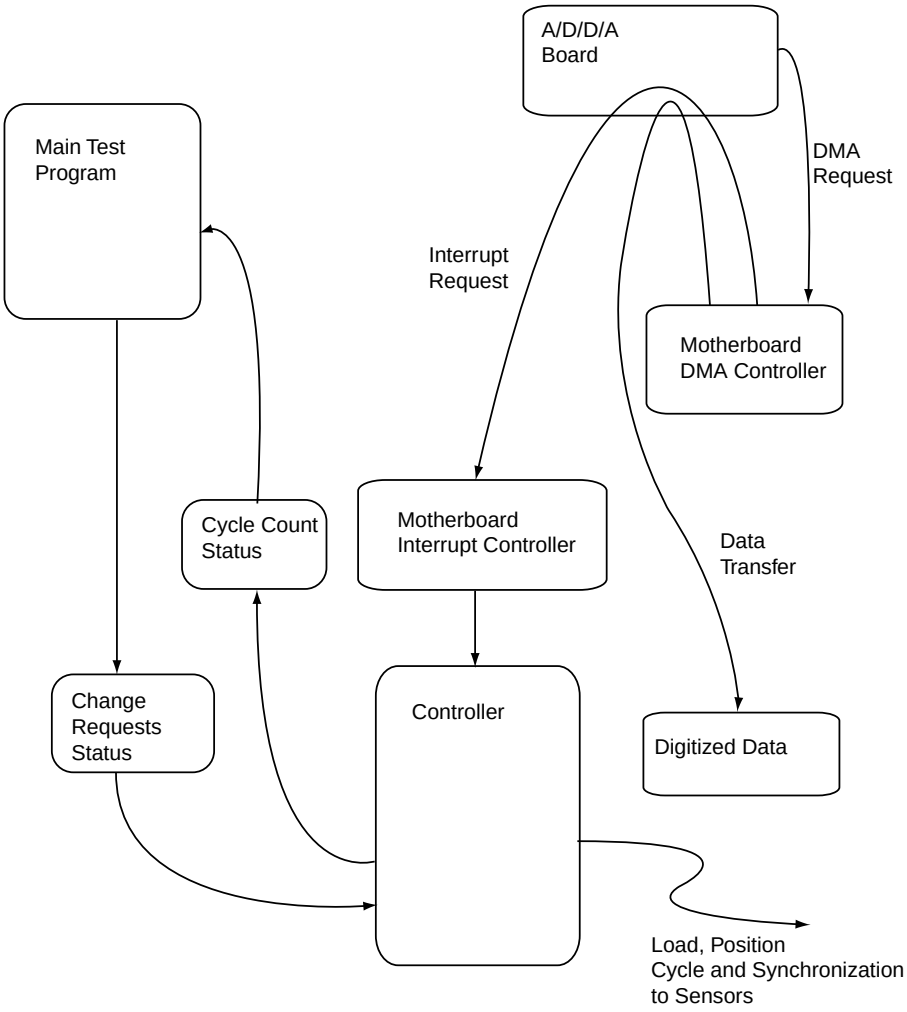

Figure 2-16 Control software

Three types of reference structure are defined in the current implementation. These are point references, i.e. one load level repeated continuously; cyclic references made up of one cycle of a sine wave; and ramps which traverse linearly from one load to another. A test is made up of sub-tests, which is generally a fixed number of constant amplitude cyclic loading. For each sub-test, the program stores a cyclic reference structure at two frequencies. The slower frequency is slow enough to reduce the vibration in the load frame sufficiently to allow good microscope images. The program also stores two point load references for each sub-test, one each for the minimum and maximum load of the test cycle. The program always maintains a point reference for no load; all other reference structures are dynamically created and destroyed as required by the sub-test. An array of the possible reference structures is saved in the controller module. All other modules have access to a set of handles that represent the elements of that array. The sub-test definitions are kept in a global test definition structure which contains an array of structures that have all information required to perform a sub-test. Between sub-tests, a routine that manages the test schedule is called. It requests that the reference structures for the next sub-test be created, and stores the resulting handles in the structure that defines that sub-test. Then the main program calls the subroutine that runs the type of sub-test. On entry, the controller is maintaining the minimum load from the previous sub-test. The test routine requests that the controller ramp to the current minimum load and then change to the cyclic load reference in one function call. The routine then loops continuously, checking for user input and to see if the number of cycles in the sub-test is complete, and periodically requesting that the real-time data be displayed on screen. The test routine may also call other similar routines when needed. For example the constant cyclic load routine will call routines that run the machine in a pre-defined slower cycle (identical amplitude, but approximately 3 times as long). This occurs on a defined schedule so that the microscope is guaranteed a better picture. The user can request that the slow cycle be run, or that the machine stop at maximum or minimum load. There is also a routine that is used to perform a test cycle very slowly so that measurements can be taken at each load level. This is called a crack-opening cycle in the program, and it is also used to inject an overload cycle into the test.

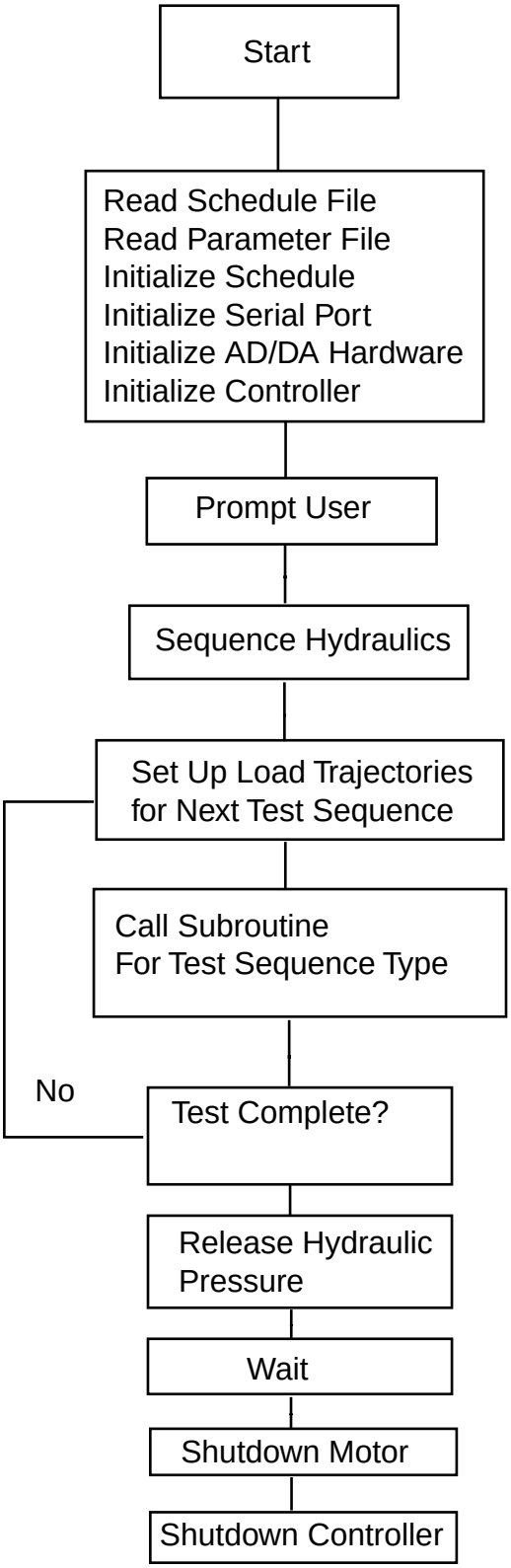

Figure 2-17 Flow Chart of Controller Software

2.2.3.5 Controller/Interrupt Routine

The controller is an Interrupt Service Routine (ISR) that services the Direct Memory Access (DMA) completion interrupt. The A/D board is initialized to take 20 readings per frame, which represents 10 readings each for 2 channels. These are channels are connected to the load cell output and cylinder position LVDT output. The DMA controller on the PC motherboard is programmed to read 20 single 16 bit words and store them sequentially in a given memory location for each transfer. It is also programmed to reload the initial address for the next transfer after each transfer of 20 readings is complete. When a reading is taken, the result is put into a FIFO on the A/D board and a DMA request is issued. The DMA controller on the motherboard retrieves the data and stores it in system ram (in sequence). When the 20^{th} reading is stored, the DMA controller asserts a signal that is looped back to an interrupt line by the A/D board. At this point, control is given to the Controller ISR. Thus once the DMA controller and A/D board are initialized to work together, no periodic programming of either element needs to take place in order for further data to be collected. The controller ISR adds the 10 readings together for each channel and uses these values to calculate the control law. Since the A/D and D/A only have 12 bit resolution, this allows the most dynamic range possible, since there is no truncation of any intermediate result until the analog output value is calculated. It also avoids a needless division. If the controller is controlling to a periodic reference, then communications are enabled. The controller sends 5 packets of data: a packet to transmit maximum load reading; a packet to transmit the minimum load reading; a packet to synchronize LCR readings; a packet to trigger an ultrasonic reading at low load, an a packet which is used to trigger video and an ultrasonic readings at high load .

2.3 Damage Sensing System

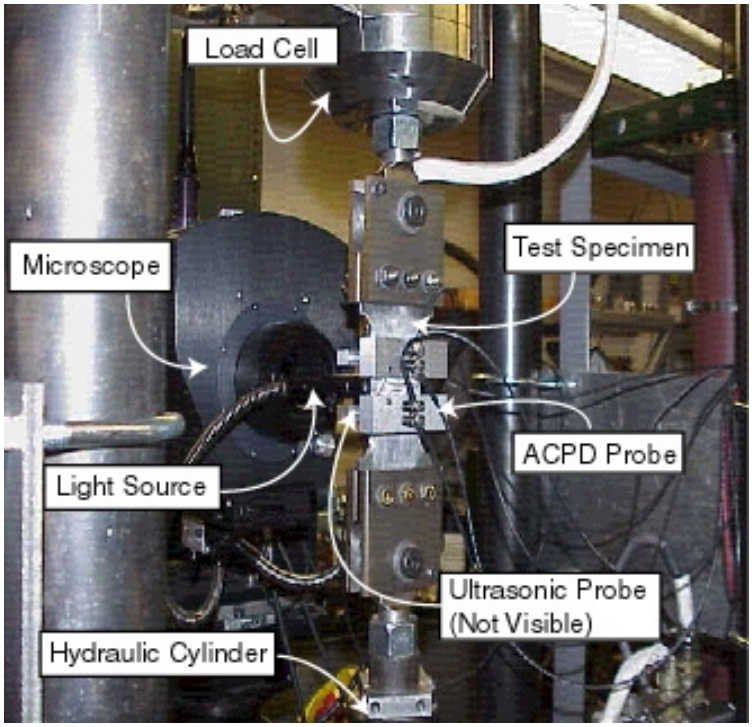

Figure 2-18 Test Setup

Figure 2-18 shows an overview of the damage sensor system. In addition to the instruments, there are 4 computers used in the system. The first computer controls the load frame and acquires analog signals. One computer controls the LCR meter, and another controls the ultrasonic equipment. The final computer controls the microscope and video, collects data from the other computers over an Ethernet network, and runs the real time NDE algorithm. An Ethernet network and an RS-232 serial data line connect the computers. The control computer sends messages on the serial data line to synchronize the remaining computers to the applied load cycle. Only the control computer can send out data on the serial line, which is connected in parallel from the control computer to each of the remaining three computers. The advantage of this system is that it is easy to add extra sensors. The disadvantage is that there is extra complexity and the network connection is a bandwidth bottleneck. If the sensors are well calibrated, it is possible that all crack length measurements can be calculated on the sensor side of the network connection. During calibration studies, high bandwidth

sensors such as ultrasonic flaw detection systems can put a high load on the network connection. The final part of this section discusses the integration of the instruments into a system and the software required to run the testing.

2.3.1 Damage Sensors

The purpose of this section is to briefly describe the damage sensors used in this research. Four types of damage sensors were used. The first, a long distance traveling optical microscope, was primarily used to calibrate the other sensors. The most interesting work accomplished in this research was real-time application of ultrasonic flaw detection and sizing. Two other methods of crack length determination, compliance and potential drop were not fully developed as part of this research, but are presented here for completeness.

2.3.1.1 Optical Measuring System and the progression of crack length

The purpose of the optical measuring system is to calibrate the crack length measurements of the other instruments. To that end, it is essential to understand the strengths and weaknesses of the optical system. The strengths of the system are clear, namely, a direct measurement of the visible portion of the crack is possible with very little noise involved, barring operator disinterest. However, even for this testing, a considerable portion of the test is performed before the crack is visible. Furthermore a discussion of the progression of the crack is in order

The major weakness of the optical method is that the crack must be visible on the side of the specimen that is being observed, or for convenience, the “front”. One unfortunate circumstance is that a crack initiates on the “back” of the specimen, and propagates through the specimen’s entire thickness. The upshot of this pattern is that the crack on the back of the specimen remains longer than the crack on the front for the entire length of the test.

2.3.1.1.1 Long Distance Traveling Video Microscope

All of the methods of crack size determination considered in this section require calibration. In this effort, a long distance microscope is used for calibration. Clearly the microscope is unsuitable for field applications, but for many laboratory specimens it is

highly suitable as a calibration standard or "truth model." The primary instrument for measuring crack length is a Questar QM100 Step Zoom Long distance microscope. This microscope is mounted on a 3-axis stepper motor driven precision stage. The microscope can resolve images on the order of 2 microns at a distance of 6in to 14 in. The long distance between the microscope and the specimen is a key feature, because it allows mounting of sensor probes without interference from the microscope optic. The microscope is shown in Figure 4.2 The encoders on the stage have 20-micron resolution, which is increased to 5-micron resolution with quadrature encoding. The motion controllers improve upon this resolution by microstepping the stage motors. Crack length is measured by moving the microscope so that a cursor superimposed on the microscope image is over the crack tip. The microscope is used as the lens for a digital 8-bit monochrome progressive scan (non-interlaced) video camera that is capable of asynchronous operation (i.e., is not limited to a constant frame rate like a normal video camera). Since the crack tip will move out of the field of view of the microscope during the test, and since the image is the most accurate at its center, the motorized stage must be used to move the microscope in coordination with the progress of the crack.

2.3.1.1.2 Synchronization

Since the specimen is being deformed during a stress cycle, the crack moves vertically during each cycle. Thus the camera must take images with a very fast exposure time and synchronized with the motion of the specimen. This has been performed in the past by using strobed light sources synchronized to the motion of the specimen. Recently, non-interlaced cameras have become available with asynchronous reset capability and short image acquisition time, eliminating the need for strobed light. Synchronization with the load is made possible through RS-232 serial communication with the load frame control computer, which sends a particular message when the desired load is reached. The computer hosting the frame grabber must respond to this message by starting a frame acquisition. This method is dependent on the performance of the computer hosting the frame grabber due to a series of time delays. After the message arrives at the serial port, the computer operating system must invoke the serial port interrupt routine. After the interrupt routine completes its processing, the operating

system must invoke the routine that processes the message, decodes it as a video synchronization message and starts a frame acquisition. Due to the algorithms used to calculate multitasking priority by the operating system scheduler, extra delays may be injected before the acquisition is started. The observed performance of this method of synchronization is that some vertical motion is observed at 10Hz, but at 5Hz the image is effectively motionless. Initial work indicates that further improvements can be achieved by reducing the vibratory motion of the load frame.

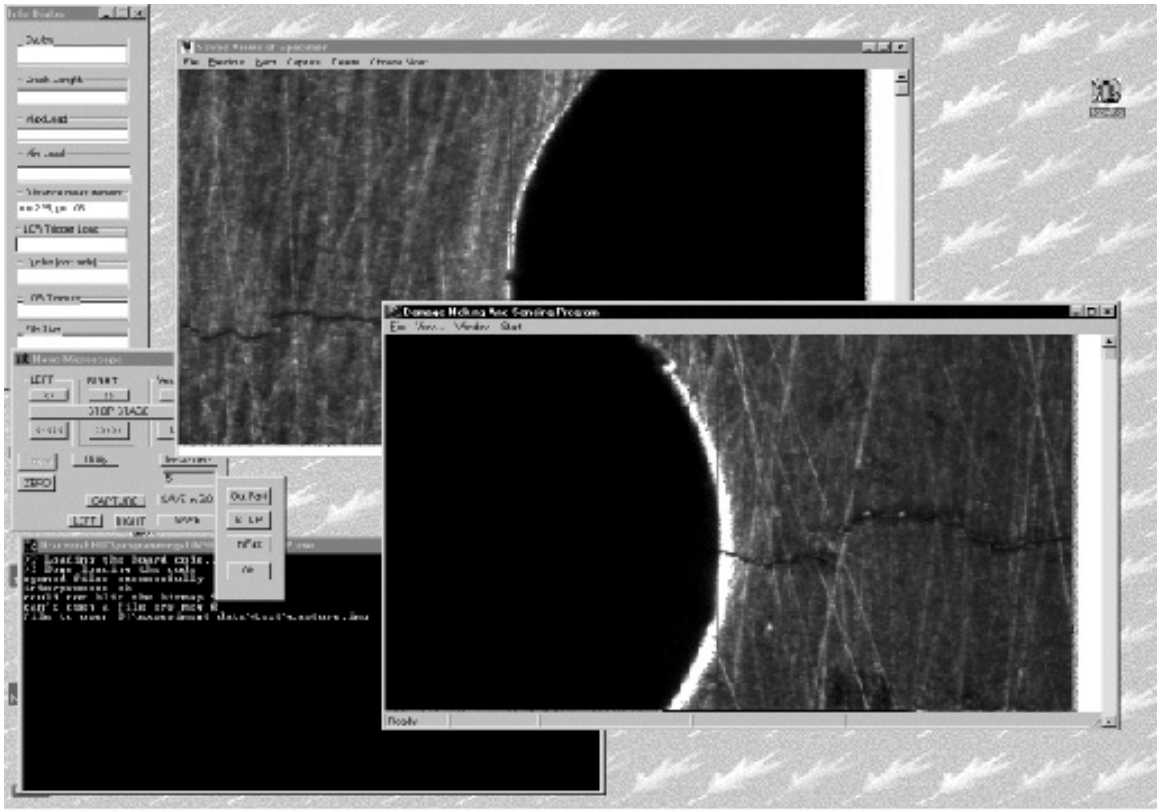

Figure 2-19 Microscope control program

2.3.1.1.3 Crack Tip/Microscope Motion Coordination

Since the field of view of the microscope is about ½ centimeter at highest magnification, significant crack growth could conceivably be monitored without moving the microscope. However, this effort required the ability to be able to follow the crack anywhere on the specimen. The method of crack length measurement used in this work

is to move the microscope until a cursor superimposed on the video image is over the crack tip. Figure 2-19 is screen shot of the microscope and motion stage user interface. The operator records the initial position of the notch edges. As the crack propagates, the operator periodically moves the microscope until the cursor is over the crack tip, saves a microscope image, and saves the motion stage position, i.e. crack tip position. This procedure is repeated for both sides of the notch, since it is very rare that the cracks initiate at the same time, or are the same length. The saved images are displayed in a separate window and it is possible to review the images during the test. Since each image takes up about 380 kilobytes in raw form, each image is compressed using JPEG standard compression. Using this method it is possible to save about 5000 images per test. The saved images are very useful for crack measurements since the difference between two consecutive images taken from the same location is fairly striking if crack propagation has occurred. The saved images can be viewed in actual order or only for one side at a time. The position of the crack tip is saved for each side of the specimen so that the motion controller can be used to quickly return to either crack tip location from anywhere in the range of motion of the stage. The position of all three stages is recorded so that the proper focus and elevation are maintained. During testing, the control computer periodically drops the load cycling frequency to below 5Hz for 10 cycles and sends a special synchronization message. The computer hosting the frame grabber waits 2 cycles for the load frame vibration to die down and then saves an image. When the image acquisition is complete, the computer moves the microscope stage to crack tip on the other side of the notch. The operator can interrupt this behavior.

2.3.1.2 Potential Drop Crack Length Detection Methods

Since metallic specimens are conductors with characteristic impedance, researchers have long been interested in measuring crack length through measuring the change in potential drop when a current is injected through a specimen. The ACPD measurement scheme is shown in Figure 2-20. An alternating current is passed through the specimen. The voltage is measured across the notch. As shown in the Figure, there are parasitic current paths that affect the measurement. These are mitigated somewhat by providing a current path through the guard resistors back to a summing amplifier in the LCR meter which subtracts the current passing through the parasitic paths from the

current that actually passes across the notch. A ground strap is connected across the load cell in order to protect it as much as possible from ACPD injected noise, and the load frame itself is connected to the ground of the LCR meter through a resistor in order to guard against potential differences that can lead to long settling times in the impedance readings.

Some researchers [Jablonski] have found that each specimen must be measured in an uncracked state in order to determine a parameter which then can be used in a standard calibration equation. The ACPD measurements were performed with a Hewlett Packard 4284A Precision LCR Meter which is capable of measuring impedance down to 0.01 milliohm at frequencies up to 1Mhz. Data from the HP4284 is available to the computer through a IEEE-488 interface bus.

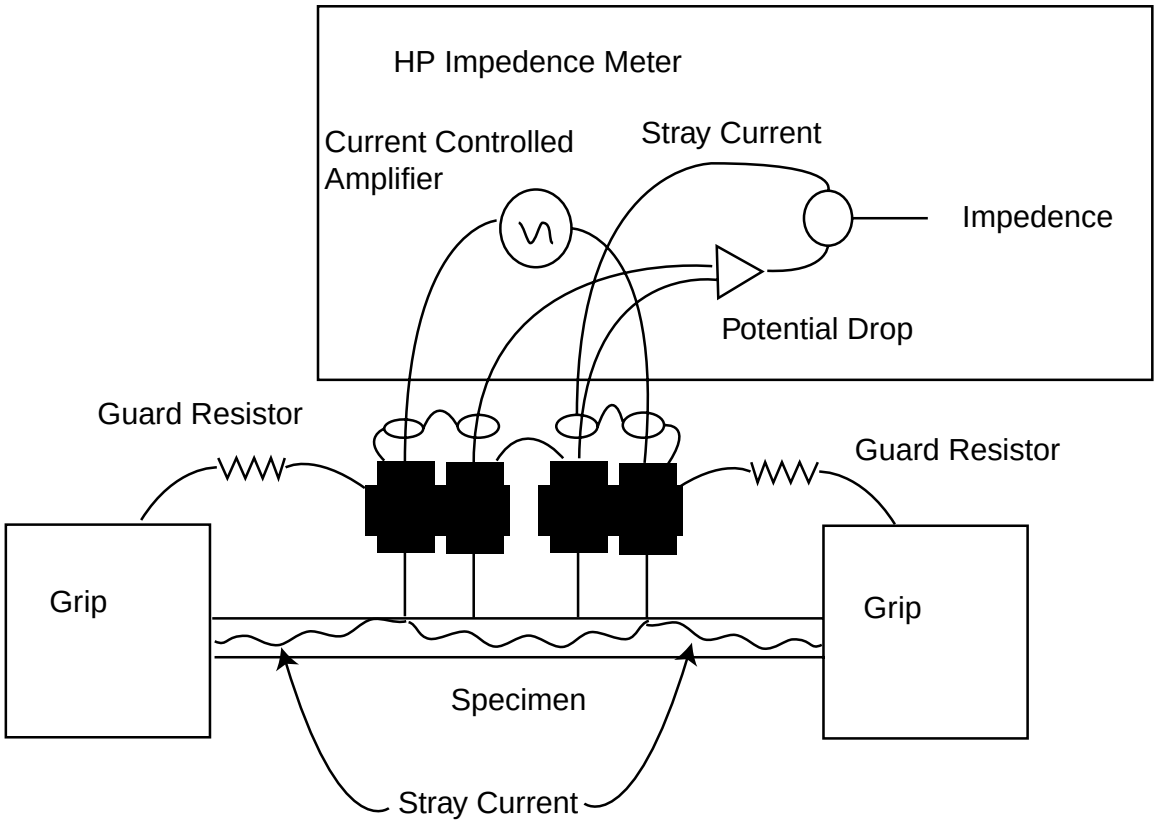

Figure 2-20 ACPD Measurement Setup

The high frequency signals used in ACPD cause the "skin effect," where most of the current flows in a small thickness near the surface of the specimen (Connolly,1995).

The skin thickness δis given by:

$$\delta = \frac{1}{\sqrt{\pi \mu \sigma f}} \tag{2.2}$$

where μ is the permeability of the material; σ is the electrical conductivity of the material; and f is the frequency of the signal in Hertz. For aluminum, $\mu = 1.26 \cdot 10^{-6}$ and $\sigma = 3.57 \cdot 10^{7} \left(\Omega^{-1} \cdot \mathrm{m}^{-1}\right)$, and thus the skin thickness is about 0.01in at 100khz and .003in at 1Mhz. Jablonski found that the relationships used by Connolly for materials that have thin skin thickness don't work for 1/8in thick plates of aluminum at frequencies up to 100kHz, however he found that there is a strong correlation between crack length and impedance. The author expended a considerable amount of effort in attempting to use ACPD for crack length measurements, but the results were not consistent enough to report here. Since the method is convenient for long crack length measurements, further development efforts may be fruitful.

2.3.1.3 Ultrasonic Flaw Detection

Ultrasonic flaw detectors are commonly used in the aerospace and nuclear power industries to detect flaws in structures, and have been used by many researchers for crack length measurement [Resch and Nelson]. The detector functions by emitting high frequency acoustic pulses and measuring the signal after it has had time to propagate through the material being measured. A flaw along the path of wave propagation will change the signature of the signal. Chapter 3 discusses the use of ultrasonic damage sensing in great detail.

2.3.1.4 Compliance Measurement

The compliance of a specimen is a function of crack length, so it is possible to use an extensometer to estimate crack length. The compliance of the specimen to be used in the work is given in Anderson as:

$$Z = Z_0 + \left(\frac{a}{W}\right)\left[-1.071 + 0.250\left(\frac{a}{W}\right) - 0.357\left(\frac{a}{W}\right)^2 + 0.121\left(\frac{a}{W}\right)^3 - 0.047\left(\frac{a}{W}\right)^4 + 0.008\left(\frac{a}{W}\right)^5 - \frac{1.071}{\left(\frac{a}{W}\right)}\ln\left(1-\left(\frac{a}{W}\right)\right)\right] \quad (4.2)$$

Where: $Z = \Delta \cdot Thickness \cdot E / Load$ is the generalized compliance,

$Z_0 = L / Width$ is the nominal generalized compliance,

Δ is the extension of the gage length,

W is the half-width

a is the half-crack length.

For experiments with sensors measuring localized strain, similar relationships can be computed using finite element methods. Compliance is clearly a more effective measure of crack growth for larger cracks. Work with fiber optic strain gauge measurement of crack length using compliance is underway at the time of this writing.

2.3.2 Distributed Real Time Damage Sensing System

The primary goal in developing the damage sensing system architecture was to build a robust, responsive, extensible system for sensor data collection and analysis. A distributed, networked system of computers and instruments meets these requirements extremely well. The advantage of having a pairing of instrument and computer is that software for each instrument can run unimpeded by the real-time requirements of other instruments. This is particularly important when commercial software for instrumentation operation is required. Only rarely is such software written with interoperability between instruments being a primary design goal. While it is possible to drive multiple instruments with one computer, this drives up the complexity of the software considerably. Considering that an average instrument costs at least 10 times the cost of a very capable computer, this arrangement makes good economic sense. A particular advantage accrues when instruments are added or removed from the system. If one computer is driving multiple instruments, the software on that computer must either

be rewritten or written in such a way as to be easily re-configurable. Either case adds considerably to the software effort.

2.3.2.1 Software Organization

The instrumentation system has a networked, client-server structure, with all real-time requirements isolated on the client (instrument) side of the network connection. Each instrument has a client program and a server program. The client program triggers the instrument to take measurements synchronized with the load cycle, does initial processing, and sends the results to the server program. The server program saves data as desired for post-test analysis, performs any required further processing and stores the results in a memory-mapped file. The analysis program also opens these memory-mapped files.

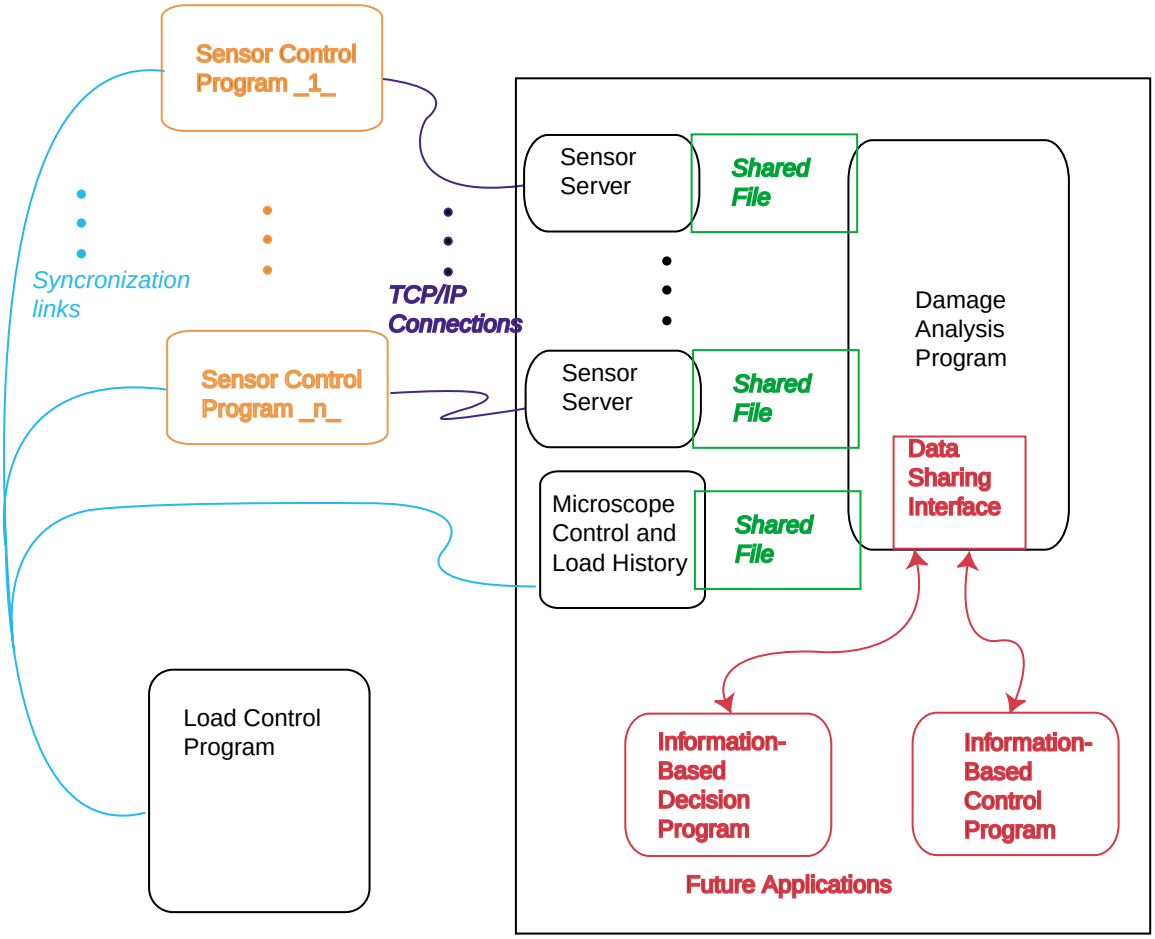

Figure 2-21 Software organization

2.3.2.2 Sensor Control Program Operation

The sensor control programs consist of a user interface and one or more threads. The user interface code for these programs is very simple, allowing the operator to set up the instrument and start taking data and also indicating the status of the communications link. In the general case, there can be three threads: the supervisor thread, the sensor thread, and the communication thread. The supervisor thread initializes itself, launches all of the other threads and then waits for communication from the load frame control computer over the serial port. Each sensor thread initializes its sensor and waits for an event to signal that a reading should be made with the sensor. The role of the supervisor thread is to parse incoming messages from the load frame controller. The load frame controller sends out 8 byte packets of data that include cycle number, load, strain, and a code that indicates the reason for the packet. The 8-byte length allows for quick response by the receiving computers, because the serial port hardware used on PC compatible computers can be programmed to generate an interrupt after the receipt of 8 bytes. If the incoming message signals that a sensor should be triggered, the supervisor thread checks to see if the sensor thread is busy. If it is busy, the supervisor thread simply skips the measurement for that load cycle. If the sensor is not busy, the supervisor thread sets up storage for a new measurement, sets an event to trigger the sensor thread, and waits for more input. There is code in the supervisor thread to recover from communications errors. The supervisor thread also triggers the communications thread to send sensor readings to the server, either after each reading or after a number of readings.

Chapter 3

Ultrasonic Damage Sensing

In structures made of ductile alloys that are subject to fatigue failures, a large part of the service life is spent in crack initiation and in the presence of very small cracks. The overriding goal of this research is to have knowledge of damage state for as much of the life of the structure as possible, and not simply to know when the life of the structure is used up. Thus, for this work, small crack detection and sizing is of primary importance. There are very few flaw sizing methods that will work with flaws that are as small as the microstructural elements of ductile metals or even extremely small cracks. There are fewer still that are suitable for installations outside of the laboratory. Ultrasonic flaw detection meets the requirements of real time damage sensing on structures in service, although to date it is uncommon or possibly has not been done. Ultrasonic flaw detectors are commonly used in the aerospace and nuclear power industries to detect flaws in structures, and have been used by many researchers for laboratory crack length measurement [Resch and Nelson].

3.1 Ultrasonic Flaw Detection

The detector functions by emitting high frequency acoustic pulses and measuring the signal after it has had time to propagate through the material being measured. Material features such as the grains boundaries, inclusions, stress state, voids, or cracks along the path of the wave will affect the propagation of the signal. A piezo-electric crystal is used to inject the acoustic waves into the specimen and array of crystals are in position across the crack plane to measure the signal. Any flaw or other discontinuity in material properties along the wave path will cause a reflection of energy back towards the wave source, and will also disturb the signal seen by a transducer on the other side of the flaw from the source. As with the propagation of any wave, it is possible that discontinuities in the propagation media will cause additive and destructive interference. Attenuation was chosen rather than reflection to avoid the issues of detecting a small

signal in noise [De Belleval and Gherbezza, 1994]. However, the analysis of attenuation poses the problem of small change detection in noisy signals [Szilard, 1982].

Two different ultrasonic flaw detectors were used in this experiment. While the experimental setup is described in more detail in the next section, this section covers the measurement techniques used. The signals used for the initial testing consist of a spike pulse which is modulated by the transducers into a band limited signal which contains frequencies from 400khz to 10Mhz. The second system uses a gated sine wave signal. For the purposes of this experiment, these systems are roughly equivalent. Both systems emit a signal for a very short portion of the measurement cycle. This allows for the attenuation of any standing waves that might otherwise develop in the test article. The wedges used for the transducers in this test are of a high enough angle that the signal will take multiple paths through the test article and reach the pickup transducers. The signal that reaches the transducer is then a characteristic pulse of some duration that must somehow be processed in order to be correlated to the corresponding crack length. Considering each measurement pulse as a vector, this suggests using a vector norm as a measurement of crack length. The most commonly used norm used with a multi-frequency pulse is the maximum value of the pulse. Two other useful norms for this application are the sum of the absolute values of the elements of the vector and the square root of the sum of the squares of the elements of the vector. Another method is to take the inner product of the pulse with a reference pulse, although this has the problem of not being equivalent to a norm, but in the case of rectified signals it has a larger range of crack size measurement.

Most of the results reported here were measured with a Krautkramer-Branson USN-52 system that is designed for production inspection applications. The system as used in this testing is shown in Figure 3-1. The USN-52 generates a pulse, which drives the single 5Mhz piezo transducer. The signal propagates through the specimen and impinges on the array of transducers on the other side of the notch. The transducer array is connected to a crosspoint switch, which is controlled by an external computer using its parallel ports. The output of the crosspoint switch is sent to the USN-52, which processes the data and sends it over a serial link to the computer controlling the crosspoint switch. This computer further processes the data and then sends the data over

a TCP/IP network connection to the main computer. A major disadvantage of this system is that it can only deliver 3 readings per minute, and these readings are not synchronized with the specimen loading. The other complicating factor for this system is that the pickup transducer is an array of 16 crystals. The initial notion was that the crack shadow would obscure each transducer element in turn, and that the signal from each transducer would diminish to zero strength when it was fully shielded from the sending transducer. This may well be the case with higher frequency signals, but it became clear in use that the interaction of the acoustic wave with the crack is much more complex than this. For example, the signal strength from all transducers in the array reach zero at approximately the same crack size. Due to this complexity it became clear that the requirement to scan 16 transducers obscures more information than it reveals, due to the reduced amount of data available. The upshot of this analysis was that the most reasonable course was to average the energy of the 8 transducers on each side of the crack. This becomes a good measure of the crack length on the associated side of the specimen. Because of this experience, the second system only has one emitting transducer and 2 receiving transducers, one for each side of the notch.

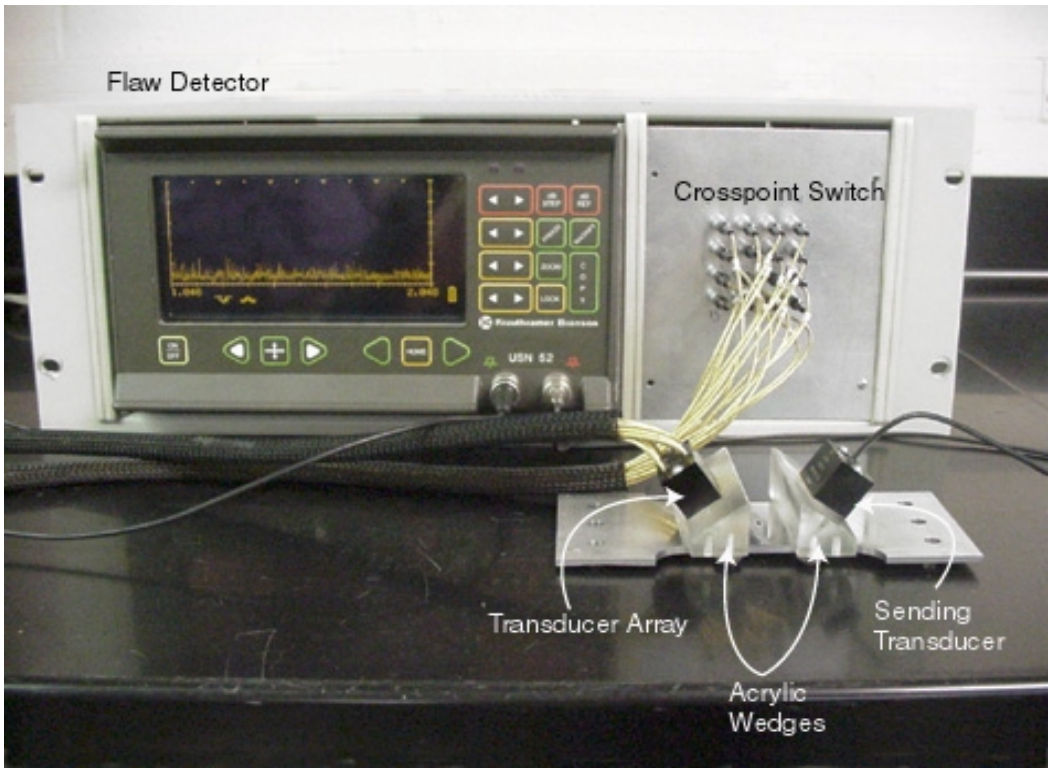

Figure 3-1 Ultrasonic flaw measuring system

Figure 3.2 shows the signal received on an un-cracked specimen of 6061-T6 aluminum. This signal is not rectified which is superior from the point of view of analysis, but due to the design of the USN-52, the only half as many measurements can be performed in the same amount of time. Since the norm of the rectified signal and the un-rectified signal is the same, the rectified signal is used for most of these experiments. A rectified signal for an un-cracked specimen of 7075-T6 aluminum is seen in Figure 3.2. The notation Sk. 6 identifies the specimens donated by Sikorsky. In these figures the pulse is seen as repeating multiple times. This represents the effect of different transmission modes the signal takes through the specimen [Langenberg, et. al.]. Figure 3.3 represents the evolution of the ultrasonic signal over the duration of an experiment. This is the result of the same experiment and transducer as Figure 3.7. The vertical axis is signal strength, the axis along the front of the figure is the time duration of the pulse and the axis coming out of the paper is cycles.

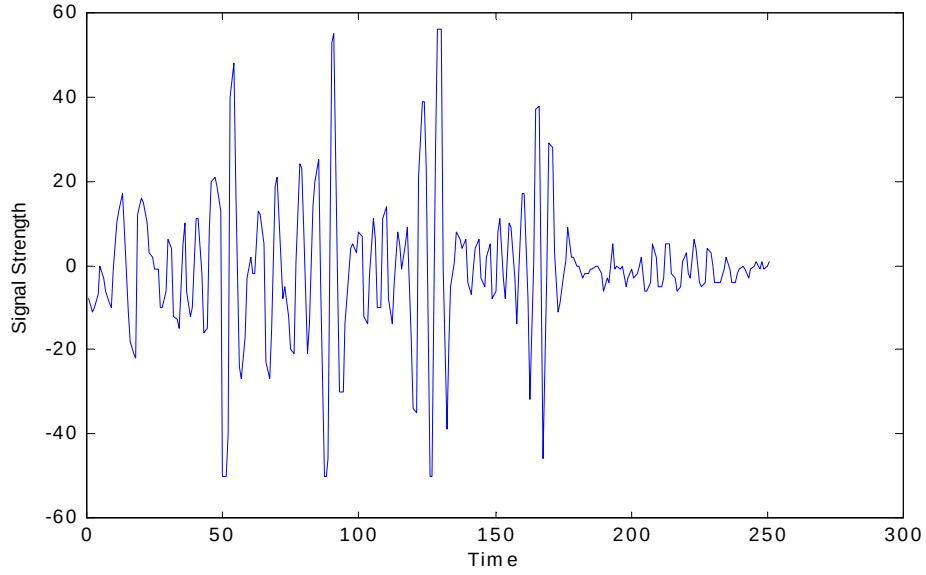

Figure 3-2 Ultrasonic signal 6061-T6 Specimen 20, Cycle 1

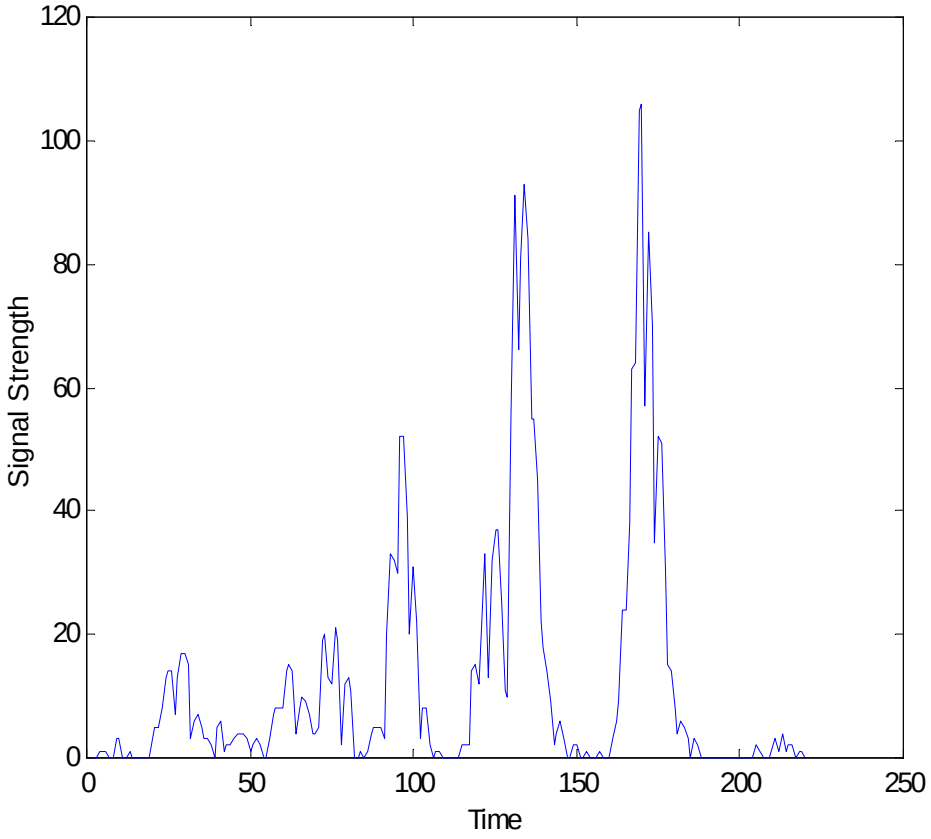

Figure 3-3 Rectified ultrasonic signal 7075-T6 Specimen Sk. 6, Cycle 1

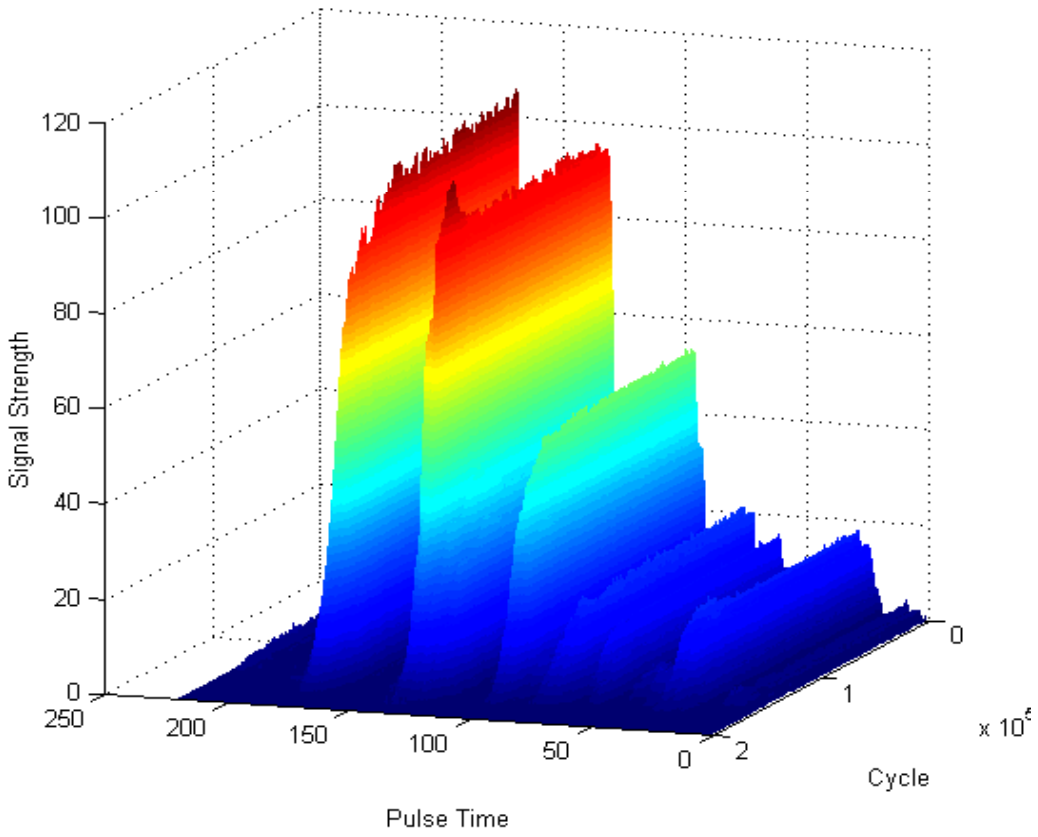

Figure 3-4 Ultrasonic signal 7075-T6 Specimen Sk. 6

3.1 Ultrasonic Crack Length Measurement for 7075-T6

The results in this section were obtained using the Krautkramer-Branson USN-52 flaw detection system. As previously discussed, this it is not possible to synchronize this instrument to the load. Three methods or norms were used to analyze the ultrasonic signals: energy, inner product of each signal with a reference signal, and the peak value from a given reading. As seen in the processed data in Figures 3-5, 3-6, and 3-7, not only are these signals noisy, but it is also possible to see that there are two levels of signal being measured. The least noisy signal comes from the peak value or L_∞ norm. It is possible to see some of the complexity of these results due to the array of sensors. In particular, the signal energy level of channel 4 increases dramatically just as the energy

of the other channels starts to decrease significantly. This behavior is seen whenever the two sides do not crack at the same time. Averaging the energy on each side of the notch generally removes these effects. However, one larger sensor on each side of the notch is a preferable approach, because of the added expense of an array. Furthermore, much of the signal processing can be simplified when the measurements are synchronized with the loading.

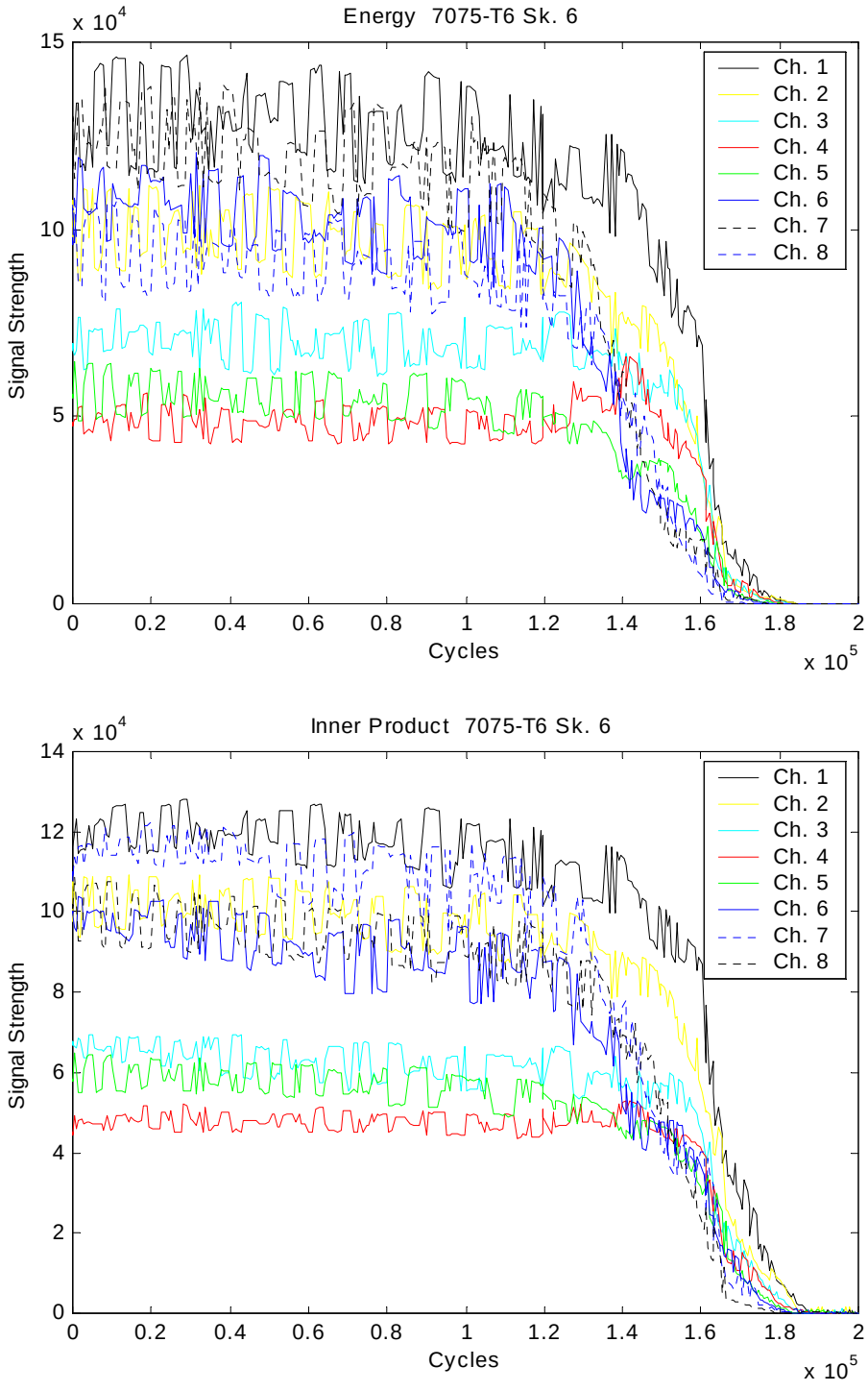

Figure 3-5 Energy and inner product with reference for channels 1-8, 7075-T6 specimen Sk. 6

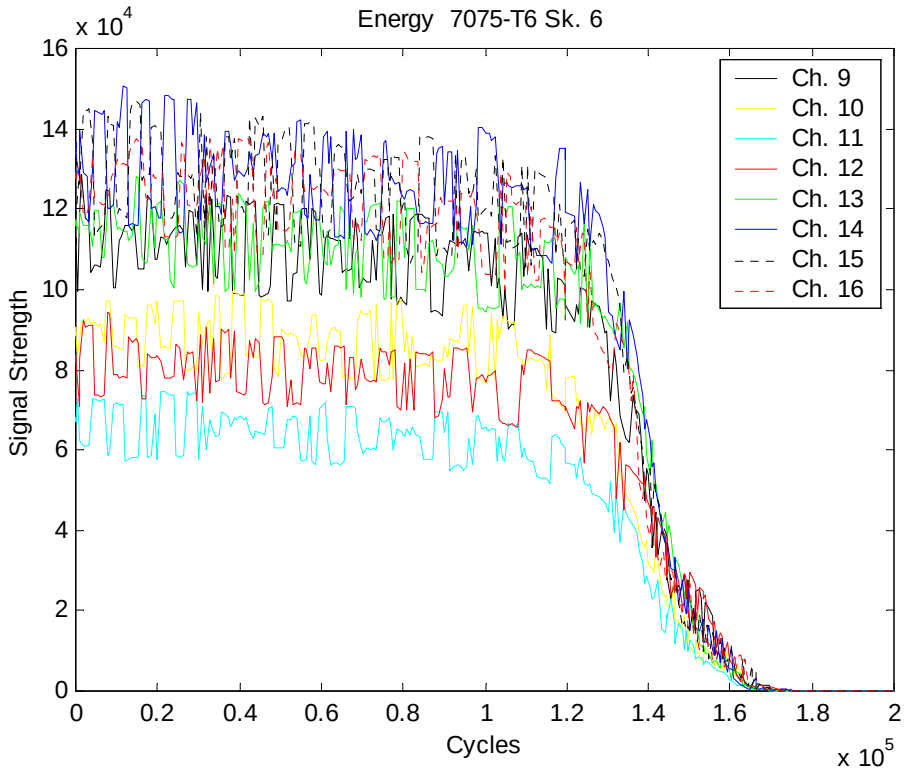

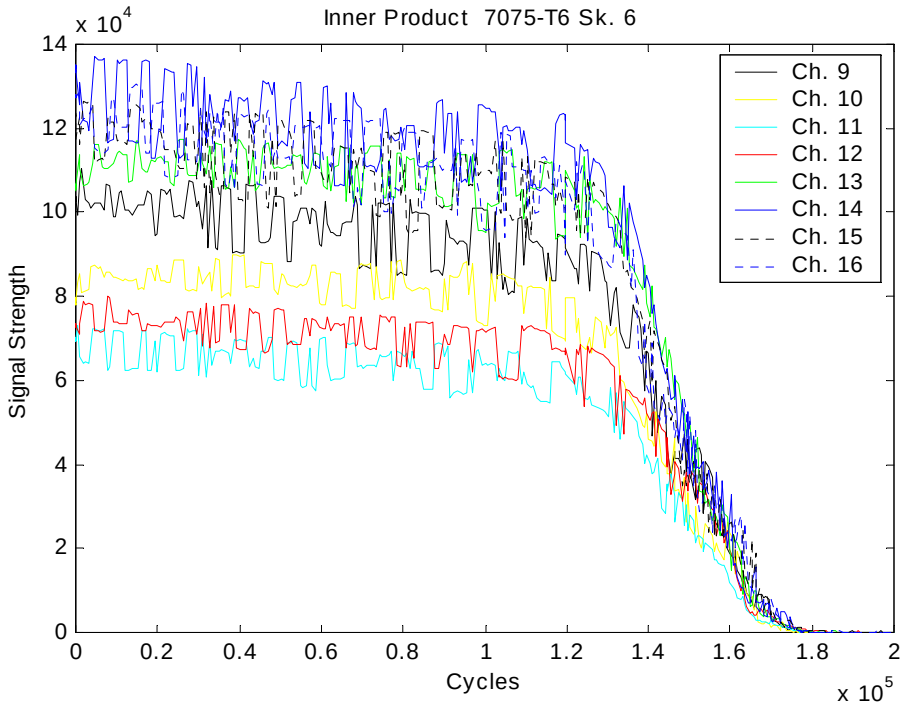

Figure 3-6 Energy and inner product with reference for channels 9-16, 7075-T6 specimen Sk. 6

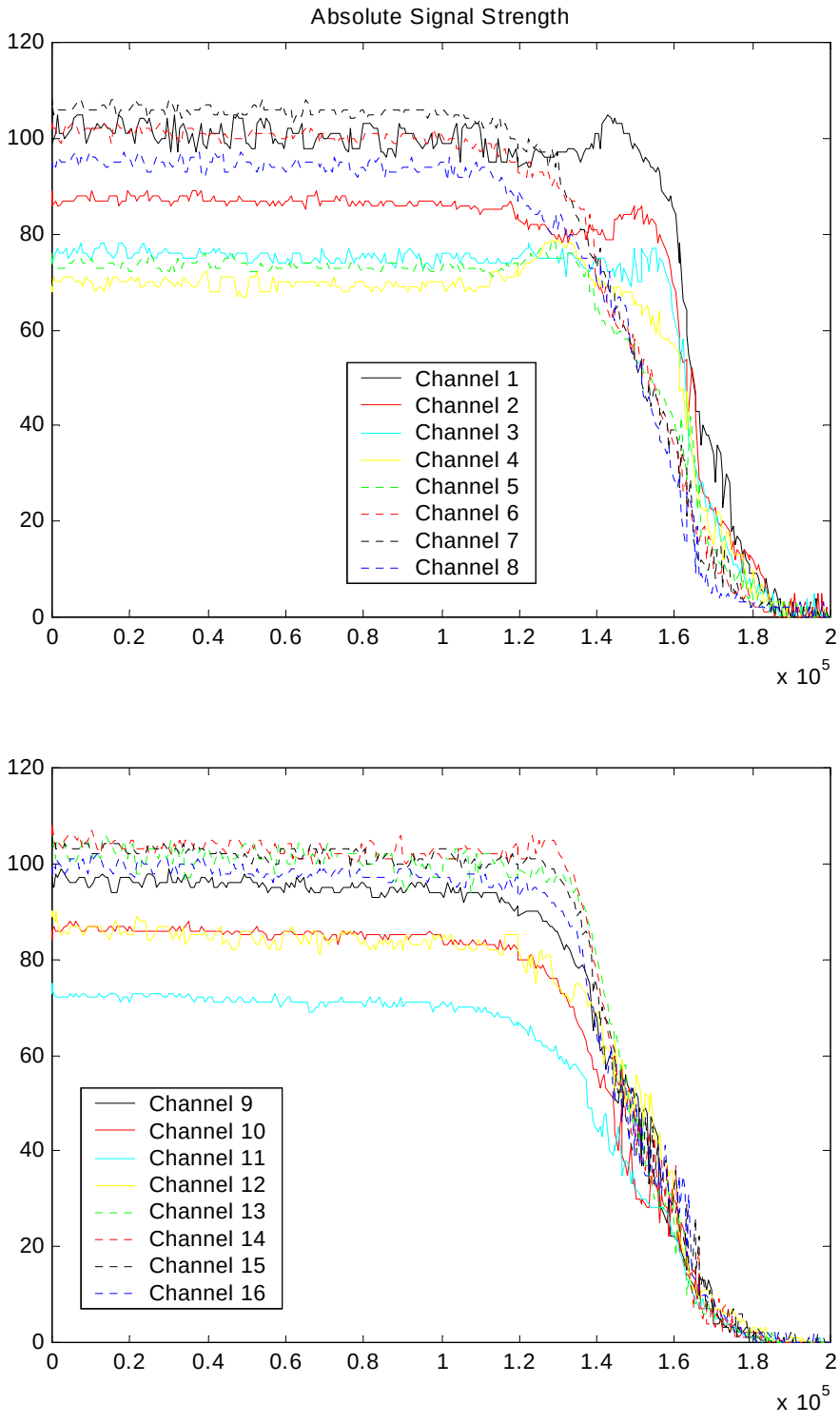

Figure 3-7 Peak value of ultrasonic signal Specimen Sk. 6

The approach taken here to reduce the data shown in Figures 3-5, 3-6, and 3-7 is to calculate a signal attenuation from the initial signal. This approach is self-calibrating because the absolute signal level is not used in the analysis. The first step was to take each new measurement on a given channel and then add the most recent measurements from the other channels to generate the signal for each side of the notch at a given. The result was filtered using the Matlab function, ***filtfilt***, which provides zero-phase high order filtering of the signal. After this step, the maximum signal level was obtained. The microscope measurements of crack length were processed to fit on the same scale as the ultrasonic attenuation by taking the crack length from the edge of the notch and scaling it. The scaling factor was chosen so that the average microscope measurement crossed the 100% attenuation line approximately at the same place as the ultrasonic signal reached 100% attenuation.

The signals presented in this section were measured using the full wave rectification mode of the USN-52. Thus, using an inner product of the signal with a reference signal is analogous to using the energy of the signal. However, there are advantages to using the inner product method, because the signal emphasizes longer crack lengths to a greater degree than the energy measurement. For the work in the following sections, the peak value or L_∞ norm measurement was used because it matches the microscope crack measurements the closest as can be seen in Figure 3-8 through Figure 3-14. On all of the specimens, surface cracking was observed within 10,000 cycles from the initiation of testing. The testing on these specimens was with block loading. After cracks had initiated on both sides of the notch, the load was decreased 3 times in blocks of 15000 cycles each, and then the load was returned to its initial value. This leads to the unusual looking crack growth rates seen on some specimens, particularly specimens Sk. 9 in Figure 3-13 and Sk. 10 in Figure 3-14.

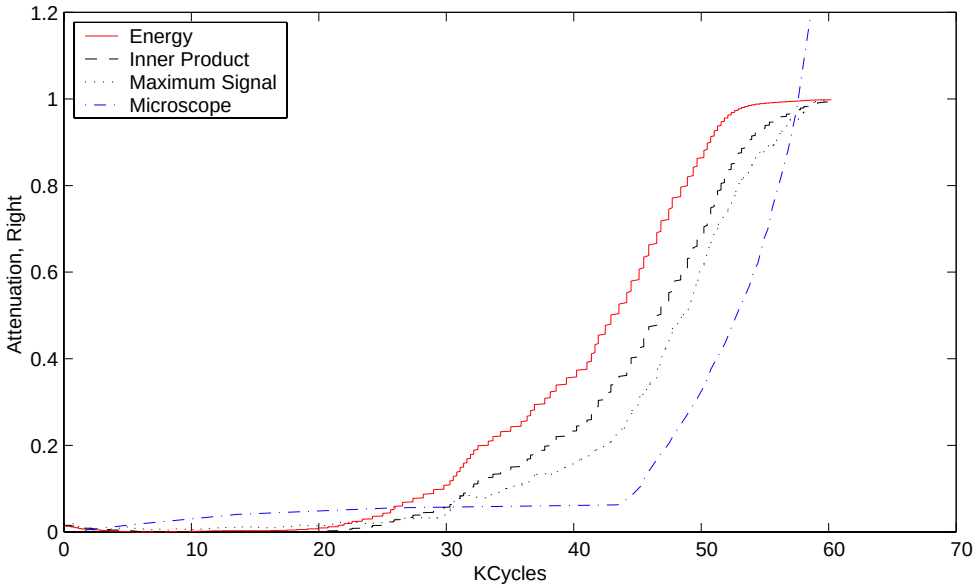

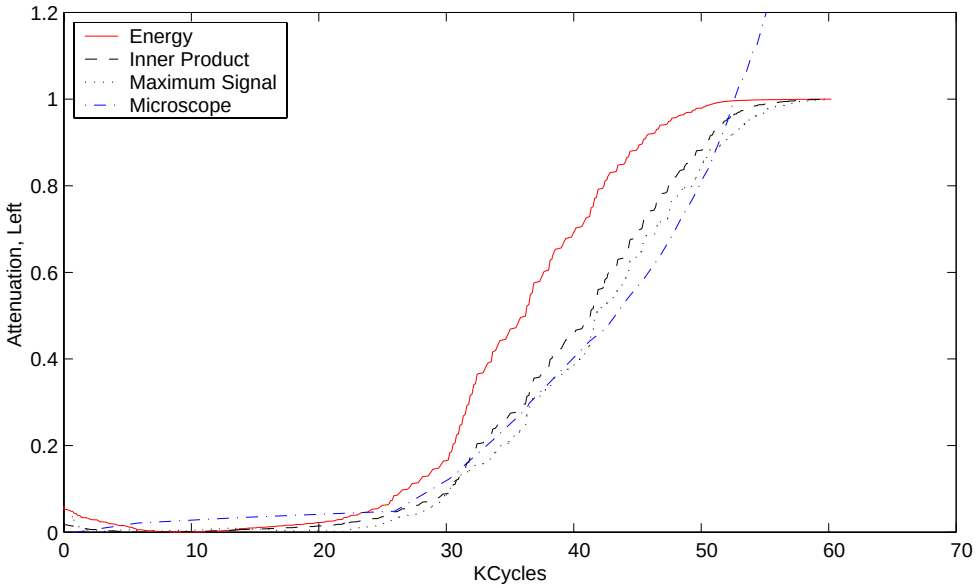

Figure 3-8 Ultrasonic attenuation vs. microscope crack length, Specimen Sk. 4

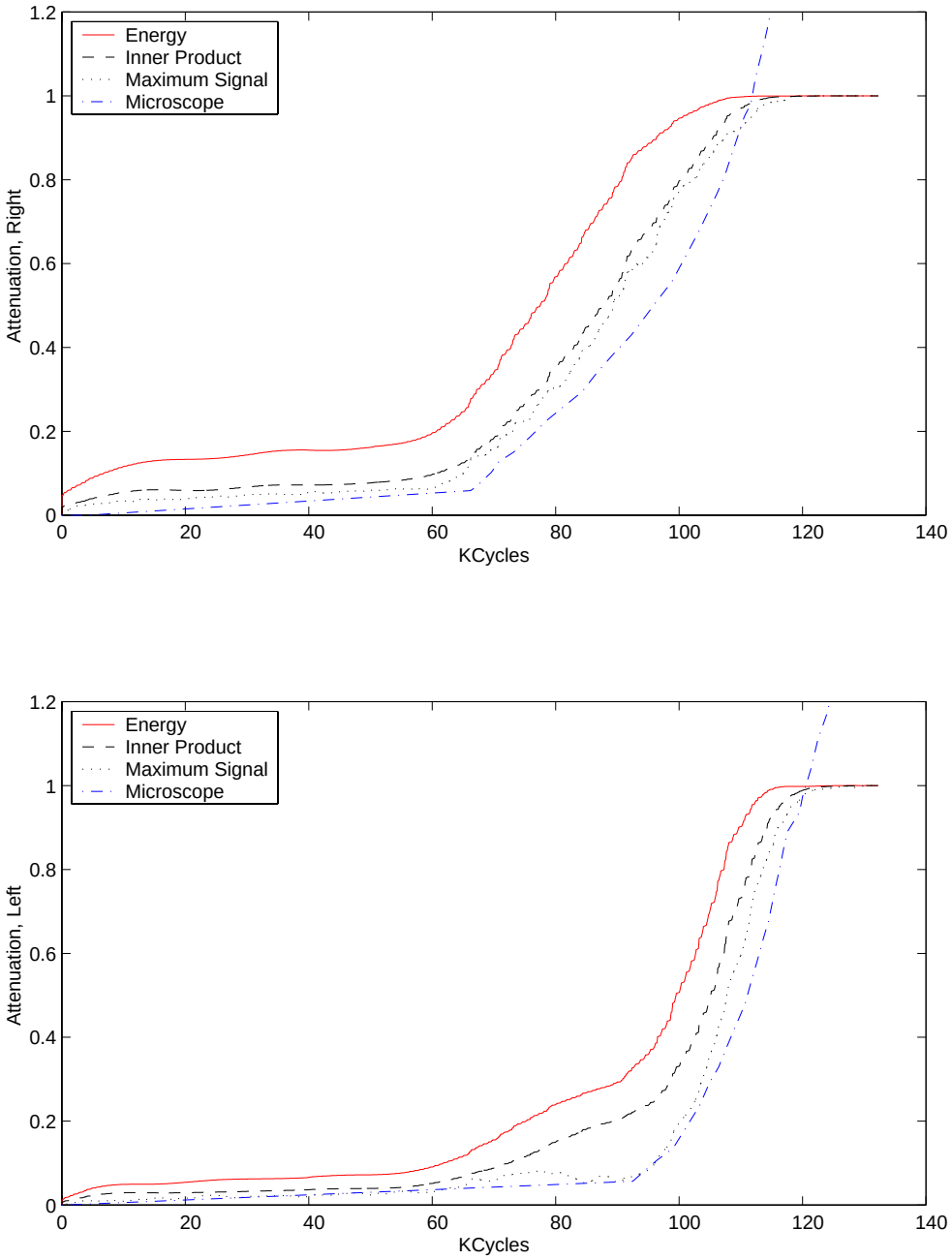

Figure 3-9 Ultrasonic attenuation vs. microscope observations specimen Sk. 5

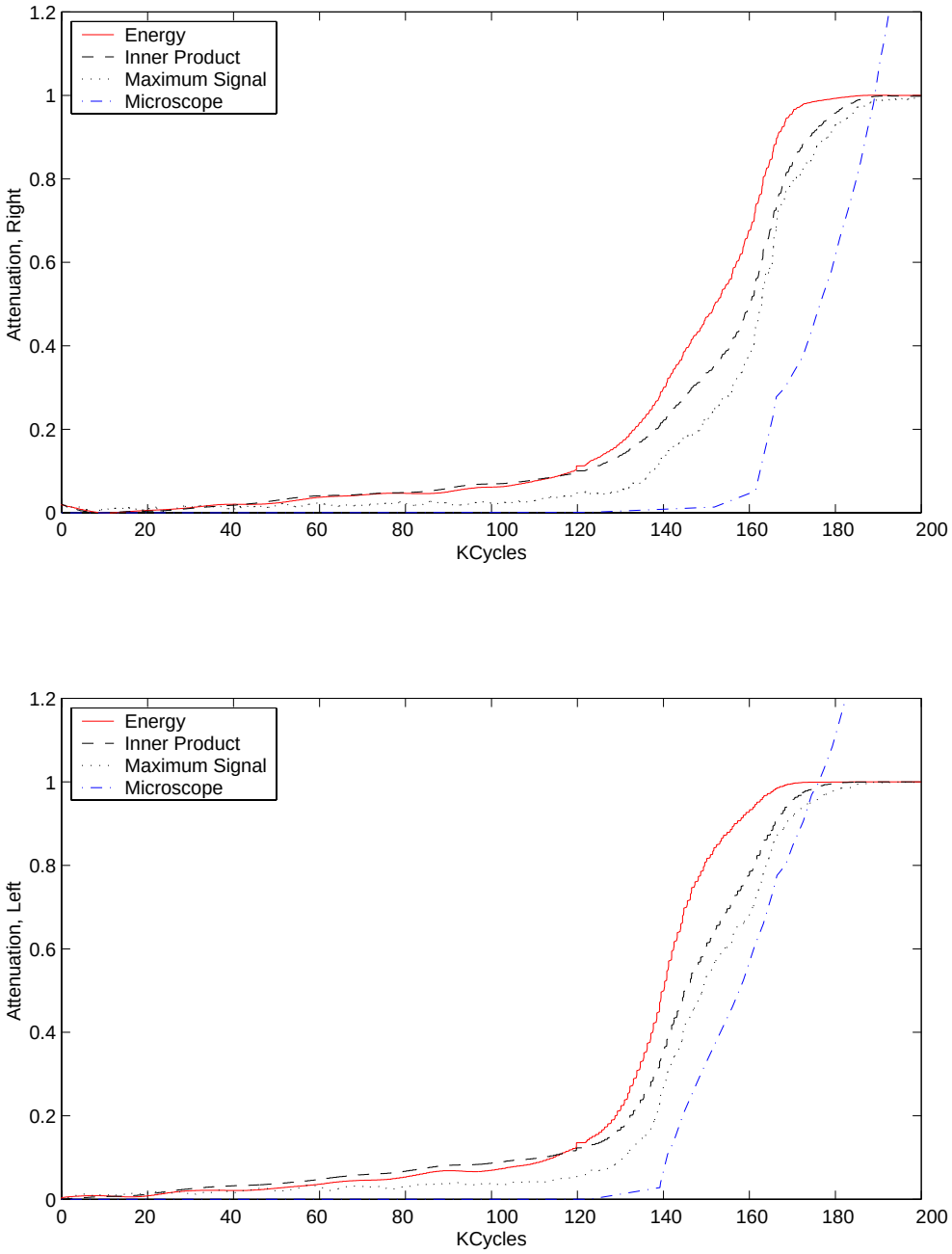

Figure 3-10 Ultrasonic attenuation vs. microscope observations specimen Sk. 6

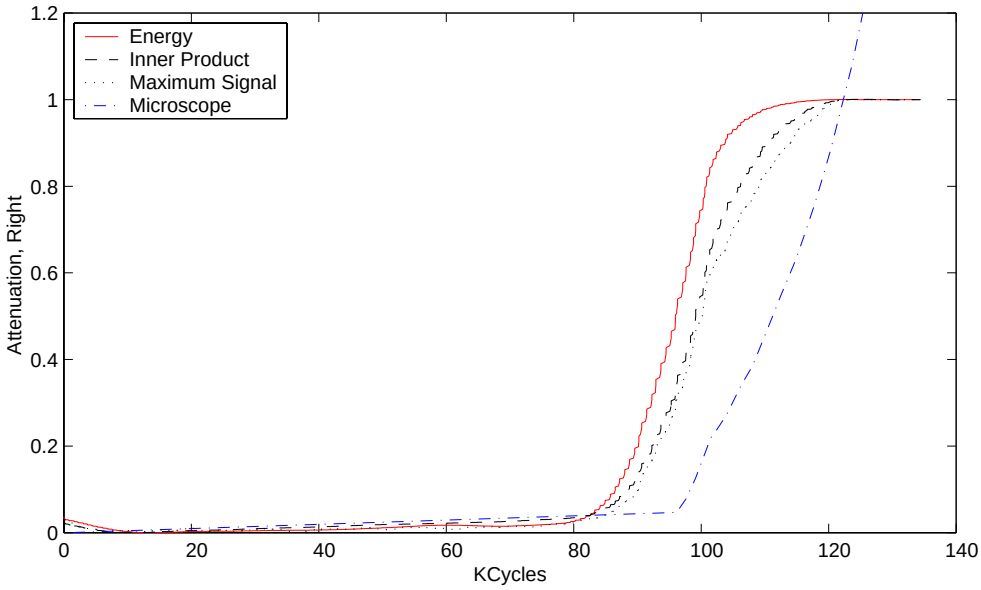

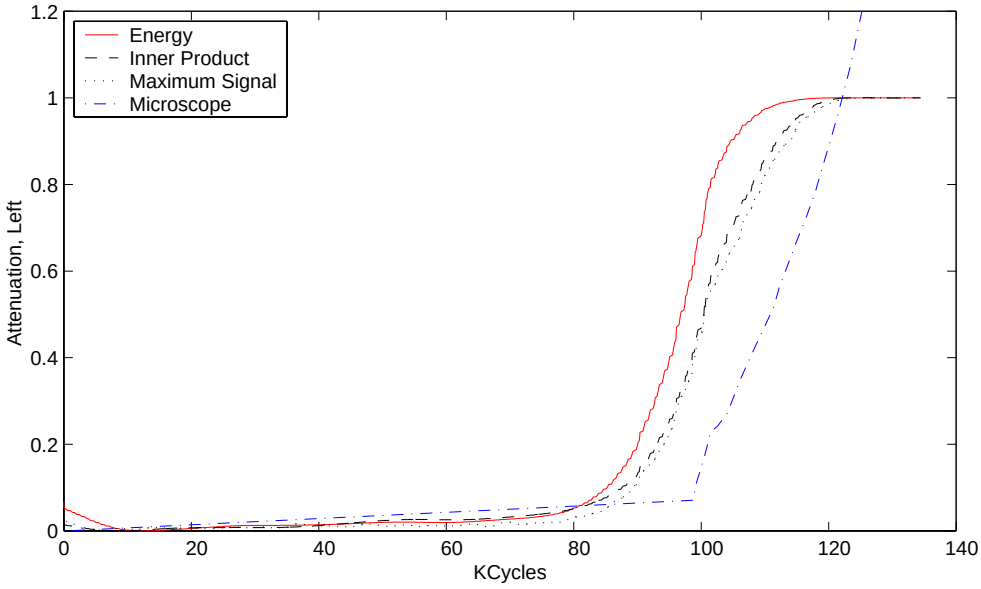

Figure 3-11 Ultrasonic attenuation vs. microscope observations specimen Sk. 7

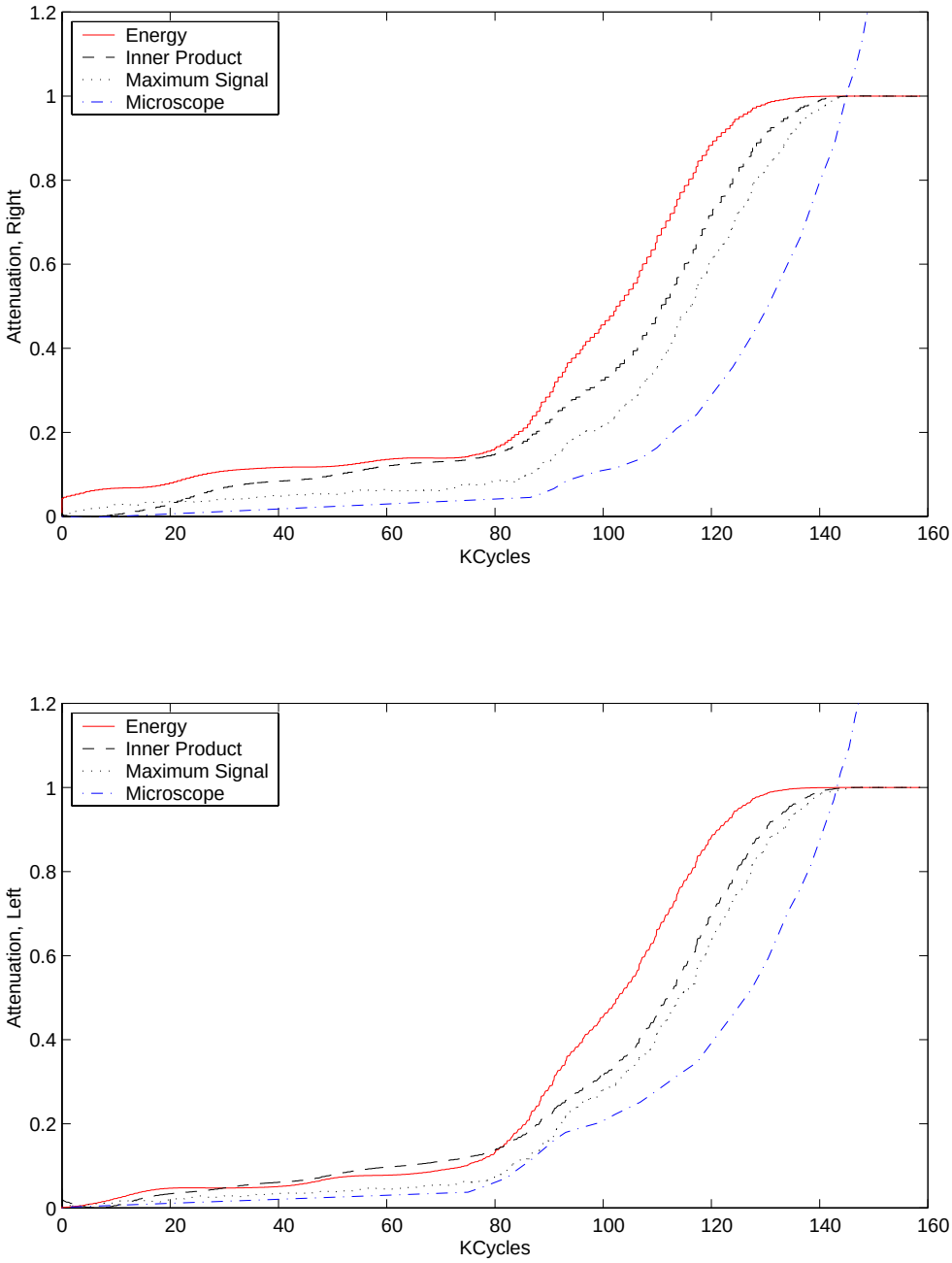

Figure 3-12 Ultrasonic attenuation vs. microscope observations specimen Sk. 8

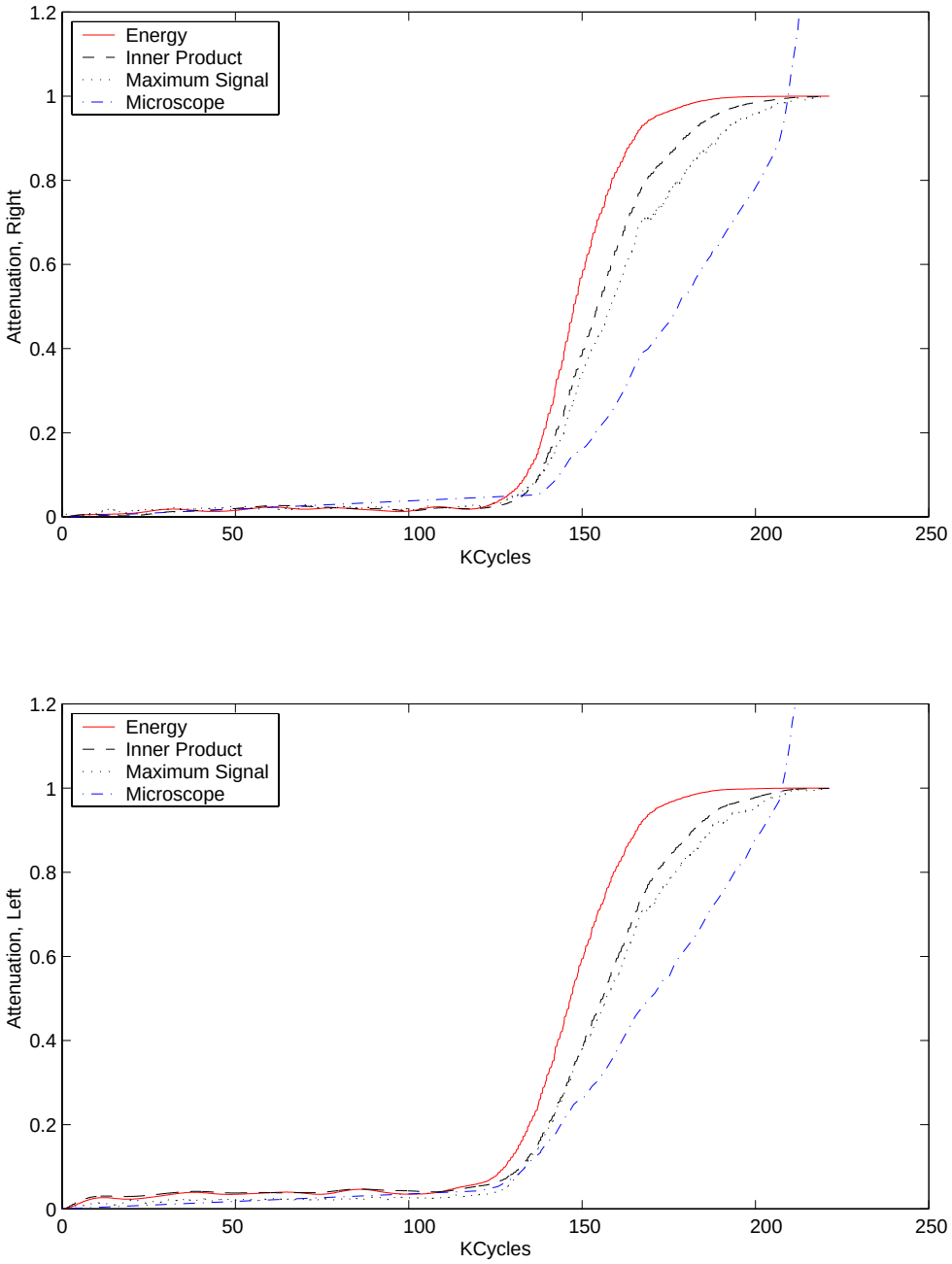

Figure 3-13 Ultrasonic attenuation vs. microscope observations specimen Sk. 9

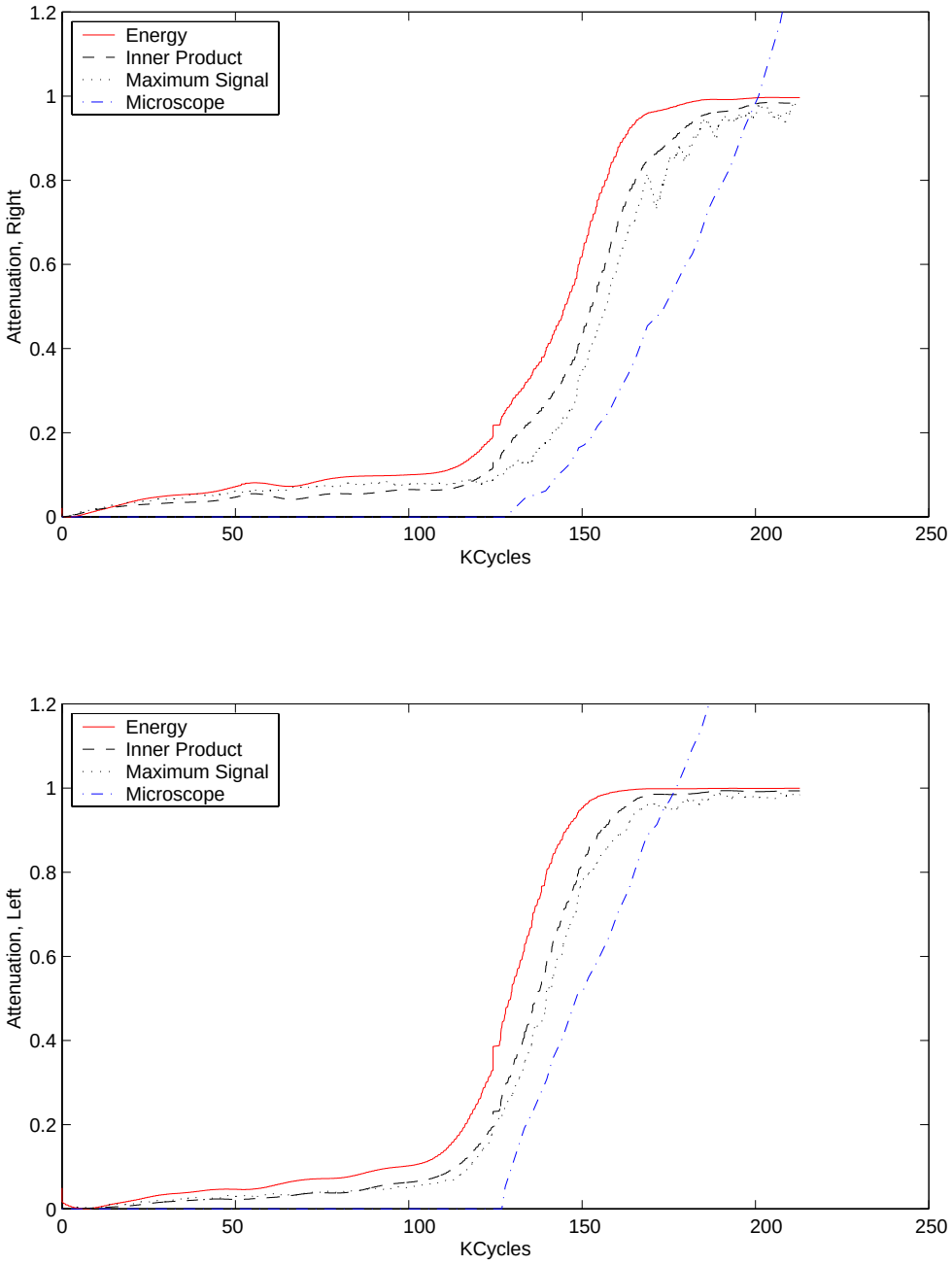

Figure 3-14 Ultrasonic attenuation vs. microscope observations specimen Sk. 10

Figures 3-8 to 3-14 show a comparison of ultrasonic measurements and scaled crack length measurements. In order to use the ultrasonic instrument for crack length measurements, a 5th order polynomial calibration curve was generated using least squares fit of the maximum signal value to crack length.

$$c_u = \alpha_5 u^5 + \alpha_4 u^4 + \alpha_3 u^3 + \alpha_2 u^2 + \alpha_1 u^1 + \alpha_0 + c_0$$

where u is the ultrasonic attenuation, c_u is the ultrasonic measurement of crack length, and c_0 is ½ the notch width. The coefficients of this equation are:

α_0=0.0191, α_1=0.8615, α_2=-3.1553, α_3=9.3721, α_4=-11.6545, α_5=5.5743

This calibration curve, derived from the results shown in Figure 3-8 to Figure 3-14, is shown in Figure 3-15. Lower order polynomials did not properly capture the desired behavior for small attenuation. The polynomial structure of the calibration curve is not unique as there exist other mathematical forms that would fit the data. For example, the orthogonal functions such as Legendre polynomials or transcendental functions could also be used. This is a subject of future research with a trade-off between accuracy and computational speed fro real-time measurements. As shown in Figures 3-16 to 3-22, this calibration yields excellent agreement with the microscope data. It must be noted that the ultrasonic instrument may be more accurate than optical microscopy in measuring the condition of the specimen, since the microscope can only capture the condition on one face of the specimen and the ultrasonic measurements are affected by the cross section of the crack. This is particularly the case when the crack is small, because then the 2-D geometry of the crack is the least well represented by a measurement on the surface. The other consideration while using the microscope is that it is possible for the two sides to have a constant bias in length. It is likely that the calibration curve could be improved with better knowledge of crack configuration when the cracks are very small. Figures 3-16 through 3-22 show a comparison of microscope crack length measurements with the ultrasonic crack length measurements. The agreement is good for most specimens for attenuation up to about 80%. One item to note is shown in Figure 3-17 on the left ultrasonic measurement (red trace) from 60-90 kilocycles. The excursion in the data that is shown there is due to the interaction between the ultrasonic waves as the right side of

the notch develops a crack and the left is not yet cracked. In practice, this is of little concern, since the most important point is that a crack has developed at the notch.

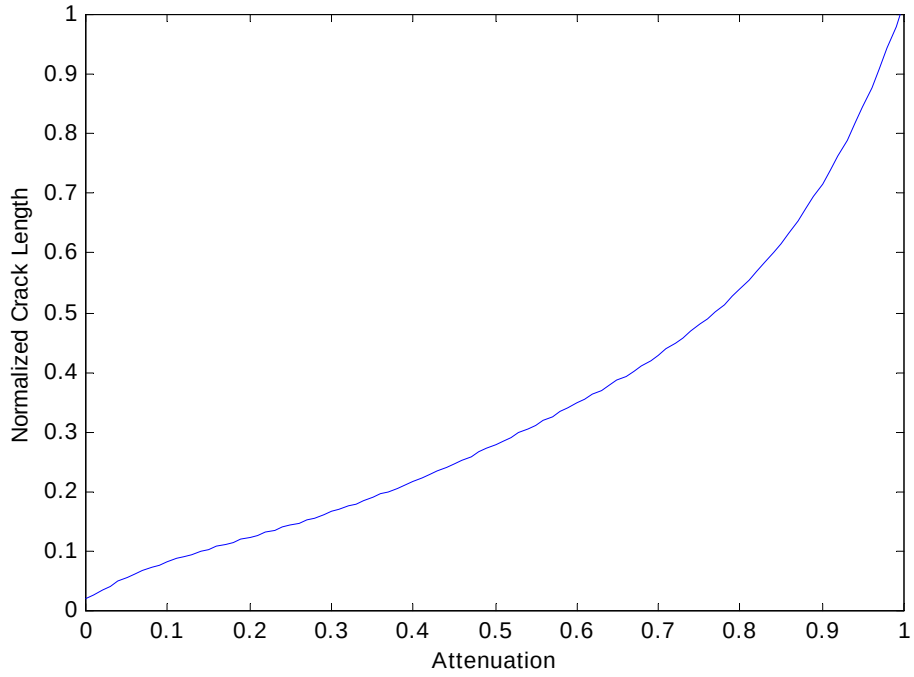

Figure 3-15 Calibration curve of crack length to attenuation

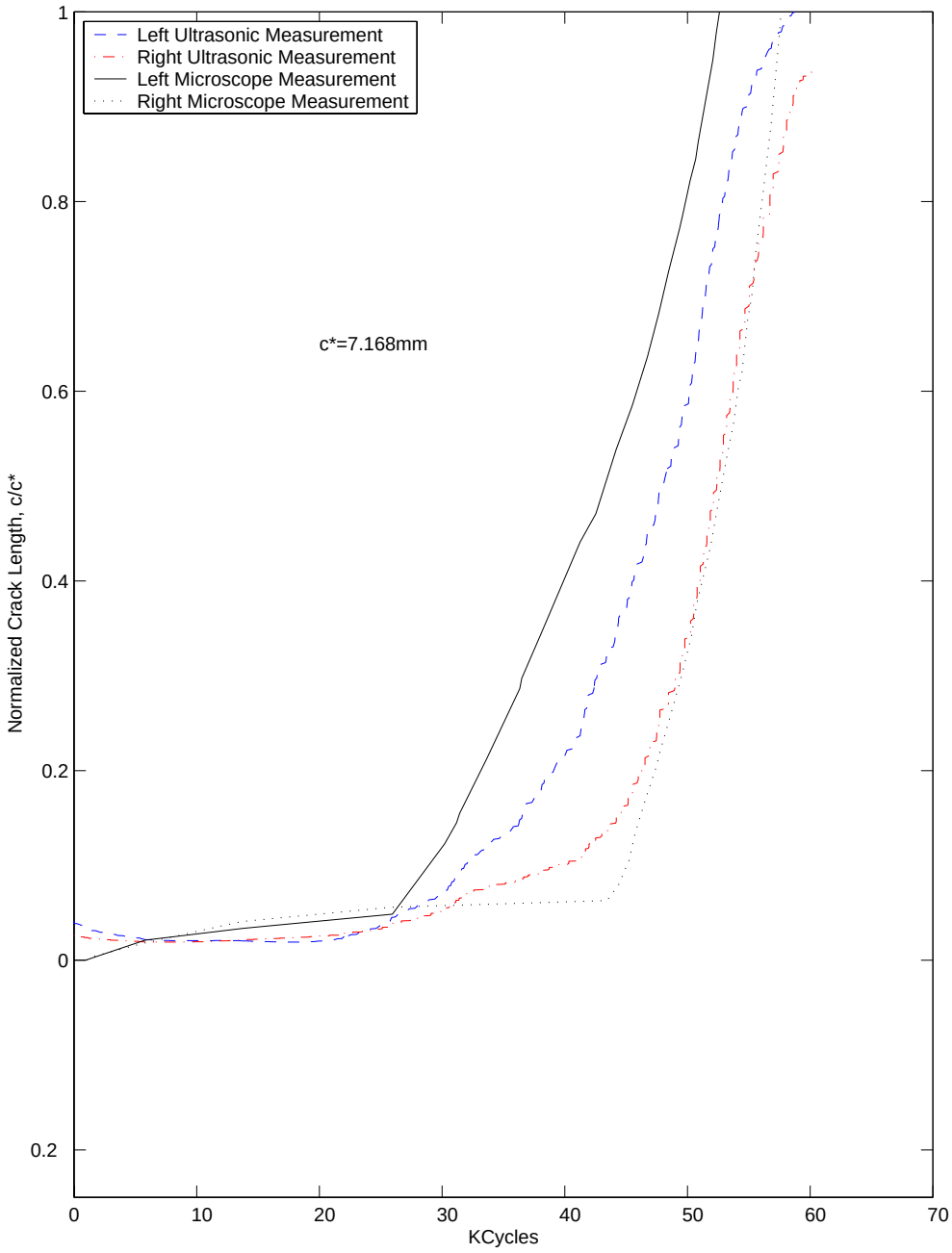

Figure 3-16 Ultrasonic vs. microscope measurements of crack length, specimen Sk. 4

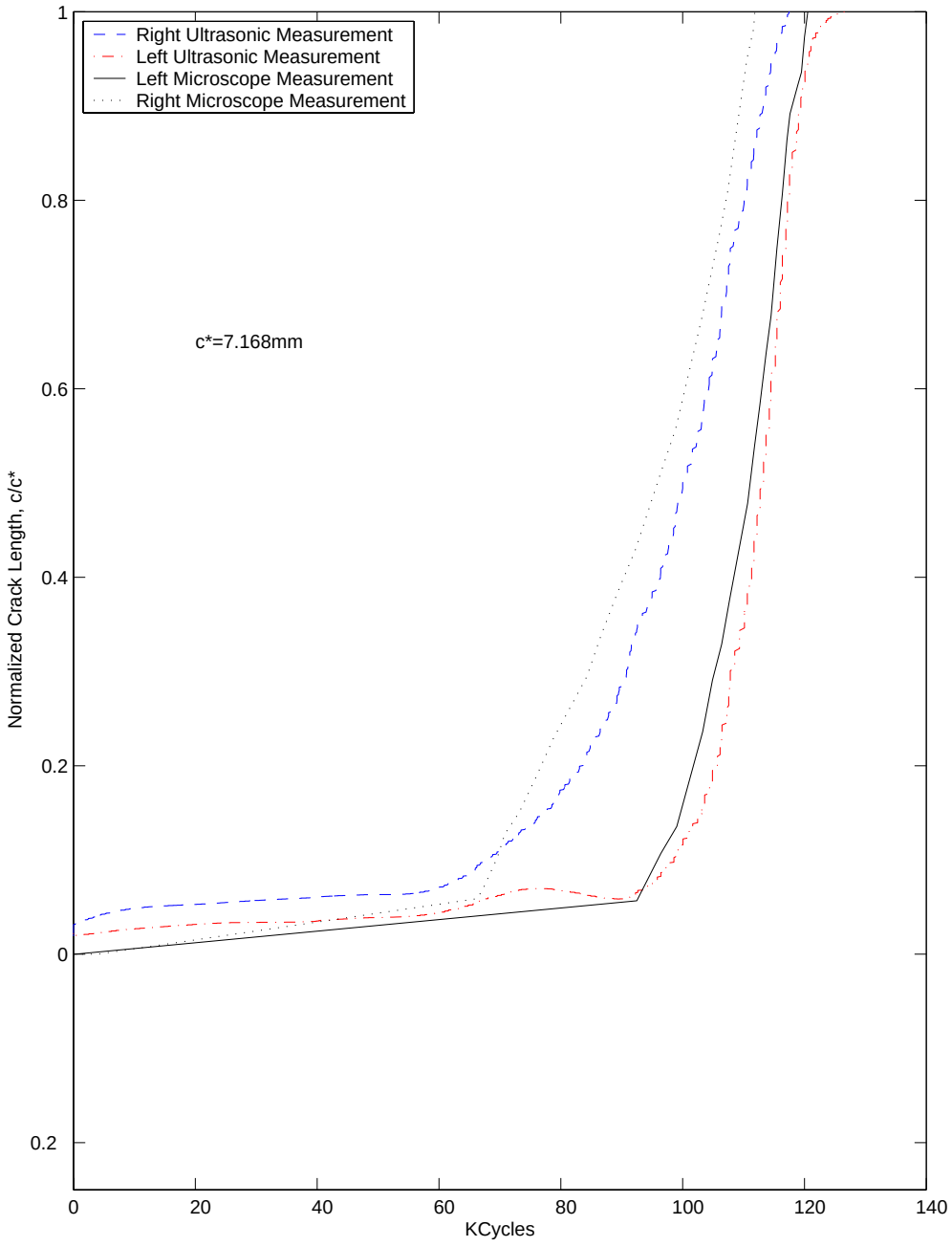

Figure 3-17 Ultrasonic vs. microscope measurements of crack length, specimen Sk. 5

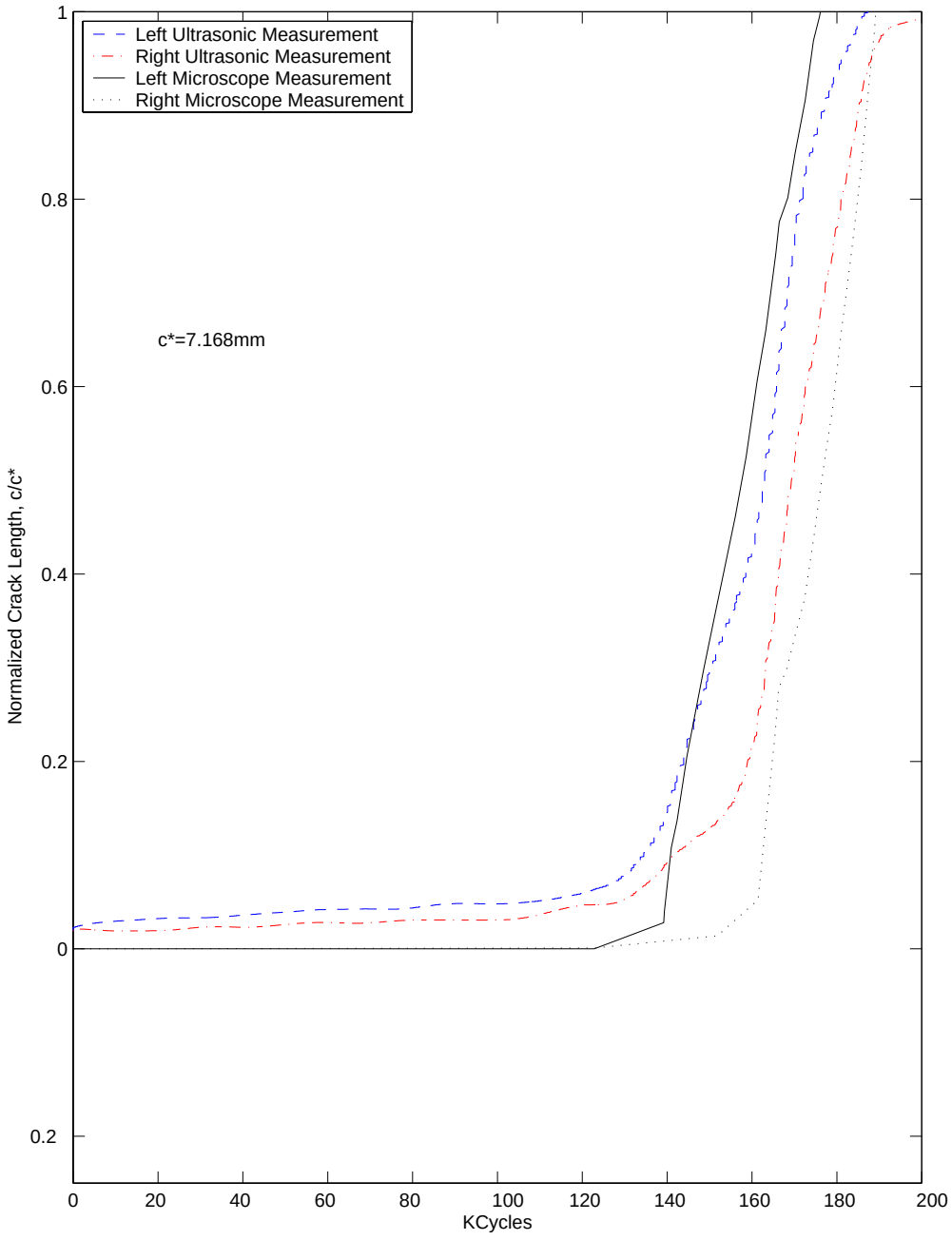

Figure 3-18 Ultrasonic vs. microscope measurements of crack length, specimen Sk. 6

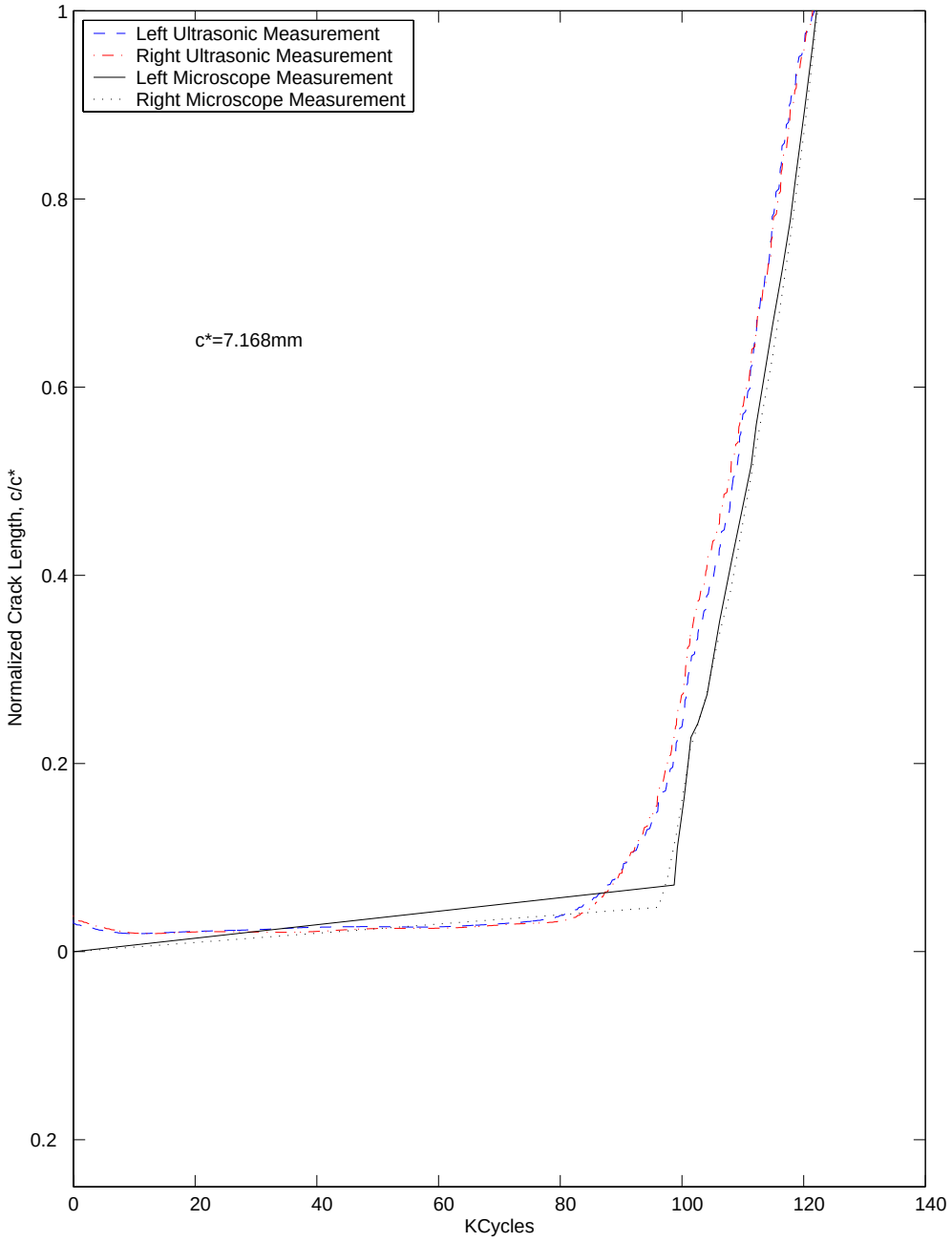

Figure 3-19 Ultrasonic vs. microscope measurements of crack length, specimen Sk. 7

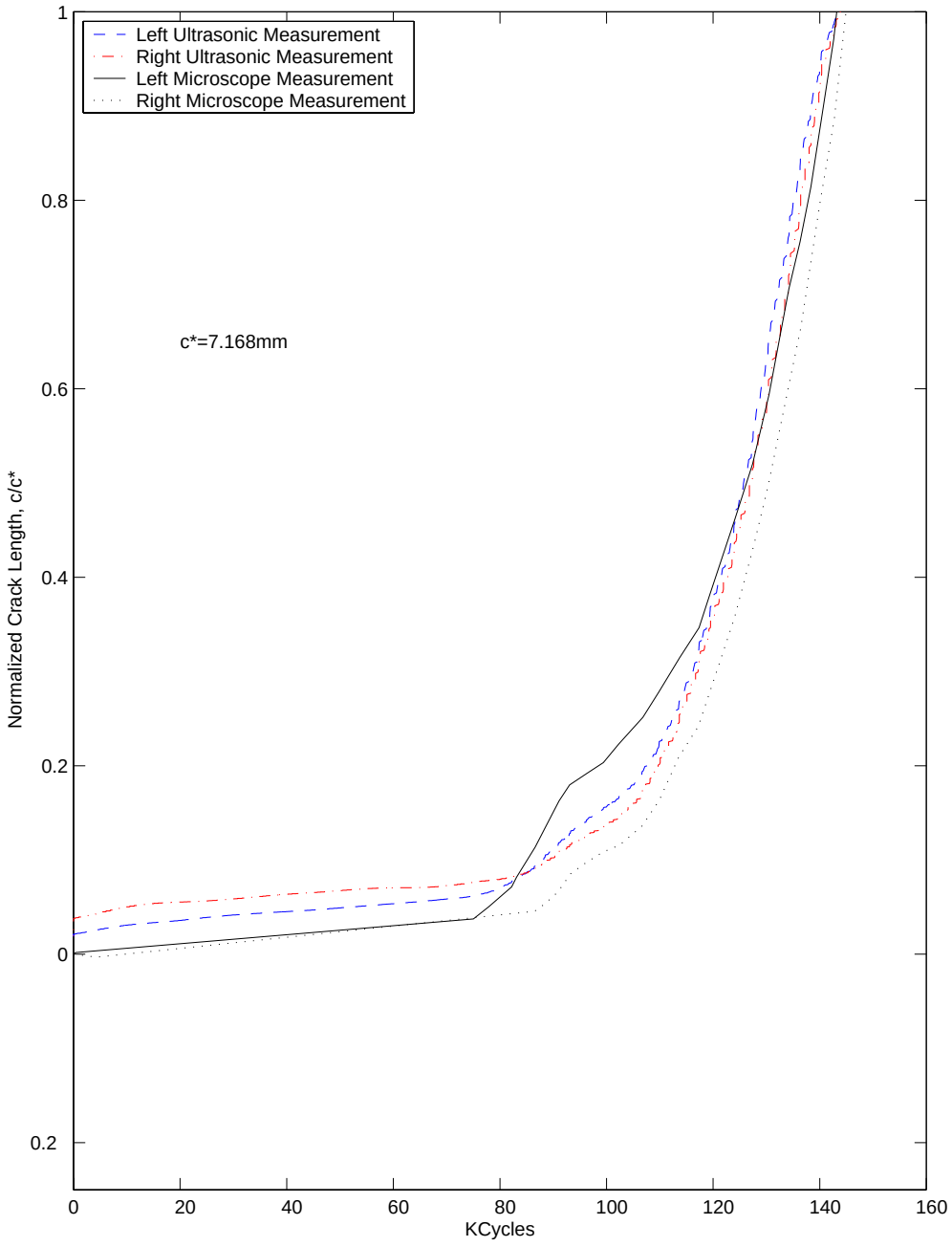

Figure 3-20 Ultrasonic vs. microscope measurements of crack length, specimen Sk. 8

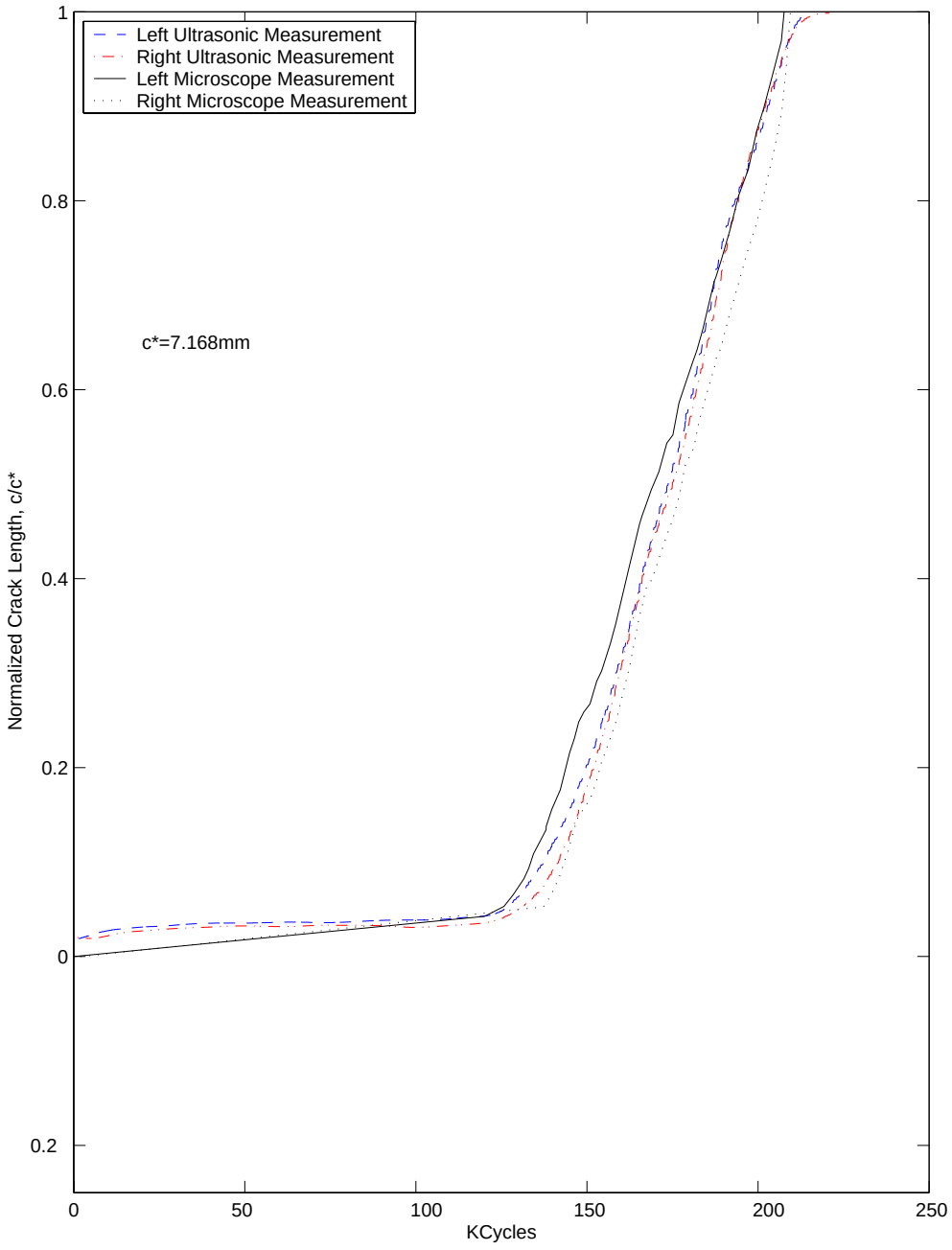

Figure 3-21 Ultrasonic vs. microscope measurements of crack length, specimen Sk. 9

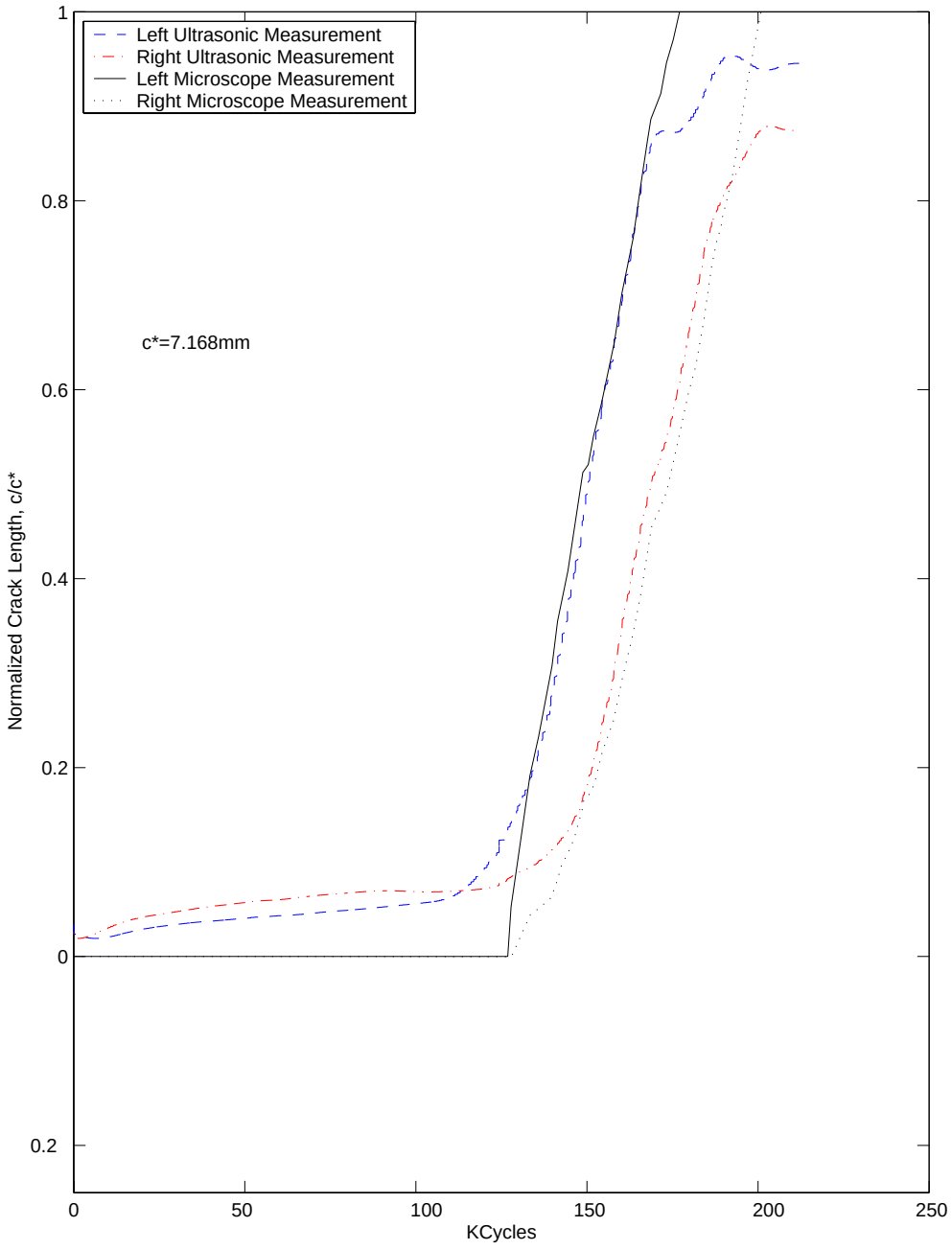

Figure 3-22 Ultrasonic vs. microscope measurements of crack length, specimen Sk. 10

3.2 Ultrasonic Crack Length Measurement for 6061-T6

The studies detailed in this section were performed on specimens machined out of commercial grade 6061-T6 rectangular bar stock 3" by 1/8" in the same configuration as shown in Chapter 1. The characteristic sequence of events for these tests was that after a long period of no discernable surface activity small surface cracks would appear and grow steadily. This contrasts with the results from the testing of 7075-T6 where very small surface cracks of length on the order of 50 microns formed very early in the testing. Thus in Figures 3-23 to 3-28, when the crack length shown is zero no surface cracks were visible, and any cracks that existed were less than 20 microns long. The measurements were taken using the un-rectified mode (typically called RF mode) of the USN-52. This introduces more delay into the measurements, and it invalidates the inner product method used with the rectified measurements presented in the previous section.

Although these measurements are difficult to calibrate to crack length, it is clear that in almost every case, ample warning of impending surface crack formation is available from these measurements. The exception is specimen #27. One issue to note is that due to the method used to generate this data, the ultrasonic signal is delayed somewhat, so that in the case of a faster ultrasonic system, it should be possible to provide more warning of impending surface cracks. One thing to note about these figures is that since none of the specimens were cycled to rupture, the filtered data appears to diverge from what one might expect at the end of the test. This is due to the fact that measurements were taken after the load was taken off of the specimen and included in the generation of these data sets. On a partially cracked specimen, when the load is removed, there is a large recovery of signal strength, and that has a significant effect on the filtered data, but not during the important portion of the test before and just after formation of surface cracks.

The reason for the gaps in the specimen numbers is that prior to specimen #20, ultrasonic data was not collected in a useable format. The data from specimens 21, 22, and 23 was lost due to power outages or equipment failures. Possibly more interesting is the gap from specimen 28-31. These were measured using the receiver

bandwidth on the USN-52 of 0.3-4Mhz. Since the transducers have a characteristic frequency of 5Mhz, much of the most useful parts of the signal were filtered out. Additionally, a higher gain was required to get a reasonable signal which introduces considerable noise into the signal. In any event the data from these specimens is not useable.

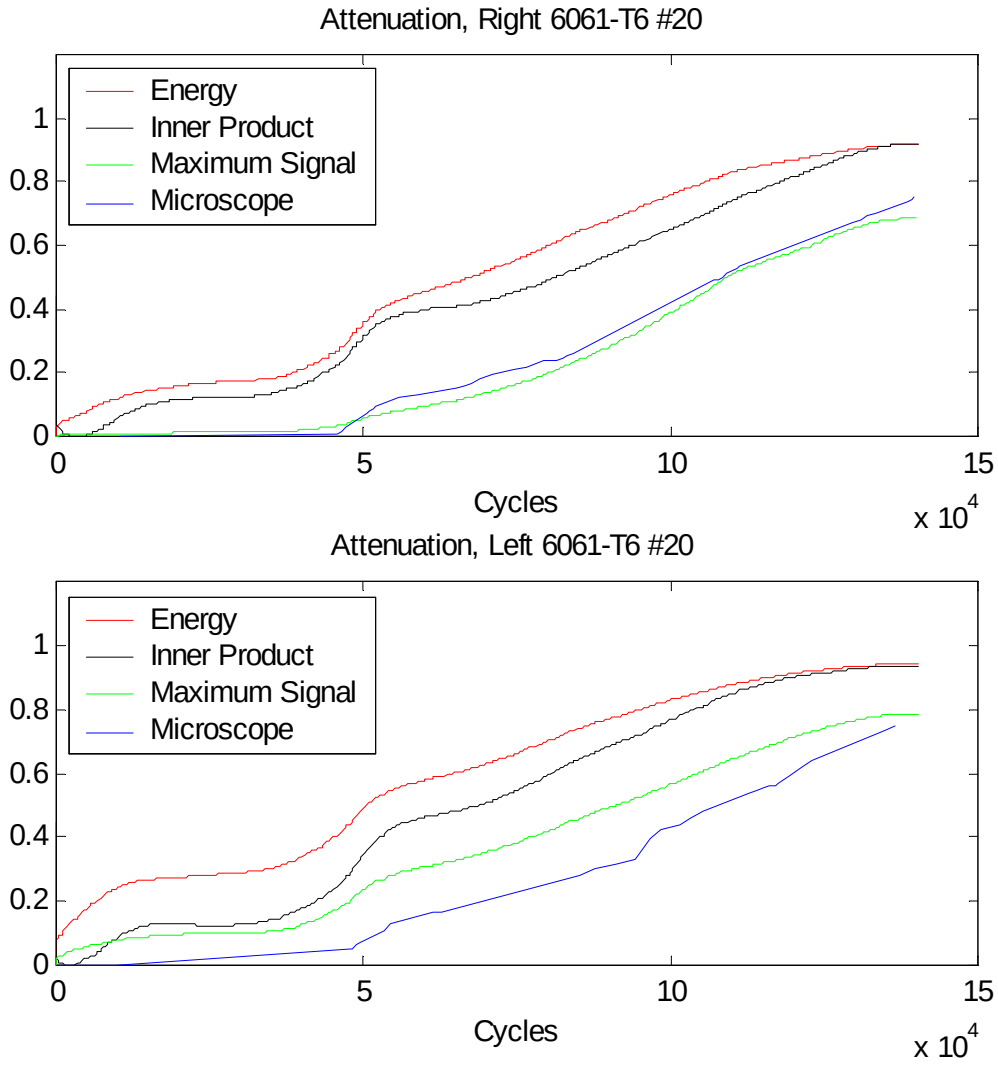

Figure 3-23 Energy vs. microscope observations 6061-T6 specimen #20

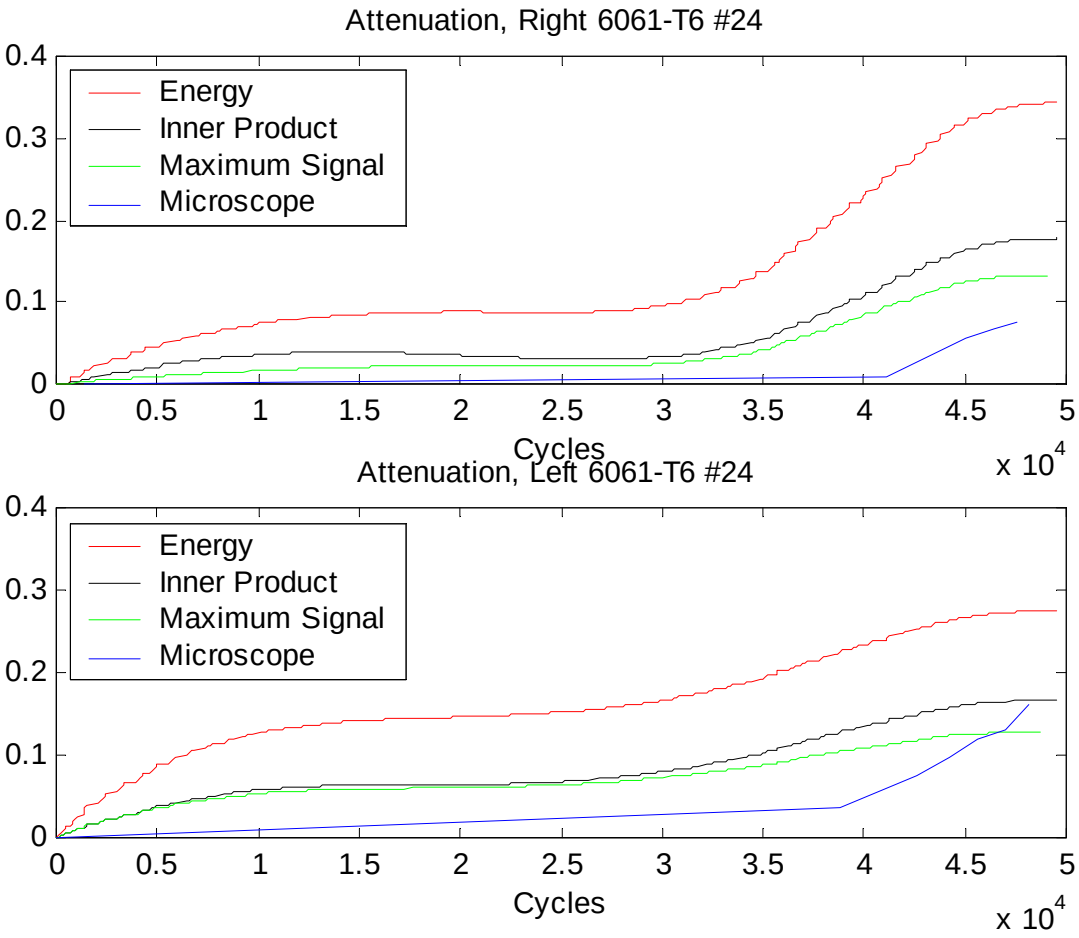

Figure 3-24 Energy vs. microscope observations 6061-T6 specimen #24

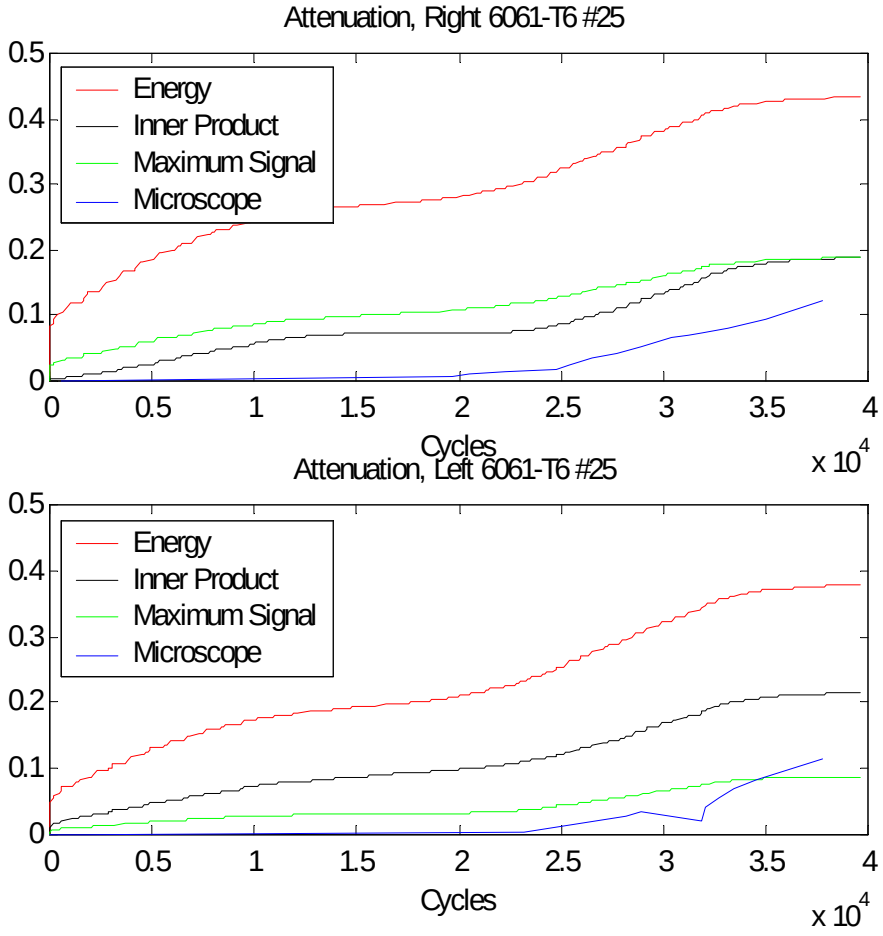

Figure 3-25 Energy vs. microscope observations 6061-T6 specimen #25

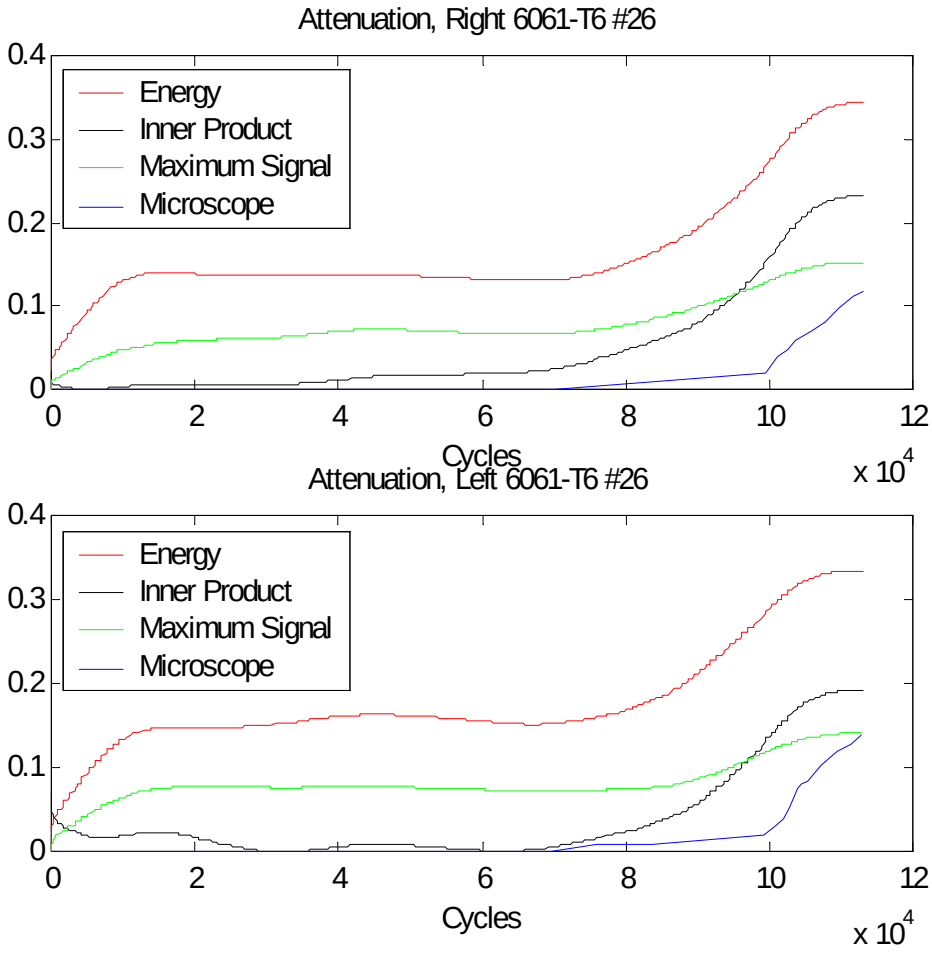

Figure 3-26 Energy vs. microscope observations 6061-T6 specimen #26

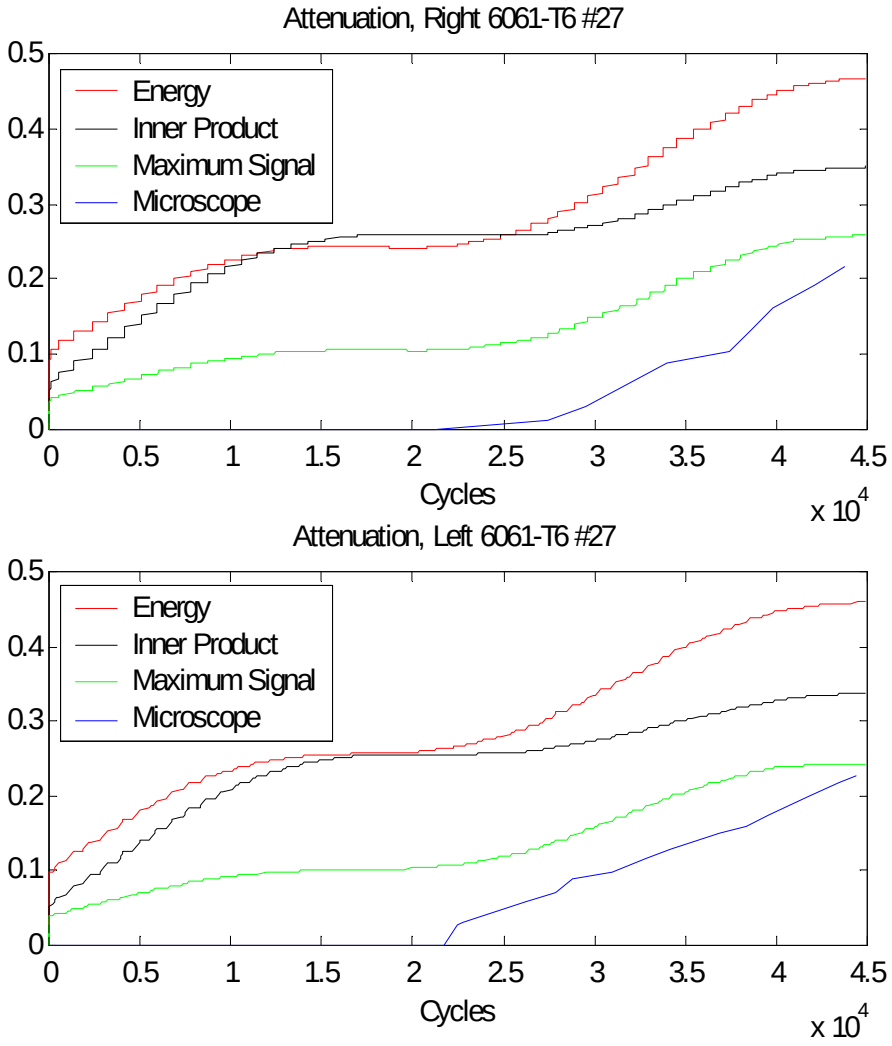

Figure 3-27 Energy vs. microscope observations 6061-T6 specimen #27

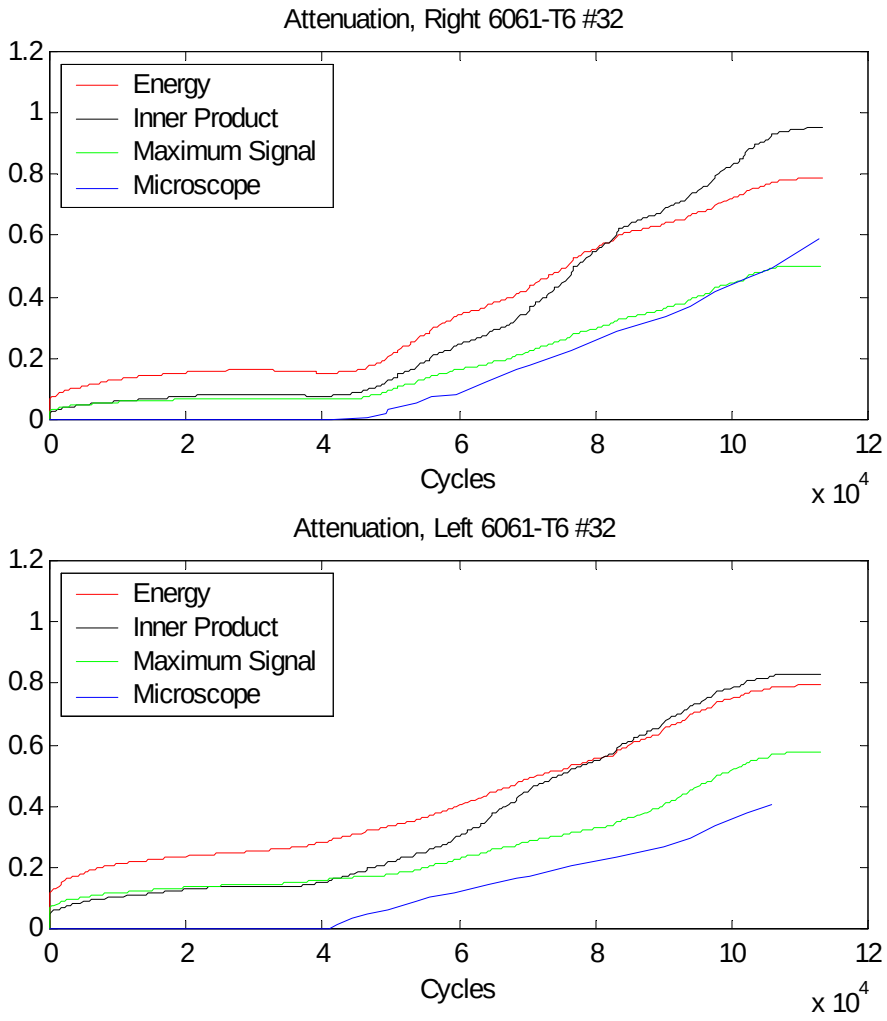

Figure 3-28 Energy vs. microscope observations 6061-T6 specimen #32

Unfortunately, most of these experiments were ended before enough data for good calibration between ultrasonic attenuation and microscope crack length measurement could be performed, and thus the results are not as good. The calibration curve is shown in Figure 3-29, and a comparison of ultrasonic and microscopic crack length measurements are shown in Figures 3-30 and 3-31.

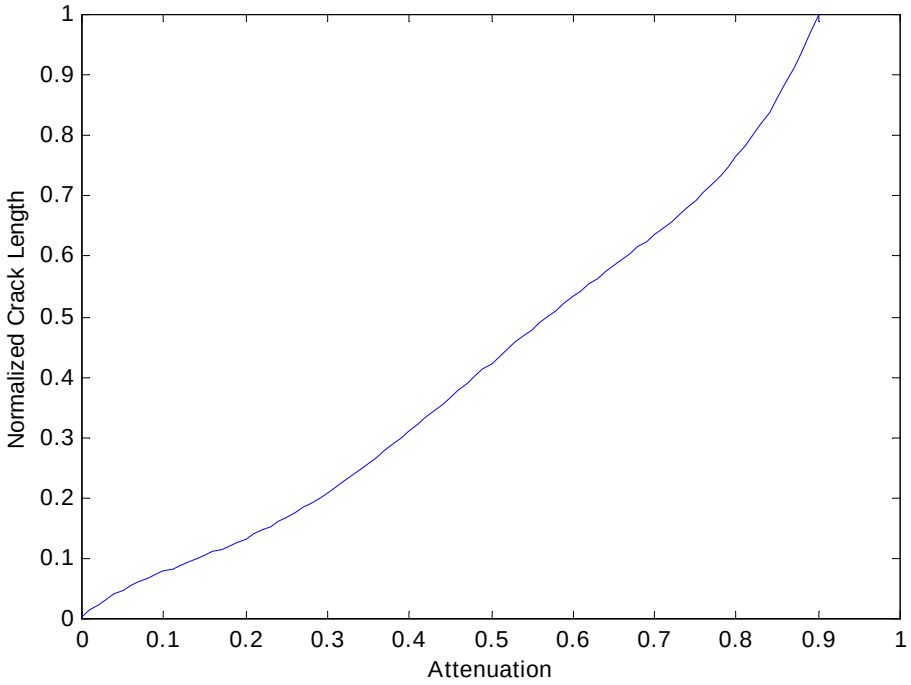

Figure 0-29 Calibration curve of crack length to attenuation

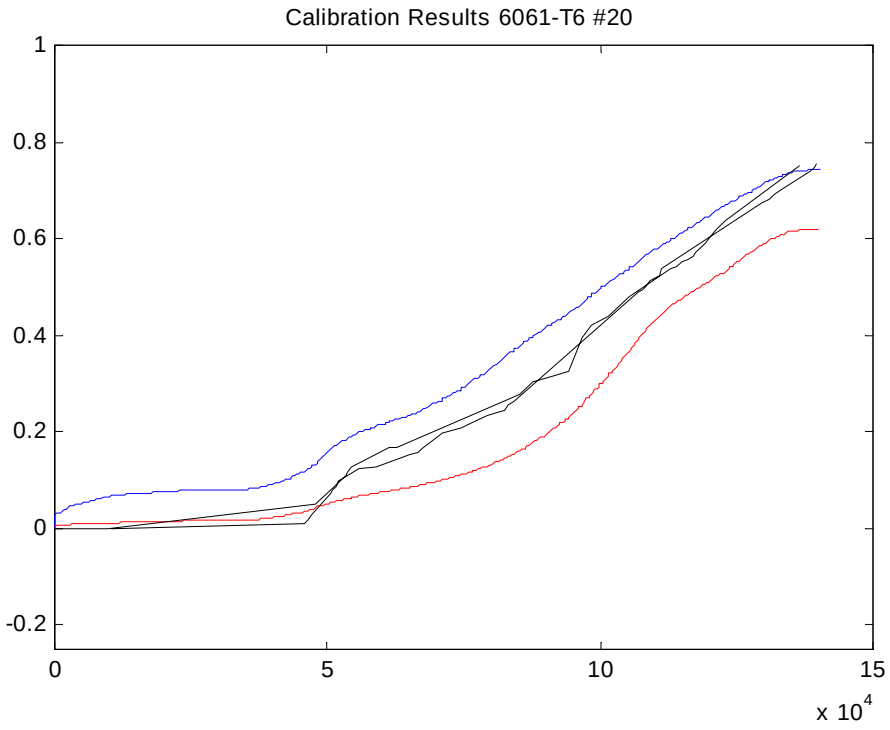

Figure 3-30 Comparison of ultrasonic vs. microscope measurements of crack length, specimen 6061-T6 #20

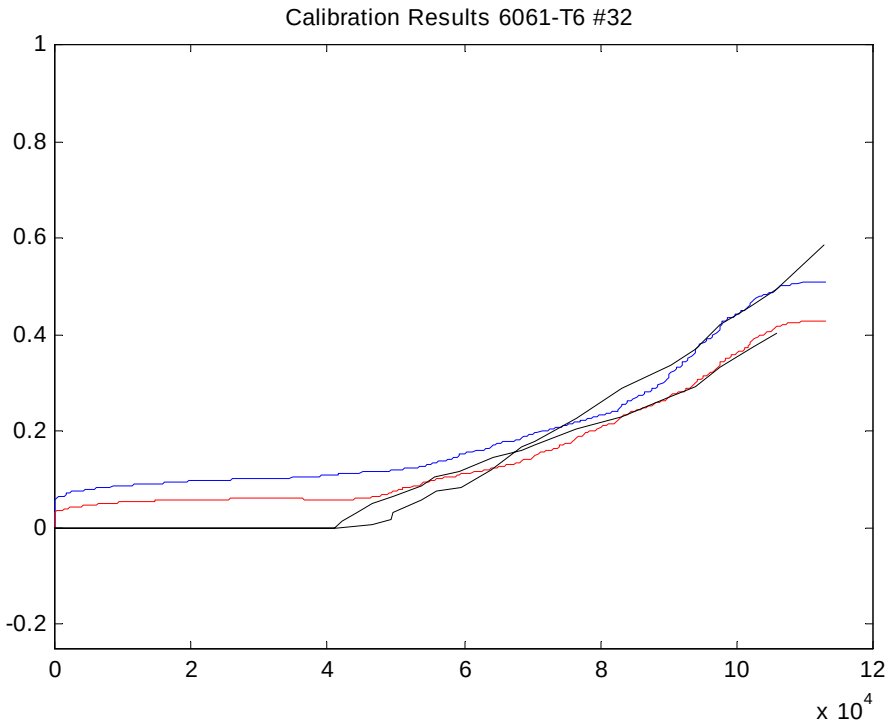

Figure 3-31 Comparison of ultrasonic vs. microscope measurements of crack length, specimen 6061-T6 #32

3.3 Ultrasonic Measurements Synchronized With Loading

Although the USN-52 demonstrated the potential benefits of ultrasonic flaw detection, the problems with the signal evident in Figures 3-9 and 3-10 displayed a significant weakness of that system. Thus, a different system was developed that could be synchronized with the load applied on the specimen. A schematic of the apparatus is shown in Figure 3-23. A Matec TB1000 Gated Amplifier PC add-in card drives a piezo-electric transducer with a gated sine wave with amplitude of 300V. To be more explicit, the excitation signal consists of short bursts of a sine wave of constant amplitude interrupted by relatively long periods of 0V. This signal propagates through the specimen, past the notch, and is captured by two transducers arrayed on either side of the notch. This signal is routed through a high frequency selector switch to a National Instruments NI5911 Oscilloscope card in the PC. The selector switch is controlled with

the parallel port of the PC. The acquisition of the ultrasonic signal is synchronized with the load applied to the specimen. Data is acquired at the low load and at the high load, alternating between the two pickup transducers on subsequent cycles. Thus in 2 cycles, each transducer will be sampled twice, once at low load and once at high load. The oscilloscope is triggered by the TB1000 once it is enabled from the software.

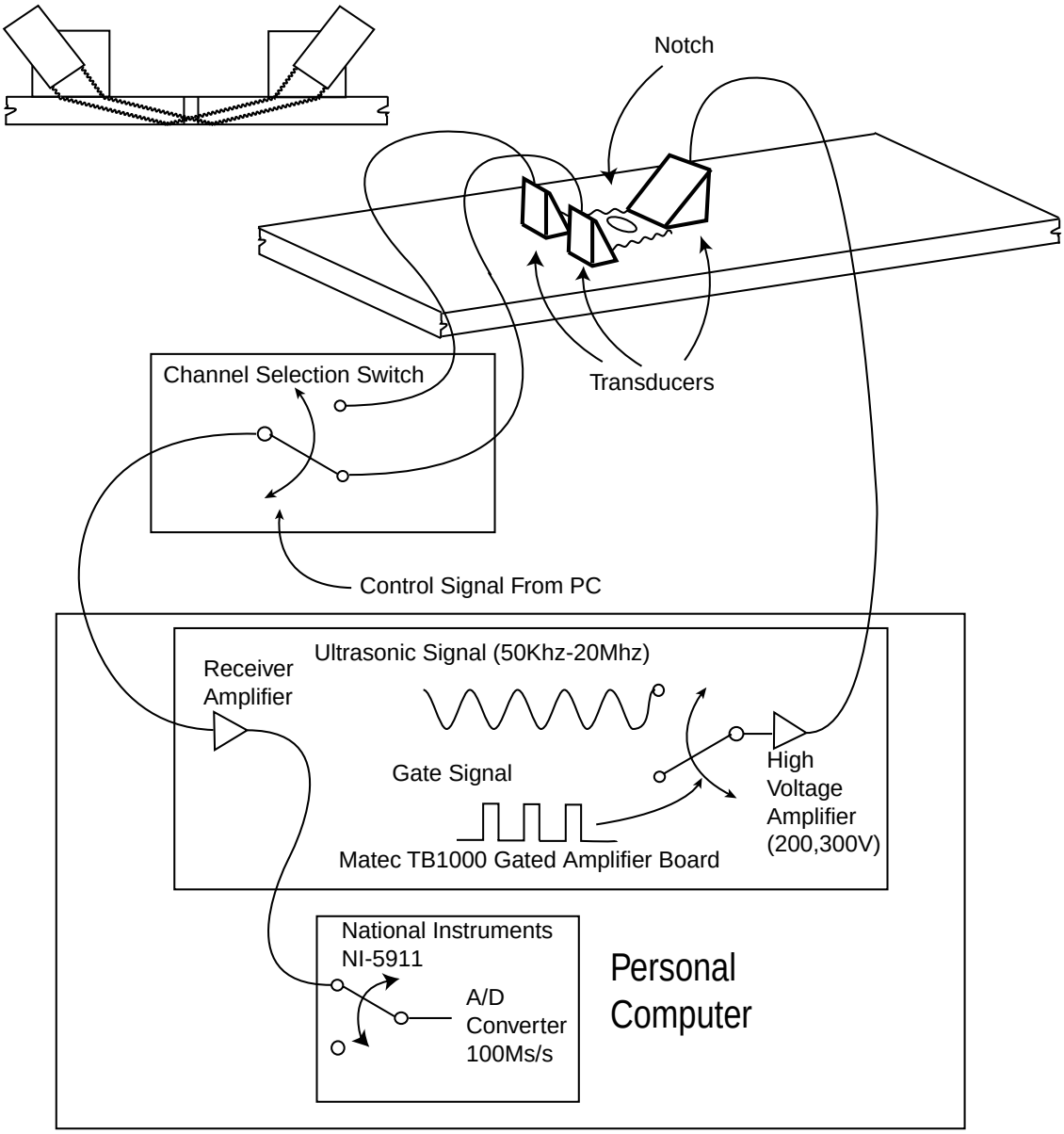

Figure 3-32 Ultrasonic flaw detection system

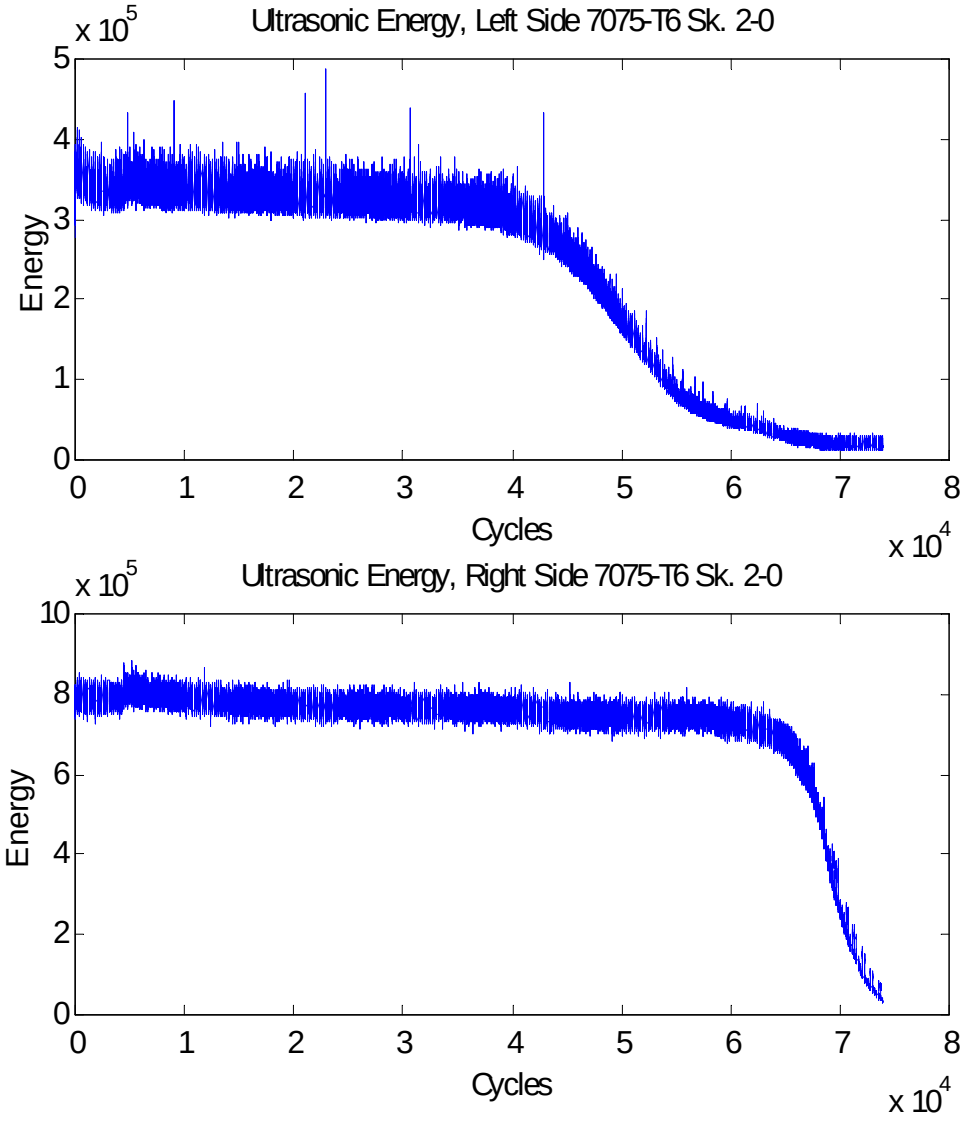

Figure 3-33 Unfiltered ultrasonic energy specimen Sk. 2-0

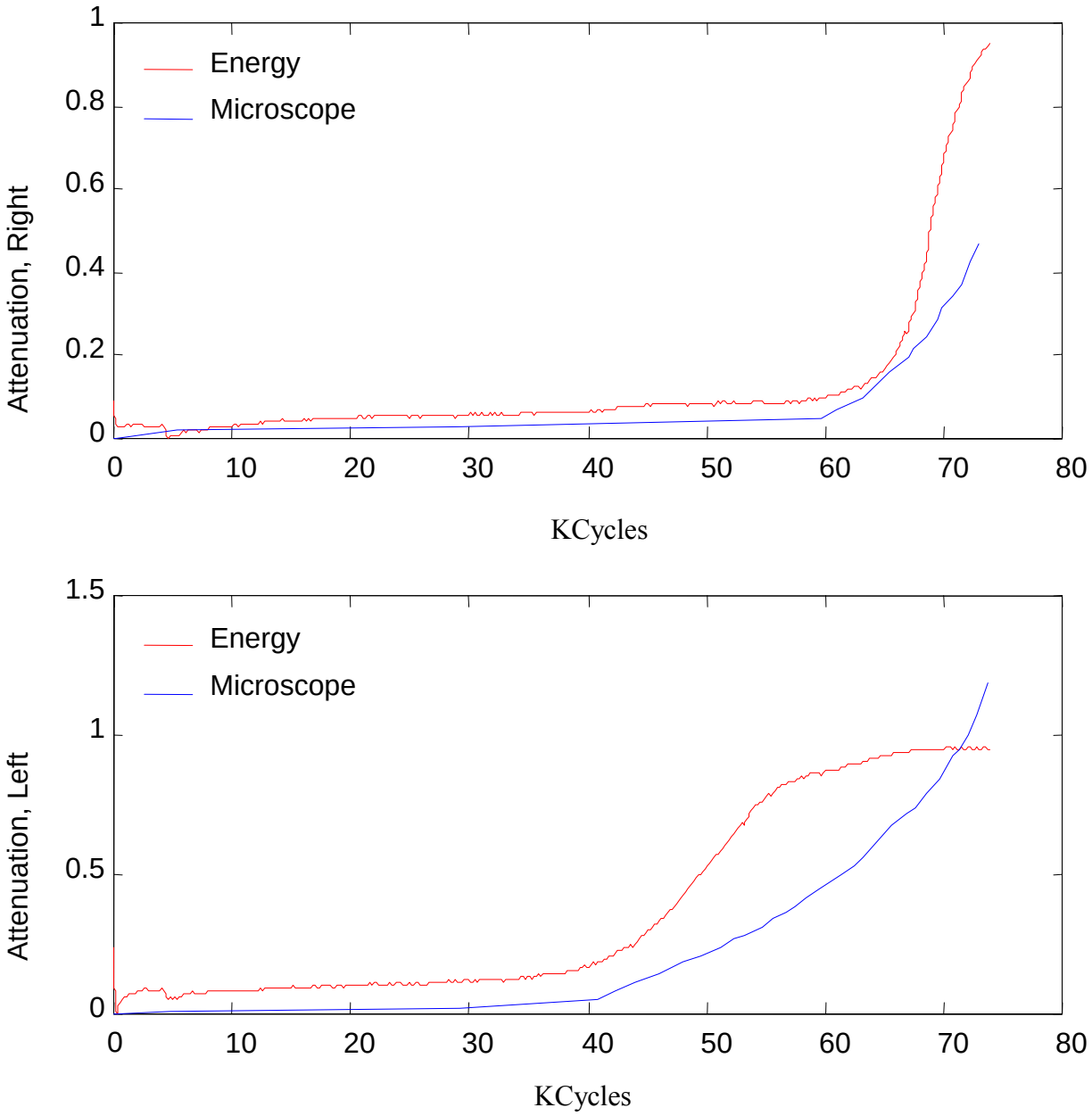

Figure 3-34 Ultrasonic attenuation vs. microscope observation specimen Sk. 2-0

The measurements shown in Figure 3-24 were taken at the maximum load condition at each cycle. A measurement is also taken at the minimum load, and on average these measurements are higher strength than measurements taken at the maximum load at the same cycle. As can be seen from Figure 3-25 the attenuation on the left of the notch shows a good correlation to the microscope observation of crack length. The attenuation on right of the notch does not seem to conform to the same relationship with crack length as the left sensor. Further work with this measurement system is ongoing.

From the material presented in this chapter, it can be seen that measurements of small cracks can successfully be performed using ultrasonic attenuation. This is an extremely important development for an on-line crack length measurement system. The main shortcoming of this technique is that the signal saturates for relatively small cracks. This shortcoming can be accommodated in two ways. The first, data fusion of multiple sensors, is explored further in an appendix. The second method, crack damage model parameter estimation is explored further in the next chapter.

Chapter 4

Fatigue Crack Model Parameter Estimation

It has long been recognized that accurate methods of fatigue analysis allow for cheaper, and less conservative design of mechanical structures leading to construction of highly reliable, maintainable, and efficient machinery. Many researchers cited in Suresh (1991) have empirical and semi-empirical models based on observed experimental data and have attempted to provide a physical interpretation of these models. For various reasons, these models have proven to be less than fully successful in practice, but most importantly, only a few such models capture the inherent variability in the crack growth process. The primary idea expressed in this chapter is that crack damage estimates are obtained from a state-space model of crack growth combined with real-time measurements of crack length. This estimate is more accurate than either the measurements or the model output. Particularly, the crack damage model, even if it properly models the stochastic nature of fatigue crack growth, can only predict the estimated mean of crack growth trajectories over an ensemble of test data. However, Ray (1999) has shown by statistical analysis of available experimental results that including a random variable in the parameters of the crack growth model can capture the predominant variability in crack growth rates. The model itself is shown in the discussion that follows, but the important point is that for any given sample, the variability in the modeling errors can be reduced significantly by producing a good estimate of the random parameter early in the crack growth process. Simply put, a specimen that is cracking at a higher rate rarely improves so that a specimen that was cracking at a slower rate overtakes it. The first part of this chapter discusses fatigue crack models, and this leads to a discussion of the estimation of model parameters in the second half of the chapter.

4.1 Cumulative Fatigue Damage Models

Most fatigue damage models are based on experimental data generated by constant amplitude cyclic loads to test specimens, but these results are not directly

applicable to real structures that are subjected to complex time-dependent loads with varying amplitudes, mean stresses, and frequencies. The task, then, is to predict the life of a component subjected to varying amplitude loads using constant amplitude test data. The Palmgren-Miner cumulative damage law (Hertzberg, 1989) provides a simple method to estimate the fatigue life of a component experiencing variable amplitude loading. The Palmgren-Miner rule defines damage as the ratio of the number of cycles at a given stress amplitude to the number of cycles to failure at that stress amplitude. The damage, *D*, accumulated in the material due to variable amplitude loading is then the sum of the damages due to each stress amplitude:

$$D = \sum_i D_i = \sum_i \frac{n_i}{N_i} \tag{4.1}$$

where n_j is the number of load cycles at the stress level i and N_j is the total number of cycles to failure at the same stress level. Palmgren-Miner predicts failure when the total damage is equal to one. The difficulty with this model is that it does not account for sequence effects (Suresh, 1991). Many nonlinear cumulative damage rules have since been in an attempt to overcome the shortcomings of the Palmgren-Miner rule such as the Henry, Gatts, Corten-Dolan, Marin, and Manson double-linear rules (Bannantine et al. 1990) and the recent work of Ray and Wu (1994). However, although these methods result in more accurate predictions than the Palmgren-Miner rule for two-step load histories, there is no guarantee of their accuracy under actual service load histories.

4.2 Fatigue Crack Growth Models

Typical constant amplitude crack propagation data shows that most of the life of a component is spent while the crack length is relatively small and that crack growth rate depends on the crack length itself. Additionally, crack growth rate increases with increased applied stress. Paris and Erdogan (1963) suggested that the crack growth rate is related to the applied stress and crack length via the stress intensity factor range as:

$$\frac{dc}{dN} = C\Delta K^m \tag{4.2}$$

where C and m are material constants; stress intensity factor range $\Delta K = \sqrt{\pi c}\ Y(c)\Delta S$, and $Y(c)$ is a function of the geometry of the component and crack length. Equation 4.2, known as the Paris Equation, is a common method of predicting crack growth for constant amplitude stress cycles with zero stress ratio, and is the basis of most fatigue crack growth models. It was developed and validated using both K increasing (constant amplitude load) and K decreasing (near threshold) testing. Since these are very different loading conditions, one could assume that this model would work under arbitrary loading. However, these load conditions have monotonically changing plastic zone size, and thus any sequencing effects are masked by the nature of the load change. Other researchers have modified the Paris Equation to account for the sigmoidal shape of the da/dN vs. ΔK curve, and the effect of mean stress. An improvement that was originally to predict unstable crack growth but is more often used to account for the effects of mean stress in fatigue crack growth rates is Forman's equation (Bannantine et al. 1990):

$$\frac{dc}{dN} = \frac{C\Delta K^m}{(1-R)\,K_c - \Delta K} \tag{4.3}$$

where K_c is the critical stress intensity and R is the stress ratio. Another method used to account for stress ratio effects is the Walker model (Bannantine et al. 1990):

$$\frac{dc}{dN} = C\left[(1-R)^m\ K_{\max}\right]^n \tag{4.4}$$

where $K_{\max}$ is the maximum stress intensity.

The attractive feature of the models based on the Paris model is that the remaining life of a component may be estimated from the results of an inspection without any regard to the load history. This is particularly important to the aircraft industry where an inspection can ensure that there is no detectable crack present and crack growth analysis can further ensure that the largest possible crack will not grow to the critical size before the next inspection. Such damage tolerant techniques, although highly conservative, are useful to the aircraft industry and have been required by military standards MIL-A-83444 *Airplane Damage Tolerance Requirements*. The total crack growth due to variable

amplitude loading is usually obtained simply by summing the effects due to each stress cycle, which is analogous to the Miner's rule for cumulative damage accumulation. Frequently, sequence or memory effects are not considered, so that the predicted crack growth depends only on the current level of damage and applied stress, and not on past loading. A common methodology applies a crack growth retardation correction factor for structural elements that do not undergo loading reversals (Chang and Engle, 1984). However, well-publicized problems with the durability of aircraft designed with such methods are clear evidence of the need for further research in this area. Several methods have been to yield more accurate and reliable fatigue crack growth predictions under variable amplitude loading. The Newman model, which uses the crack closure concept, proposed first by Elber (1971), is one such model, which has resulted in improved prediction of fatigue crack growth under a wide variety of loading conditions.

4.2.1 Newman's Fatigue Crack Growth Model

The conventional approach to determining the fatigue life of components is to consider crack initiation and propagation separately. Methods such as the strain life approach (Hertzberg 1989; Suresh 1991) are used to calculate the fatigue crack initiation life while fracture mechanics methods such as the Paris model (Paris and Erdogan 1963) are used to compute the crack propagation life. It is common (and often required) in the aircraft industry to assume a worst case crack which simply avoids analysis of the initiation phase entirely. While the Paris model is valid in the macro-crack range, the Newman model (Newman 1981; Newman et al. 1986) represents the fatigue crack growth process down to micro-cracks of the order of tens of microns that is comparable to the material defect or crystal imperfection size. This method, therefore represents a unified approach to model both the crack initiation and crack propagation stages.

The Newman model for crack growth is of the form:

$$\frac{dc}{dN} = C_1 \times \left(\Delta K_{eff}{}^{C_2}\right) \times \left(\frac{1 - \left(\frac{\Delta K_o}{\Delta K_{eff}} \right)^2}{1 - \left(\frac{K_{\max}}{C_5} \right)^2} \right) \tag{4.4}$$

where

$$\begin{aligned} \Delta K_o &= C_3\left(1 - C_4 \frac{S_o}{S_{\max}}\right) \\ K_{\max} &= S_{\max}\sqrt{\pi c}\, F \\ \Delta K_{eff} &= (S_{\max} - S_o)\sqrt{\pi c}\, F \end{aligned} \tag{4.5}$$

and S_0 is the crack opening stress; F is a correction factor for the finite width of the specimen; c is the crack length; and $S_{\max}$ is the maximum applied remote stress. Alternatively, a table-lookup form can be used to determine the crack growth rate as a function of ΔK_{eff}. Then, the crack growth rate is expressed as:

$$\frac{dc}{dN} = \exp\left(m\,\ell n(\Delta K_{eff}) + b\right) \tag{4.6}$$

where m is the slope and b is the intercept of the linear interpolation of the (log scale) $\Delta K_{eff} - {}^{dc}\!/_{dN}$ look-up table. This look-up table represents a piecewise fit of the experimentally measured $\Delta K_{eff} - {}^{dc}\!/_{dN}$ relationship in the logarithmic scale. Newman's fatigue crack growth model using Eq. (4.6) is similar to the implementation of the Paris equation with one important difference: while the Paris equation involves the determination of only one set of material-dependent parameters, Newman's method requires determination of the same two parameters piecewise over a range of values. This is due to the fact that the Paris model is valid only in the crack propagation stage where the $\Delta K_{eff} - {}^{dc}\!/_{dN}$ relationship is approximately linear whereas Newman's model is valid both in the crack initiation and crack propagation stages.

4.2.2 Determination of Crack-opening Stresses

The crack opening stress, S_0, is calculated from the crack-surface displacements and the contact stresses along the surface of the crack which are, in turn, determined via finite element analysis. Newman (1981) reports details of this method. Since the finite element analysis is computationally intensive, it precludes use of this model for real-time applications. However, for constant amplitude loading, the crack-opening stress may be represented as a function of stress ratio R, applied stress level $S_{\max}$, and the three dimensional constraint α (Newman et al. 1986) as

$$S_o = \begin{cases} S_{\max}\left(A_0 + A_1 R + A_2 R^2 + A_3 R^3\right) & for \quad R \geq 0 \\ S_{\max}\left(A_0 + A_1 R\right) & for -1 \leq R < 0 \end{cases} \tag{4.7}$$

where

$$\begin{aligned} A_0 &= \left(0.825 - 0.34\alpha + 0.05\alpha^2\right)\left[\cos\left(\frac{\pi S_{\max}}{2\sigma_o}\right)\right]^{1/\alpha} \\ A_1 &= \left(0.415 - 0.071\alpha\right)\frac{S_{\max}}{\sigma_o} \\ A_2 &= 1 - A_0 - A_1 - A_3 \\ A_3 &= 2A_0 + A_1 - 1 \end{aligned} \tag{4.8}$$

and the flow stress, σ_0, is the average of the uniaxial yield stress and uniaxial ultimate tensile strength of the material. This relationship is determined by computing numerical values of crack-opening stresses as a function of constraint, stress ratio, and stress level using the analytical closure model for a center-crack tension specimen.

4.3 State Space Fatigue Crack Damage Model

Patankar and Ray (2000) have formulated a state-space model of fatigue crack growth for life-extending controller analysis and synthesis that accounts for the impact of variable-amplitude loading on crack growth rate (e.g., crack retardation and sequence effects). Patankar and Ray (1999) have also shown that the predicted structural durability (and hence the controller design) could be grossly inaccurate if the fatigue crack damage model does not capture the effects of variable-amplitude cyclic stress.

The state-space model of fatgue crack damage has been validated with the test data of McMillan and Pelloux (1967) and Porter (1972) along with explanations of the underlying physical phenomena. The model is an extension of the Fastran model [Newman, 1981, 1992] which is based on the concept of small cracks in homogeneous materials. The Fastran model is represented by a nonlinear difference equation in which the crack increment during the k^{th} cycle is obtained as a function of the maximum applied (far-field) stress $S_k^{\max}$ and the crack opening stress S_k^o as:

$$\left.\begin{aligned} \Delta a_k \equiv a_k - a_{k-1} &= h\left(\Delta K_k^{eff}\right) \text{ with } h(0)=0 \\ \Delta K_k^{eff} &\equiv \sqrt{\pi\, a_{k-1}}\, F(a_{k-1}, \tilde{w})\,(S_k^{\max} - S_{k-1}^{o})\, U\left(S_k^{\max} - S_{k-1}^{o}\right) \end{aligned}\right\} \quad \text{for } k \geq 1 \text{ and } a_0 > 0 \tag{4.9}$$

where a_{k-1} and S_{k-1}^{o} are the crack-length and the crack-opening stress, respectively, during the k^{th} cycle and change to a_k and S_k^{o} at the expiry of the k^{th} cycle; F(•,•) is a crack-length-dependent correction factor compensating for finite geometry of the specimen with the width parameter $\tilde{w}$; the non-negative monotonically increasing function $h(\bullet)$ can be represented either by a closed form algebraic equation:

$$h\left(\Delta K_k^{eff}\right) = C_1\left(\Delta K_k^{eff}\right)^m \text{ with material constants } C_1 \text{ and } m, \tag{4.10}$$

or by table lookup [Newman, 1992]; and $U(x) = \begin{cases} 0 \text{ if } x < 0 \\ 1 \text{ if } x \geq 0 \end{cases}$ is the Heaviside function.

We now present the structure of the difference equation that is excited by the cyclic stress input to generate the crack opening stress. To this end, we first consider the steady-state solution of the difference equation under constant amplitude load. This issue has been addressed by several investigators including Newman (1984) and Ibrahim et al. (1986). The steady-state crack-opening stress S^{oss} under a constant amplitude cyclic load is a function of the minimum stress $S^{\min}$, the maximum stress $S^{\max}$, the constraint factor α (which is 1 for plane stress and 3 for plane strain), the specimen geometry, and the flow stress S^{flow} (which is the average of the yield strength S^{y} and the ultimate strength S^{ult}). These relationships are shown to be good for most ductile alloys by Newman (1984).

The objective is to construct the difference equation for (non-negative cycle-dependent) crack opening stress S_k^{o} such that, under different levels of constant-amplitude load, the forcing function S_k^{oss} at the k^{th} cycle matches the crack-opening stress derived from the following empirical relation [Newman, 1992] that is valid for non-zero peak stress (i.e., $S^{\max} \neq 0$):

$$S_k^{oss} = S^{oss}(S_k^{\max}, S_k^{\min}, \alpha, F) = \left(\tilde{A}_k^0 + \tilde{A}_k^1 R_k + \tilde{A}_k^2 (R_k)^2 + \tilde{A}_k^3 (R_k)^3\right) S_k^{\max} \tag{4.11}$$

where $R_k = \frac{S_k^{\min}}{S_k^{\max}}\, U\left(S_k^{\max}\right)$ for all $k \geq 0$; (4.12)

$$\widetilde{A}_k^0 = \left(0.825 - 0.34\,\alpha_k + 0.05\,(\alpha_k)^2\right)\left[\cos\left(\frac{\pi}{2}\,\frac{S_k^{\max}}{S^{flow}}\,F(a_{k-1}, \widetilde{w})\right)\right]^{1/\alpha_k} \tag{4.13}$$

$$\widetilde{A}_k^1 = \left(0.415 - 0.071\,\alpha_k\right)\left(\frac{S_k^{\max}}{S^{flow}}\,F(a_{k-1}, \widetilde{w})\right) \tag{4.14}$$

$$\widetilde{A}_k^2 = \left(1 - \widetilde{A}_k^0 - \widetilde{A}_k^1 - \widetilde{A}_k^3\right) U\left(R_k\right) \tag{4.15}$$

$$\widetilde{A}_k^3 = \left(2\widetilde{A}_k^0 + \widetilde{A}_k^1 - 1\right) U\left(R_k\right) \tag{4.16}$$

The constraint factor α_k used in Equations. (4.13) and (4.13) is obtained as a function of the crack length increment Δa_k in Eq. (4.9). As discussed in Chapter 1, α_k represents the state of plane stress or plane strain under which the crack growth is occurring. A procedure for evaluation of α_k is presented in the Fastran manual [Newman, 1992]. Since α_k does not significantly change over cycles, it can be approximated as piecewise constant for limited ranges of crack length.

The following constitutive relation, in the form of a nonlinear first order difference equation, recursively calculates the crack-opening stress S_k^o upon completion of the k^{th} cycle [Patankar and Ray, 2000]:

$$\begin{aligned} S_k^o = {} & \left(\frac{1}{1+\eta}\right) S_{k-1}^o + \left(\frac{\eta}{1+\eta}\right) S_k^{oss} + \left(\frac{1}{1+\eta}\right)\left(S_k^{oss} - S_{k-1}^o\right) U\left(S_k^{oss} - S_{k-1}^o\right) \\ & + \left(\frac{1}{1+\eta}\right)\left[S_k^{oss} - S_k^{oss\_old}\right] U\left(S_{k-1}^{\min} - S_k^{\min}\right)\left[1 - U\left(S_k^{oss} - S_{k-1}^o\right)\right] \end{aligned} \tag{4.17}$$

$$\eta = \frac{t\,S^y}{2\widetilde{w}E} \tag{4.18}$$

where the forcing function S_k^{oss} in Eq. (4.17) is calculated from Eq. (4.11) as if a constant amplitude stress cycle $\left(S_k^{\max}, S_k^{\min}\right)$ is applied; similarly, $S_k^{oss\_old}$ is given by Eq. (4.11) as if a constant amplitude stress cycle $\left(S_k^{\max}, S_{k-1}^{\min}\right)$ is applied. For constant-amplitude

loading, S^{oss} is the steady-state solution of S_k^o. In general, the inputs S_k^{oss} and $S_k^{oss\_old}$ to Eq. (4.17) are different from the instantaneous crack-opening stress S_k^o under variable-amplitude loading. The Heaviside function $U\left(S_k^{oss}-S_{k-1}^o\right)$ in the third term on the right hand side of Eq. (4.17) allows fast rise and slow decay of S_k^o. The last term on the right hand side of Eq. (4.17) accounts for the effects of reverse plastic flow. Depletion of the normal plastic zone occurs when the minimum stress $S_k^{\min}$ decreases below its value $S_{k-1}^{\min}$ in the previous cycle, which is incorporated via the Heaviside function $U\left(S_{k-1}^{\min}-S_k^{\min}\right)$. Note that the overload excitation and reverse plastic flow are mutually exclusive.

The dimensionless parameter η in Eq. (4.18) depends on the component thickness t, half-width w, yield strength S^y, and Young's modulus. Following an overload cycle, the duration of crack retardation is controlled by the transients of S_k^o in the state-space model, and hence determined by the stress-independent parameter η in Eqs. (4.17) and (4.18). Physically, this duration depends on the ductility of the material that is dependent on many factors including the heat treatment of specimens [Schijve, 1976]. Smaller yield strength produces a smaller value of η, resulting in longer duration of the overload effect. Smaller specimen thickness has a similar effect [Schijve, 1976]. Equations 4.9 to 4.16 describe the state-space model where the crack length a_k and crack opening stress S_k^o are the state variables.

The net effect of a single-cycle overload (i.e., increased $S_k^{\max}$) is a jump in the effective stress range $\Delta S_k \equiv S_k^{\max} - S_k^o$ resulting in an increase in the crack growth increment in the present cycle. Shortly after the expiration of the overload (i.e., $S_k^{\max}$ returning to the original lower value), S_k^o starts decreasing slowly from its increased value. The result is a decrease in ΔS_k, which causes the crack growth rate to diminish. Subsequently, after returning to the original constant-amplitude stress, as S_k^o slowly

relaxes back to its original state, the crack growth rate resumes the original value. A single overload initially increases crack growth rate for a few cycles and then gradually decreases over a much higher number of cycles until it reaches the original value. The crack growth is therefore retarded due to the fast rise and slow decay of S_k^o.

4.4 Parameter Estimation

We consider small cracks in center cracked specimens. The geometry factor F, is given by: $F = \mathrm{Sec}\left(\frac{\pi}{2}\frac{c}{w}\right)$ where w is the half width of the specimen. For c<<w, $F \approx 1$, and this approximation is used in the following analysis to simplify the equations.

Normalizing the crack length c as $\theta = \frac{c}{w}$, and also normalize the stress range, ΔS, where $\Delta S = S^{max} - S^{O}$ as $\sigma_t \equiv \frac{\Delta S}{\Delta S^*}$ where ΔS^* is a fixed nominal stress range.

The governing equation for the stochastic process of crack growth is:

$$\delta\theta_t(\zeta) = (\Omega(\zeta) + v_t(\zeta))(\theta_t(\zeta))^{\frac{m}{2}}(\sigma_t)^m \delta t \qquad (4.19)$$

where

ζ indicates a random sample;

$\delta\theta_t(\zeta)$ is the crack growth increment;

t is the current time upon completion a cycle;

δt is the increment in number of stress cycles;

$\Omega(\zeta)$ is a random material parameter

v_t is a zero-mean white Gaussian process related to material inhomogeneity

m is the exponent material parameter ($2.5 \le m \le 5$ for ductile alloys).

None that $\Omega(\zeta)$ and $v_t(\zeta)$ are statistically independent for all t.

Rearranging Equation (4.19) yields:

$$\frac{\delta\theta_t(\zeta)}{(\theta_t(\zeta))^{\frac{m}{2}}} = (\Omega(\zeta) + v_t(\zeta))(\sigma_t)^m \delta t \tag{4.20}$$

Approximating the above difference equation in the limit as a Riemann Sum, and integrating both sides:

$$\frac{1}{1-\frac{m}{2}}\left(\theta_t(\zeta)^{1-\frac{m}{2}} - \theta_0(\zeta)^{1-\frac{m}{2}}\right) = \Omega(\zeta)\int_0^t (\sigma_\tau)^m d\tau + \int_0^t (\sigma_\tau)^m v_\tau(\zeta) d\tau \tag{4.21}$$

Following Ray (1999) define an incremental measure of damage from time t_0 to time $t>t_0$ as:

$$\psi(\zeta, t_0) = \frac{1}{1-\frac{m}{2}}\left(\theta_t(\zeta)^{1-\frac{m}{2}} - \theta_0(\zeta)^{1-\frac{m}{2}}\right) \tag{4.22}$$

which is a non-negative quantity for m>2.

Starting with $\psi(\zeta, t_0) = \Omega(\zeta)\int_0^t (\sigma_\tau)^m d\tau + \int_0^t (\sigma_\tau)^m v_\tau(\zeta) d\tau$ (4.23)

the following results are obtained:

$$E[\psi(\zeta, t_0)] = E[\Omega(\zeta)]\int_0^t (\sigma_\tau)^m d\tau$$

$$Var[\psi(\zeta, t_0)] = Var\left[\int_0^t (\sigma_\tau)^m \Omega(\zeta) d\tau\right] + \int_0^t (\sigma_\tau)^{2m} \alpha_\tau d\tau \tag{4.24}$$

where α_t is the (time dependent) intensity of the white Gaussian noise $v_t(\zeta)$. If, setting

$$E[\Omega] = \mu_\Omega \text{ and } Var[\Omega(\zeta)(\sigma_\tau)^m] = C \tag{4.25}$$

based on the observation of Ray (1999) yields:

$$E[\psi(\zeta, t_0)] = \mu_\Omega \int_0^t (\sigma_\tau)^m d\tau \text{ and } Var[\psi(\zeta, t_0)] = C(t - t_0)^2 + \int_0^t (\sigma_\tau)^{2m} \alpha_\tau d\tau \tag{4.26}$$

For the constant amplitude case, i.e. $\sigma_t = \sigma$, and homogeneity of material structure , i.e. $\alpha_t = \alpha$

$$E[\psi(\zeta, t_0)] = \mu_\Omega (\sigma_t)^m (t - t_0)$$

$$Var[\psi(\zeta, t_0)] = C(t - t_0)^2 + \sigma^{2m}\alpha(t - t_0) \tag{4.27}$$

Note that for sufficiently large t, the variance in the damage measure is dominated by the term $C(t-t_0)^2$, which represents the variability captured by the random parameter Ω, as stated at the beginning of this chapter.

Given the above model of crack growth, a measurement model is now developed. Consider the case when measurements of crack length are available at arbitrary instants of time. The measurement equation is given by:

$$y_t(\zeta) \equiv \frac{\theta_t^{1-\frac{m}{2}}}{1-\frac{m}{2}} + n_t(\zeta) \tag{4.28}$$

where n_t is a zero mean stationary white Gaussian noise of known variance.

$$y_t(\zeta) - y_0(\zeta) = \psi(\zeta, t_0) + n_t - n_0 = \Omega(\zeta)\int_0^t (\sigma_\tau)^m d\tau + \int_0^t (\sigma_\tau)^m v_\tau(\zeta) d\tau + n_t - n_0 \tag{4.29}$$

$$z_k = \Omega(\zeta)\int_{t_{k-1}'}^{t_k} (\sigma_\tau)^m d\tau + \int_{t_{k-1}'}^{t_k} (\sigma_\tau)^m v_\tau(\zeta) d\tau + n_{t_k} - n_{t_{k-1}'} \tag{4.30}$$

$$z_k = y_{t_k} - y_{t_{k-1}'} \qquad \text{for } k=1,2,\ldots,q \tag{4.31}$$

We consider block loading, i.e. $\sigma_t = \sigma_k$ for all $t_{k-1} < t \le t_k$, and homogeneous material properties which yields constant $\alpha_k = \alpha$. This gives:

$$z_k = \Omega(\zeta)\sigma_k^m (t_k - t_{k-1}') + \sigma_k^m \sqrt{\alpha}\beta_{t_k - t_{k-1}'}(\zeta) + \varepsilon_k(\zeta) \tag{4.32}$$

where $\varepsilon_k(\zeta) = n_{t_k}(\zeta) - n_{t_{k-1}'}(\zeta)$, with $E[\varepsilon_k] = 0$, and $Var[\varepsilon_k] = \sigma_n^2 (t_k - t_{k-1}')$.

$$\text{Then let: } Z \equiv \begin{bmatrix} z_1 \\ \vdots \\ z_q \end{bmatrix}; \quad H \equiv \begin{bmatrix} \sigma_1^m (t_1 - t_0') \\ \vdots \\ \sigma_q^m (t_q - t_{q-1}') \end{bmatrix}; \quad E \equiv \begin{bmatrix} e_1 \\ \vdots \\ e_q \end{bmatrix} \tag{4.33}$$

Where $e_k = \sigma_k^m \sqrt{\alpha}\beta_{t_k - t_{k-1}'}(\zeta) + \varepsilon_k(\zeta)$, and thus:

$$E[e_k] = 0 \text{ and } Var[e_k] = (\sigma_k^{2m}\alpha + \sigma_n^2)(t_k - t_{k-1}') \tag{4.34}$$

So $Z = H\Omega + E$ (4.35)

This leads to:

$$R = \mathrm{Cov}(E) = \begin{bmatrix} \left(\sigma_1^{2m}\alpha + \sigma_n^2\right)\left(t_1 - t_0'\right) & 0 & \cdots & 0 \\ 0 & \ddots & & \vdots \\ \vdots & & & 0 \\ 0 & \cdots & 0 & \left(\sigma_q^{2m}\alpha + \sigma_n^2\right)\left(t_q - t_{q-1}'\right) \end{bmatrix} \tag{4.36}$$

Then the weighted least squares estimator for Ω based on a batch of data sets is given by:

$$\hat{\Omega} = \left[H^T R^{-1} H\right]^{-1} H^T R^{-1} Z \tag{4.37}$$

To reformulate the batch estimator as a recursive estimator so that the estimate can be updated with each measurement, note that:

$$\left[H^T R^{-1} H\right]_q^{-1} = 1 \Big/ \sum_{k=1}^{q} \frac{\sigma_k^{2m}\left(t_k - t_{k-1}'\right)}{\left(\sigma_k^{2m}\alpha + \sigma_n^2\right)} \tag{4.38}$$

and

$$\left(H^T R^{-1} Z\right)_q = \sum_{k=1}^{q} \frac{\sigma_k^{m} z_k}{\left(\sigma_k^{2m}\alpha + \sigma_n^2\right)} \tag{4.39}$$

are both scalar quantities, and thus:

$$\hat{\Omega}_q = \frac{\left[H^T R^{-1} Z\right]_q}{\left[H^T R^{-1} H\right]_q} \tag{4.40}$$

after q measurements. Then the update for a new measurement is given by:

$$\left[H^T R^{-1} H\right]_{q+1} = \left[H^T R^{-1} H\right]_q + \frac{\sigma_{q+1}^{2m}\left(t_{q+1} - t_q'\right)}{\left(\sigma_{q+1}^{2m}\alpha + \sigma_n^2\right)}; \quad \left[H^T R^{-1} Z\right]_{q+1} = \left[H^T R^{-1} Z\right]_q + \frac{\sigma_{q+1}^{m} z_{q+1}}{\left(\sigma_{q+1}^{2m}\alpha + \sigma_n^2\right)}$$

and then stated for completeness: $\hat{\Omega}_{q+1} = \dfrac{\left[H^T R^{-1} Z\right]_{q+1}}{\left[H^T R^{-1} H\right]_{q+1}}$ (4.41)

4.5 Estimator Results

The equations presented in the previous section were implemented and demonstrated with the experimental data for 7075-T6 aluminum. Since these experiments were not conducted using constant amplitude loading, equation 4.41 was implemented with updates each cycle. The data is not from center-cracked specimens since the cracks do not start at the same time, but this does not affect the results in any obvious way. The crack lengths from both sides were averaged together. When used cycle by cycle, the estimator effectively becomes the average of z_k / σ_k^m, and is not sensitive to the values of α and σ_n, which were set equal to each other. Since the experiments had significant changes in load amplitude, crack opening stress is highly significant to proper modeling of crack growth. In order to calculate the non-dimensional stresses σ_k, the crack opening stresses must be estimated. This estimate was performed by using the dynamic crack opening stress formulation used by the state space model of Patankar and Ray (2000) given in section 4.3, using the ultrasonic measurement of crack length for all values related to crack length, particularly dc/dn and geometry factor. The value of dc/dn is required to determine the state of constraint between plane strain and plane stress. Since the experimental crack growth increment, dc/dn, data is quite noisy even after filtering, practical implementations of this technique should use a better measure of dc/dn. This could be the crack growth equation itself.

The ultrasonic data was used after significant amount of signal processing as discussed in the previous chapter. The only filtering was the initial backward averaging. Thus these simulations reflect what is possible on-line. As can be seen from Figure 4-1, there is a transient period before the estimate becomes constant. In practice, starting with an initial estimate of Ω would reduce this transient for the average case. As can be seen from Figure 4-2 through Figure 4-9, the estimate of Ω leads to a conservative estimate of crack growth in every case (e.g. the projected failure occurs before the actual failure). These results are very good, particularly considering that the estimator was used very early in the cracking process and not updated with new estimates or new crack length measurements. Also, the estimator could have been used earlier in the experiment with a corresponding reduction in accuracy.

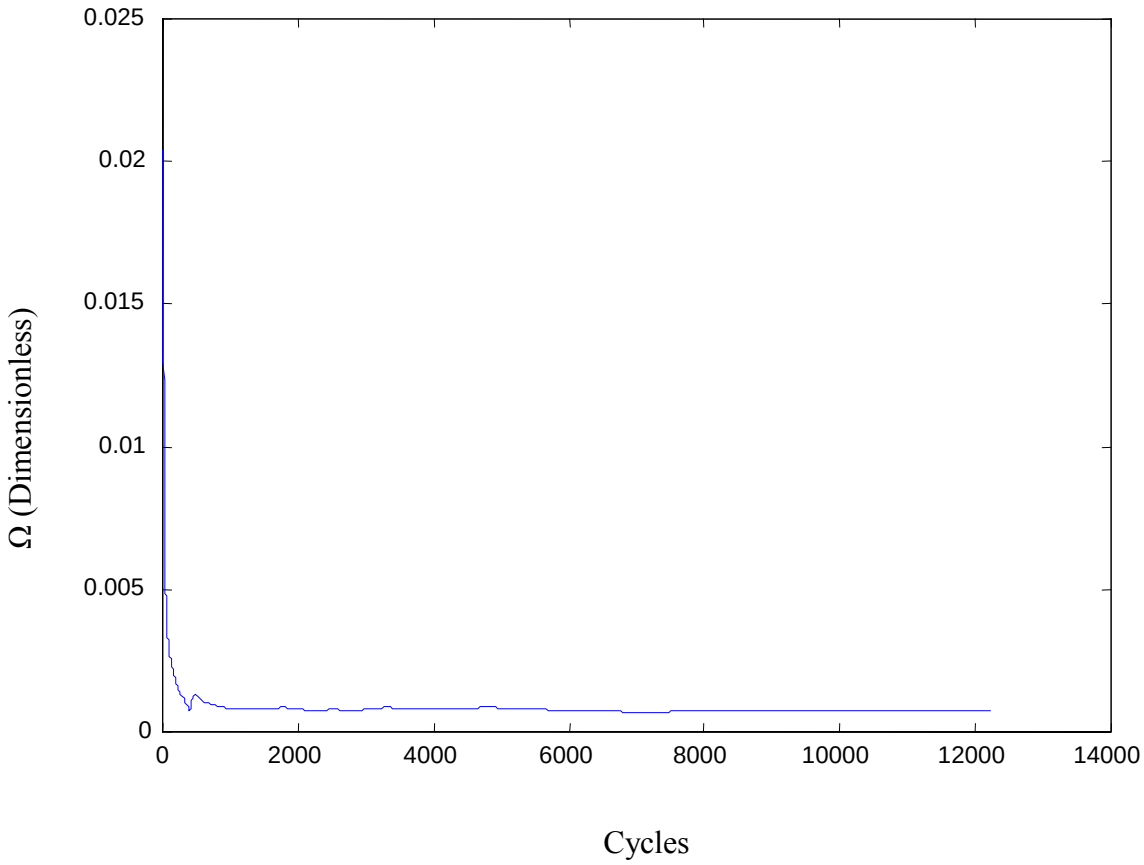

Figure 4-1 Estimator Results

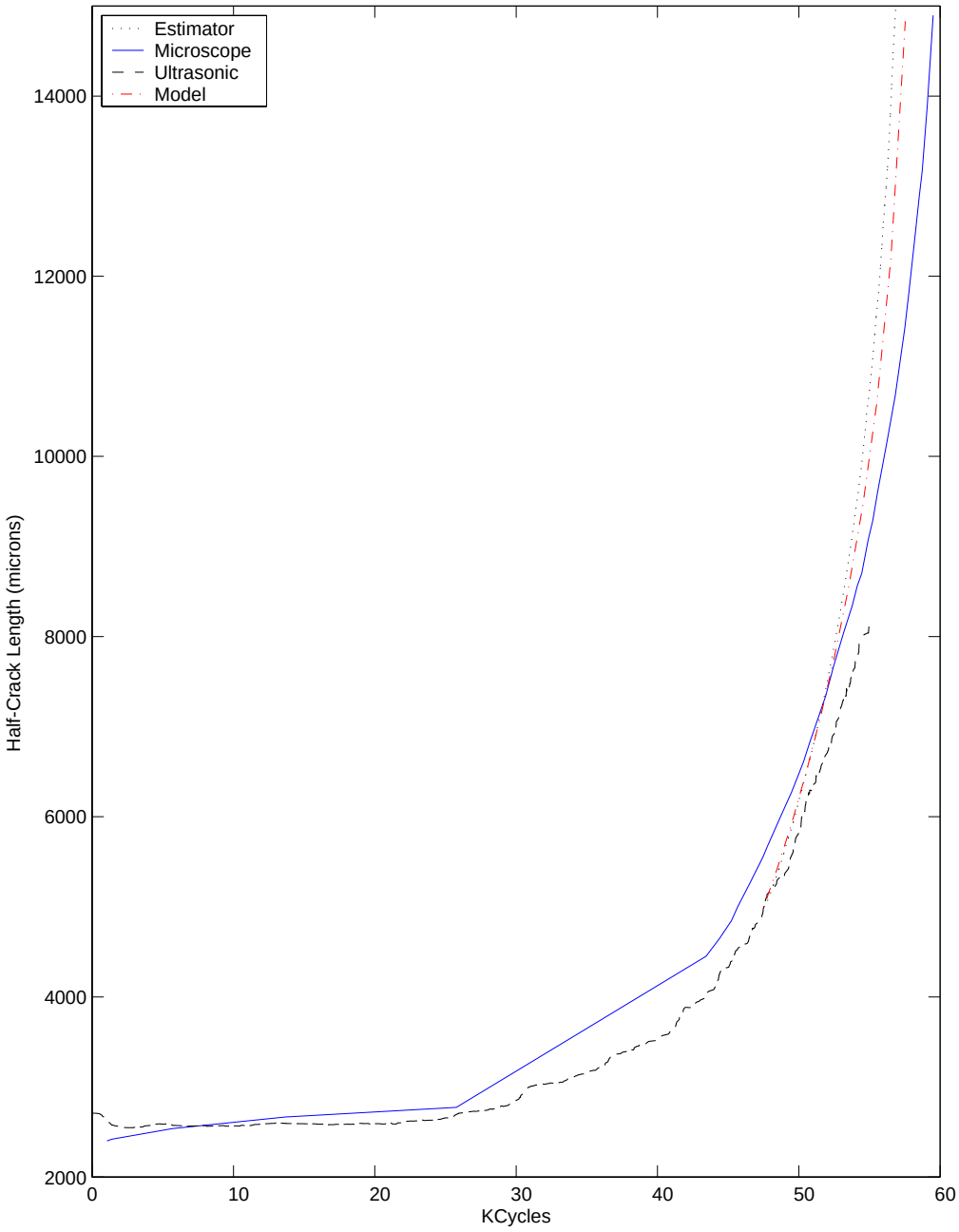

Figure 4-2 Results from parameter estimator and state-space model Specimen Sk. 4

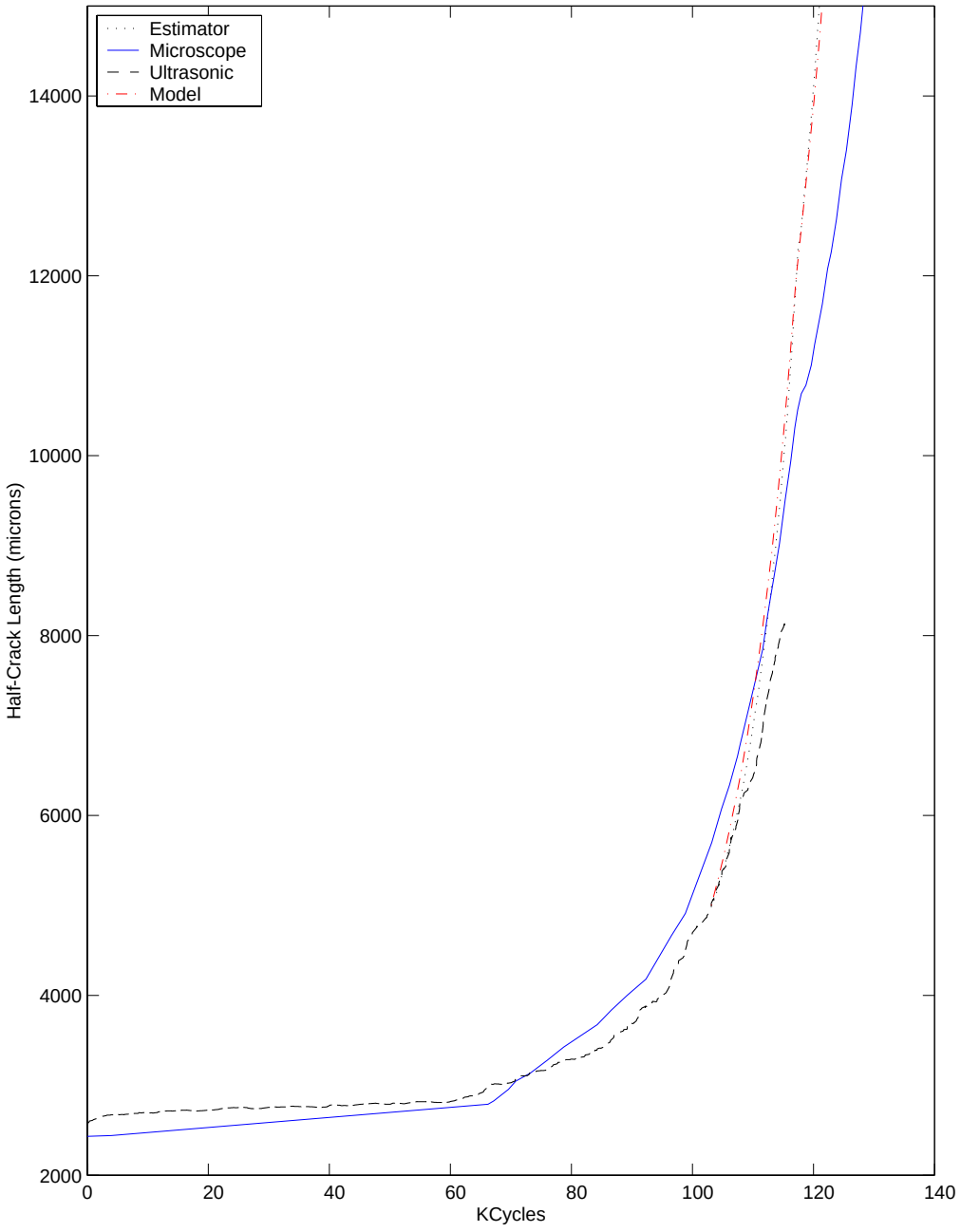

Figure 4-3 Results from parameter estimator and state-space model Specimen Sk. 5

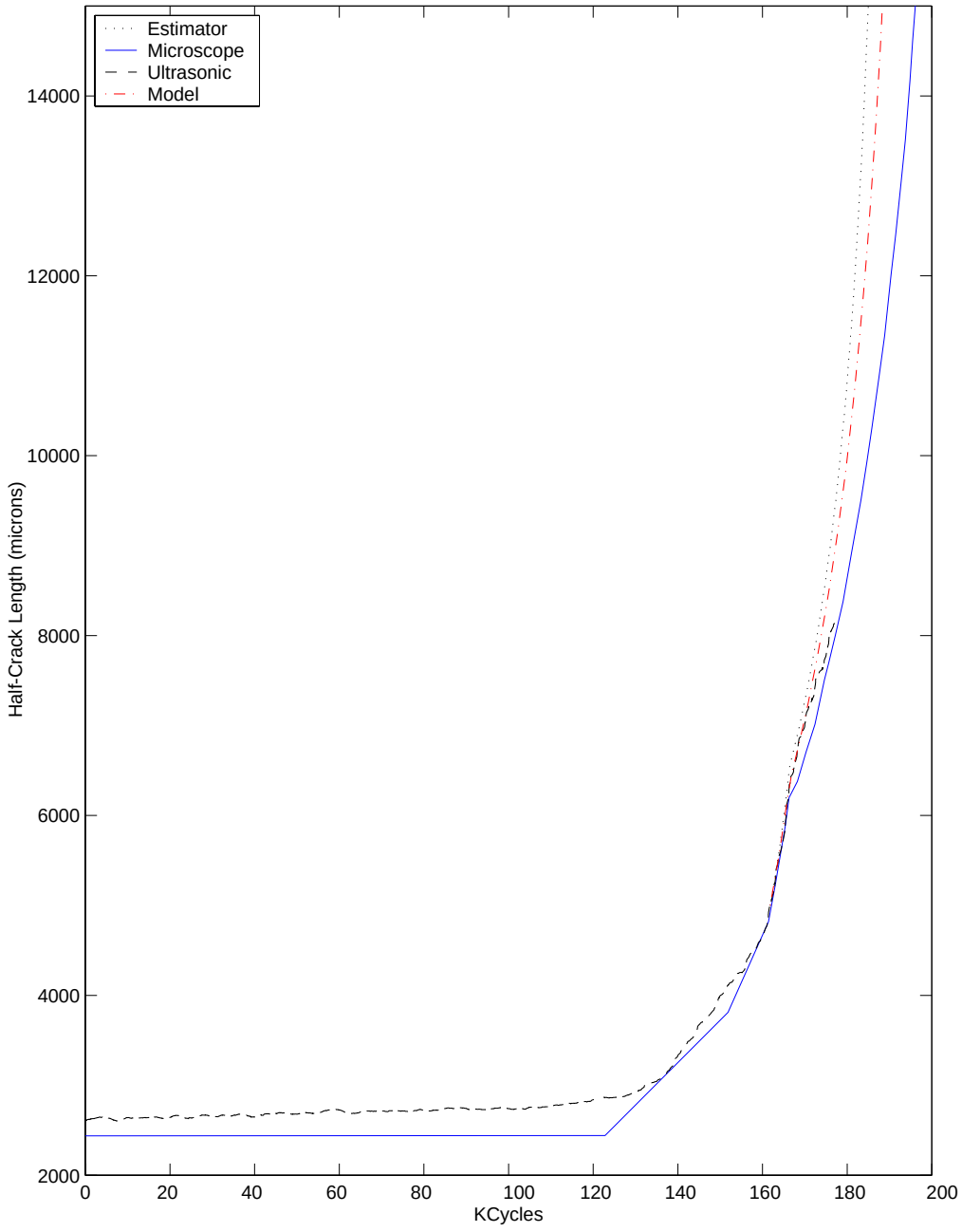

Figure 4-4 Results from parameter estimator and state-space model Specimen Sk. 6

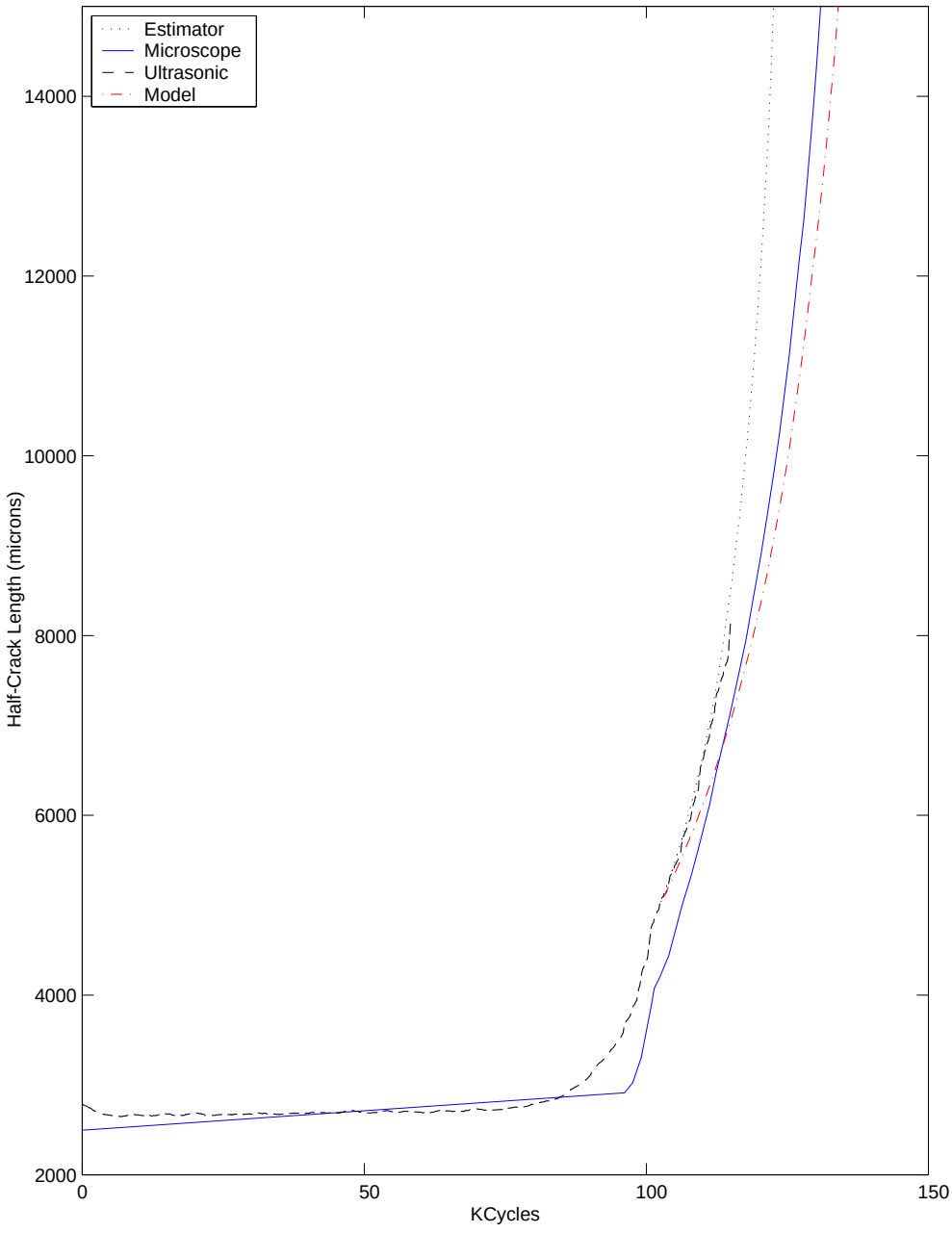

Figure 4-5 Results from parameter estimator and state-space model Specimen Sk. 7

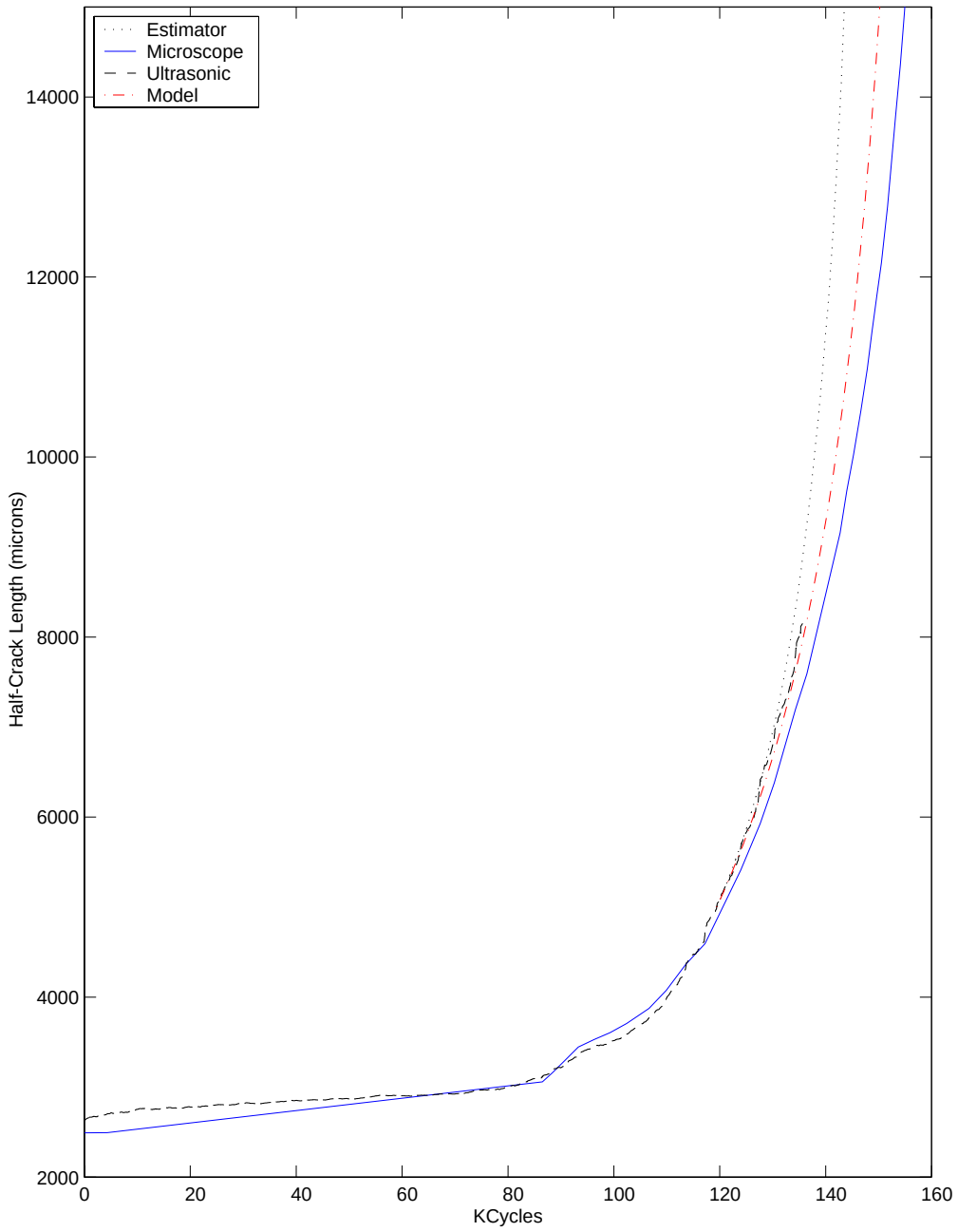

Figure 4-6 Results from parameter estimator and state-space model Specimen Sk. 8

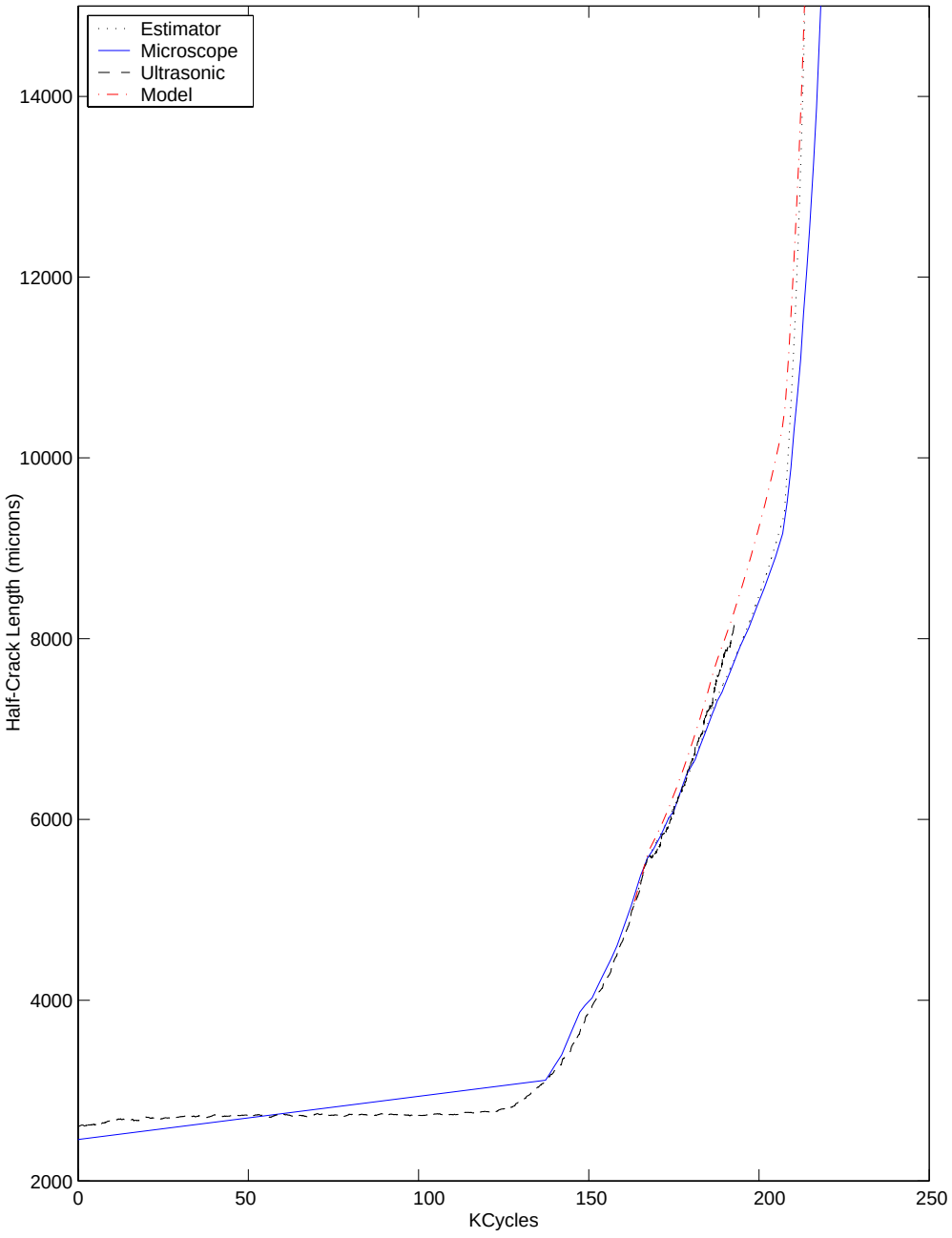

Figure 4-7 Results from parameter estimator and state-space model Specimen Sk. 9

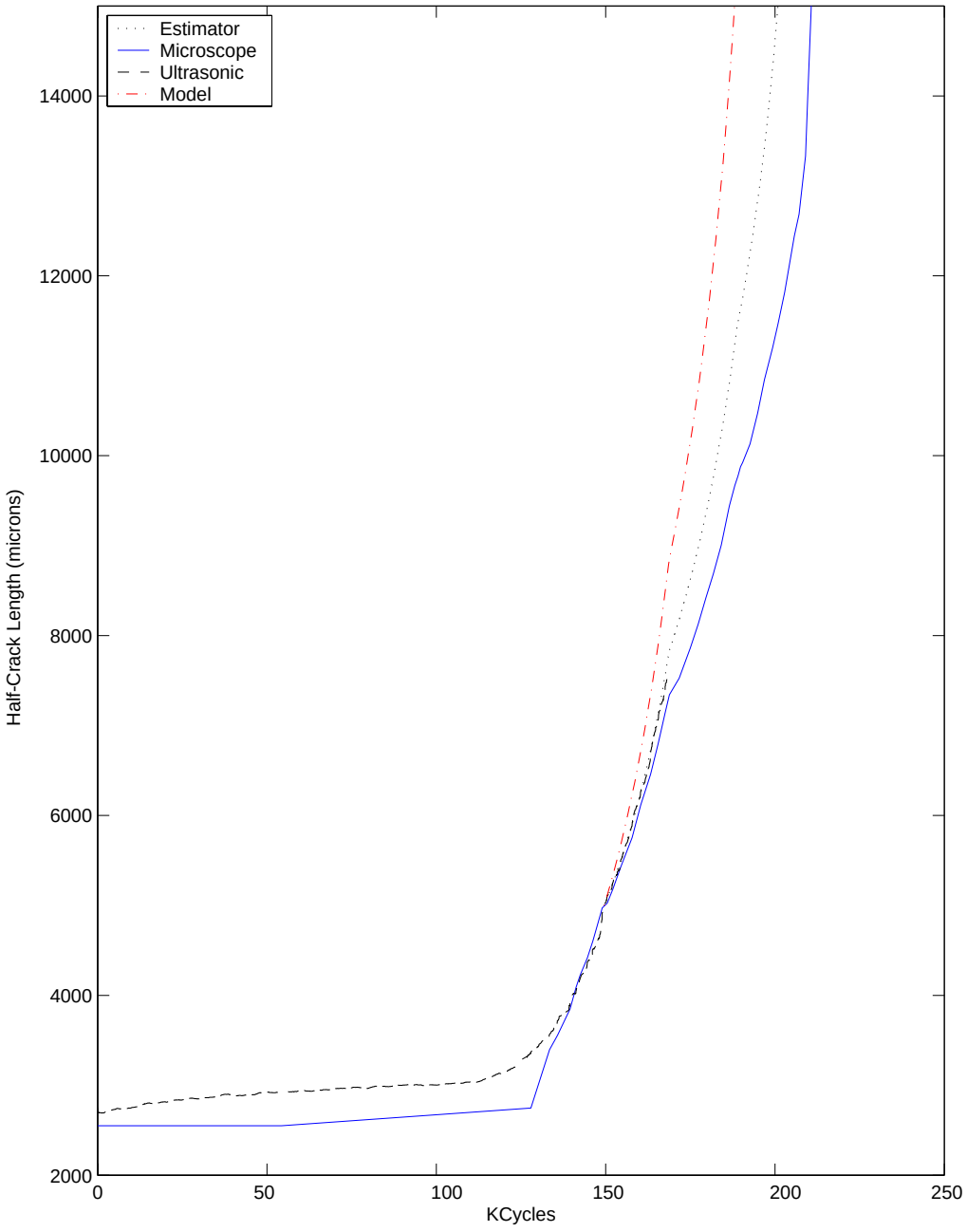

Figure 4-8 Results from parameter estimator and state-space model Specimen Sk. 10

Chapter 5

Conclusions and Recommendations For Future Work

5.1 Conclusions

The main goal of this research is to demonstrate a sensing system that is capable of measuring fatigue crack damage in real time for information-based decision and control. Clearly, more work needs to be done under laboratory conditions before such a system can be deployed into service. However, this work has outlined many of the important issues including demonstration of on-line measurement techniques, and has significantly hastened the practicality of such an on-line damage sensing system.

The main thrust of this research has been to develop a facility capable of generating fatigue cracks and measuring their propagation on-line. In the process of designing and building this facility the following important tasks have been accomplished.

The image acquisition and online visualization with the microscope has been successful at allowing accurate crack length measurements without slowing the progress of testing to any appreciable degree. Automation of the microscope and the ability to save a large number of images have allowed a much higher number of optical measurements to be taken with the same amount of operator involvement. The large capacity to save images has also allowed automation of image acquisition, thus freeing the operator from constant monitoring in the early stages of crack growth. This is particularly important due to the difficulty of measuring crack length given only one image. Since the microscope requires oblique lighting, it is impossible to remove all crack indications with polishing. Thus it is possible for the operator to erroneously imagine occurrence of crack growth when there is none. Crack growth is easy to discern when switching rapidly between images. The saved images also form a record of crack growth, which is useful in reviewing the progress of crack propagation in post-test analysis.

The collection of software packages developed during this work provide a platform for other efforts of this type and allow flexibility in adding or deleting measuring instruments in a robust manner. The ability to take real-time measurements on a cycle-by-cycle basis and synchronized to the load is an important improvement over most fatigue crack growth apparatus, particularly for efforts to measure crack opening stress.

As originally proposed, this work was planned to concentrate on the propagation of existing through cracks of known initial length. Although this is a challenging problem, a practical online damage sensing system must be able to detect cracks as they appear. It is extremely desirable to be able to obtain a measurement of crack damage before the it grows to a length that is measurable with inspection techniques available under routine maintenance. This research demonstrates successful usage of ultrasonic techniques for measurement of very small cracks. Particularly it is possible to use ultrasonic signal attenuation as a measure of crack length and to independently measure fatigue cracks on either side of a notch. Furthermore, at least in the case of 6061-T6 aluminum alloy, the progress of crack initiation can be measured before surface cracks appear. It appears that the measurements of crack growth in the 7075-T6 alloy do not allow prediction of the onset of surface cracks in the present experimental environment. However, the measurements do track the progression of crack growth very well after the formation of surface cracks and thus allow the prediction of the transition from 2-D cracks to 1-D through cracks. It was successfully demonstrated that a self-calibrating ultrasonic attenuation technique can be used to provide an ultrasonic measurement of crack length.

The work with alternating current potential drop (ACPD) measurements has not yet been very effective. Apparently measurements taken with this technique have not been sensitive to small cracks and often been non-repeatable for larger cracks. Since this is a very useful laboratory crack length measurement technique that other researchers have reported using successfully, future efforts to overcome the problems are warranted.

One of the initial goals of this research was to combine fatigue crack damage measurements with the predictions of a fatigue crack damage model in order to provide a higher fidelity estimate of fatigue crack damage than is possible from either method

alone. A proposed technique of combining these two methods is presented in Appendix B. As this research evolved to a greater emphasis on the early stages of crack formation, the lack of stochastic models of 2-D crack growth and the difficulty in determining which crack configuration to model has led to a de-emphasis of this technique. This is because the parameter estimation technique presented in Chapter 4 is potentially of much greater importance. It was shown that in the general case, a parameter estimator can predict the future progression of fatigue crack damage in a structure with lower error than a fatigue crack damage model based on typical parameters. This technique could be very powerful if ultrasonic measurements of early crack growth could be incorporated into an estimator. Even in the large crack regime, a properly tuned estimator would be an important development.

5.2 Recommendations For Future Work

As outlined in the first chapter of this dissertation, the early stages of fatigue crack growth are difficult to predict and model due to a large number of possible crack configurations. However, the experimental observations suggest that ultrasonic measurements is capable of discriminating between different crack configurations. This work would require the capability of optically monitoring the notch face as well as the surface of a specimen.

Although the 7075-T6 alloy is still an important material due to the large installed base, its poor fatigue resistance has led to the adoption of over-aged high-strength aluminum alloys. Thus similar studies of more advanced materials are called for.

The fatigue crack damage models presented in Chapter 4 either have not been extended to 2-D cracks or those extensions are not yet firmly established based on the fundamental principles of physics. Since this part of the fatigue crack growth process is vital to the service life prediction of mechanical structures, this is the work that needs to be explored further.

The research work reported in this dissertation was done using a very simple model of ultrasonic signal propagation through a specimen. These results could be

further improved more advanced modeling of ultrasonic waves and their interactions with cracks.

The parameter estimation technique outlined in Section 4 of Chapter 4 can be extended to estimate the additional parameters required to successfully model crack growth under variable amplitude loading.

Since the imaging system is automated and can reliably take high quality microscope images of the specimen, an automated crack recognition system can be constructed, particularly for the first millimeter of crack growth. This part of the experiment is the most tedious for the operator, and thus its automation would be a great improvement. Beyond this range, an automated focusing system would be required.

Appendix A

Hydraulic System Equations

Variables:

$P_T \equiv$ Tank pressure (assumed constant)

$P_R \equiv$ Return pressure

$P_a \equiv$ Accumulator pressure (state)

$P_P \equiv$ Pump outlet pressure (assumed constant)

$Q_P \equiv$ Pump volumetric flow

$Q_R \equiv$ Return flow

$Q_c \equiv$ Flow into cylinder from pump side

$x \equiv$ Servo Valve position (x and dx/dt are states)

$y \equiv$ Cylinder position (y and dy/dt are states)

$B \equiv$ Bulk Modulus of hydraulic fluid

$P_1 \equiv$ Cylinder extend side pressure (state)

$P_2 \equiv$ Cylinder retract side pressure (state)

$k_i \equiv$ valve input parameter

$u \equiv$ valve drive current (control input)

$\zeta_v \equiv$ Servo valve damping ratio

$\omega_{n\,valve} \equiv$ Servo valve natural frequency

$A_1 \equiv$ Cylinder extend area

$A_2 \equiv$ Cylinder retract area

$M \equiv$ Effective mass of cylinder

$D \equiv$ Cylinder damping

The differential equation governing the accumulator pressure is:

$$\dot{P}_a = (Q_P - Q_c) \cdot \frac{nBP_a^{\frac{n+1}{n}}}{nVP_a^{\frac{n+1}{n}} + nP_aC_a^{\frac{1}{n}} + BC_a^{\frac{1}{n}}} \quad \text{(A 1)}$$

Where C_a is defined as follows. The nitrogen in the accumulator is assumed to undergo polytropic expansion when the pressure in the accumulator pressure fluctuates. Then $P_a V_{N_2}^{\frac{1}{n}} = const. = C_a$ where $n \in [1,1.4]$. The case n=1 is associated with isothermal expansion and n=1.4 is associated with adiabatic expansion.

The differential equations governing the cylinder pressures

$$\dot{P}_1 = \frac{B}{V_1} Q_1 - \frac{A_1 B}{V_1} \dot{y} \quad \text{(A 2)}$$

$$\dot{P}_2 = \frac{B}{V_2} Q_2 - \frac{A_2 B}{V_2} \dot{y} \quad \text{(A 3)}$$

The differential equation governing the motion of the cylinder is:

$$M \frac{d^2y}{dt^2} + D \frac{dx}{dt} + K_{eff} = P_1 A_1 - P_2 A_2 \quad \text{(A 4)}$$

The differential equation governing the position of the valve is given by:

$$\frac{d^2x}{dt^2} + 2\zeta_v \omega_{n\,valve} \frac{dx}{dt} + \omega^2_{n_{valve}} = k_i u \quad \text{(A 5)}$$

The hydraulic fluid flows are given by

$$Q_p = K_p \sqrt{P_p - P_a} \quad \text{(A 6)}$$

$$Q_c = K_v x \sqrt{P_a - P_{x_1}} \quad \text{(A 7)}$$

$$Q_R = K_v x \sqrt{P_{x_2} - P_R} \quad \text{(A 8)}$$

$$Q_R = K_R \sqrt{P_R - P_T} \quad \text{(A 9)}$$

If 2*d is valve deadband, the cylinder flows Q_1 and Q_2 are Q_R and Q_c as follows:

$Q_1 = Q_R$ and $Q_2 = Q_c$ if $x-d>0$ (cylinder extending), and $Q_1 = Q_c$ and $Q_R = Q_c$ if $x+d<0$ (cylinder retracting). If $-d<x<d$ then Q_1, Q_2, Q_R and Q_c are zero.

Appendix B

Stochastic Estimation of Fatigue Crack Size

The deterministic fatigue crack growth model presented in chapter 2 adequately models only the mean fatigue crack path. By definition, deterministic models fail to represent the variability seen in fatigue crack growth in real materials. A desire to model this variability leads to stochastic models of crack growth.

The uncertainties in fatigue crack growth in engineering structures result from three primary sources:

- Uncertainty in initial crack size;
- Uncertainty in the load applied to the structure; and
- Uncertainty inherent in the crack growth process itself.

Since the first two sources of uncertainty are tightly controlled in a test such as the one proposed here, the predominance of the variability in the acquired data is due to the third source of uncertainty. However, the proposed test suffers from the additional source of uncertainty in that crack length measurements are subject to noise and the imprecision of instruments.

A variety of stochastic crack length models have been proposed in the literature. Proposed stochastic fatigue crack growth models generally fall into the categories of discrete or jump Markov processes or continuous Markov diffusion processes. In a jump process model, the fatigue crack length is divided into discrete damage states and transition between states is modeled as Markov jumps (Bogdonoff and Kozin, 1985). A comprehensive list of references for diffusion models of crack growth can be found in Sobczyk and Spencer (1992). Crack growth can be modeled by nonlinear stochastic differential equations satisfying the Itô conditions (Oksendal, 1992). This leads to the solution of the Komogorov forward and backward diffusion equations, which are nonlinear partial differential equations, that, in general, must be solved numerically by finite element or mixed finite element-finite difference methods (Enneking, 1991). These models can be used for life prediction and risk analysis (Bolotin, 1989; Sobczyk and Spencer, 1992). However, due to the numerical complexity, these models are not suitable

for on-line damage prediction. Ray and Tangirala (1996) show that since these models use additive noise instead of multiplicitive noise, the differential equations can be constructed in the Weiner form instead of the Itô form. This allows a solution of the stochastic differential equations with an Extended Kalman Filter (EKF) (Jazwinski, 1970).

B.1 Extended Kalman Filter Approach to Stochastic Estimation of Fatigue Crack Size

The extended Kalman Filter approach to fatigue crack growth modeling in the absence of measurements was developed by Tangirala and Ray (1996). The vector stochastic differential equation for fatigue crack growth is given by:

$$\frac{dc(\omega,t)}{dt} = \frac{d\mu}{dt}\upsilon(\omega,t)\forall t \geq t_{0;}$$

$$\text{given } E[c(\omega,t)] = \mu_0 \text{ and } \text{cov}[c(\omega,t_0)] = P_0 \qquad \text{(B 1)}$$

where c(ω,t) is the crack length, υ(ω,t) is a stochastic process used to introduce uncertainty into $\frac{dc(\omega,t)}{dt}$; μ represents the mean crack growth path given by the deterministic model; and w and t represent the sample point and the time parameter of the stochastic processes respectively. Since crack growth is a correlated random process and growth is never negative, Eq. B 1 is reformulated:

$$\frac{dc(\omega,t)}{dt} = \frac{d\mu}{dt}\upsilon(x(\omega,t))\forall t \geq t_{0;}$$

$$\text{given } E[c(\omega,t)] = \mu_0 \text{ and } \text{cov}[c(\omega,t_0)] = P_0 \qquad \text{(B 2)}$$

where the function υ(x(ω,t)) is chosen to be non-negative such that a negative crack growth rate is precluded; and x(ω,t) is an auxiliary stochastic process that models non-white wide-sense stationary noise as the output of a shaping filter and is given by:

$$\frac{dx(\omega,t)}{dt} = \xi(-x(\omega,t) + w(\omega,t))\forall t \geq t_{0;}$$

$$\text{given } E[x(\omega,t)] = x_0 \text{ and } \text{cov}[x(\omega,t_0)] = \frac{\xi Q_0}{2} \qquad \text{(B 3)}$$

where w(ω,t) is stationary zero-mean white Gaussian noise with intensity Q_0 and is independent of the initial crack length c(ω,t) for all $t \geq t_0$.

The stochastic differential equations (B 2) and (B 3) are now combined to yield the augmented stochastic vector $\chi=[c^T\ x^T]^T$. Linearization of the augmented state equation at the current state yields the local state transition matrix. This allows the computation first two moments of x(w,t) conditioned on the history of applied stresses and initial conditions of x by solution of the extended Kalman filter equations. The system model is given as:

$$\begin{bmatrix}\dot{c}\\ \dot{x}\end{bmatrix}=\begin{bmatrix}d\mu/dt\,\upsilon(\omega,t)\\ -\xi x(\omega,t)\end{bmatrix}+\begin{bmatrix}0\\ \xi\end{bmatrix}w(\omega,t);or$$

$$\chi = f(\chi(\omega,t),t)+G(t)w(\omega,t)$$

$$\text{given } E[\chi(\omega,t_0)]=\begin{bmatrix}\mu_0\\ x_0\end{bmatrix} \text{ and } \operatorname{cov}[\chi(\omega,t_0)]=\begin{bmatrix}P_0 & 0\\ 0 & \frac{\xi Q_0}{2}\end{bmatrix} \tag{B 4}$$

The measurements occur at discrete times, t_1, t_2 ,...,t_i (possibly at arbitrary intervals). Measurements are modeled as:

$$z(t_i)=H\chi(t_i)+v(t_i)$$

$$\text{given } E[v(w,t_i)]=0 \text{ and } \operatorname{cov}[v(w,t_i)]=R(t_i) \tag{B 5}$$

Estimates of the crack length for times between measurements are given by the solution to:

$$\dot{\hat{\chi}}(t) = f(\hat{\chi}(t),t)$$

$$\dot{P}(t) = F(\hat{\chi}(t),t)P(t)+P(t)F^T(\hat{\chi}(t),t)+G(t)Q(t)G^T(t) \tag{B 6}$$

$$\text{where } F(\hat{c}(t),t)=\left.\frac{df(\chi(t),t)}{dc(t)}\right|_{c(t)=\hat{c}(t)}$$

Measurement updates are performed at discrete times (but not necessarily at equal intervals). The update equations are given by:

$$K(t_i)=P^-(t_i)H^T(t_i)[H(t_i)P^-(t_i)H^T(t_i)+R(t_i)]^{-1}$$

$$\hat{\chi}^+(t_i)=\hat{\chi}^-(t_i)+K(t_i)[z_i-H(t_i)\hat{\chi}^-(t_i)] \tag{B 7}$$

$$P^+(t_i)=P^-(t_i)-K(t_i)H(t_i)P^-(t_i)$$

Where $P^{-}(t_i)$ and $\hat{\chi}^{-}(t_i)$ are the estimated covariance and estimated crack length prior to the incorporation of measurements respectively, and $P^{+}(t_i)$ and $\hat{\chi}^{+}(t_i)$ are the covariance and length estimates after the incorporation of measurements. Equations (B 6) and (B 7) are used recursively starting with an initial measurement:

$$\hat{\chi}^{+}(t_0) = H^{+} z(t_0)$$

$$\text{and } P(t_0) = H^{+} R(t_0) H^{+T} \tag{B 8}$$

Where the notation H^{+} indicates a generalized inverse because, in general, H is not square. Since in the case of the proposed work, there are at least as many sensors as cracks, taking the generalized inverse of H does not present any problems, but it might if there were more cracks than sensors. As stated above, the measurements need not be taken at equally spaced intervals. This is because between measurements, the damage is tracked by the damage model. However, the quality of the estimates is improved by measurements.

B.2 Lognormal Distributed Crack Length Model Formulation

Crack length, $a(\omega,t)$, is assumed to be lognormal distributed and is defined by

$$a(\omega,t) = \mu_a(t) \exp\left(z(\omega,t) - \frac{\sigma_z^2(t)}{2} \right) \quad \forall t \geq 0 \tag{B 9}$$

where t indicates the number of cycles, $\mu_a(t) = E[a(\omega,t)]$, and $\mu_a(t) > 0 \quad \forall\, t \geq 0$. Using expressions for the mean and variance of lognormal distributed random variables, Eq. (4.9) implies

$$\begin{aligned} E\left[a(\omega,t)\right] &= \mu_a(t) \\ \sigma_a(t) &= \mu_a(t) \sqrt{e^{\sigma_z^2} - 1} \end{aligned} \tag{B 10}$$

$z(\omega,t) \sim N\left(0, \sigma_z^2(t)\right)$ is the normalized zero-mean process defined as

$$z(\omega,t) = \ell n\left(\frac{a(\omega,t)}{\mu_a(t)} \right) - E\left[\ell n\left(\frac{a(\omega,t)}{\mu_a(t)} \right) \right] \tag{B 11}$$

From Eq. (4.11) it follows that

$$E\left[\ell n\left(\frac{a(\omega,t)}{\mu_a(t)}\right)\right] = -\frac{\sigma_z^2(t)}{2} = -\frac{1}{2}Var\left[\ell n\left(\frac{a(\omega,t)}{\mu_a(t)}\right)\right] \quad \text{(B 12)}$$

which is satisfied for any lognormal distribution. The crack propagation process is an explicit fuction of the continuous variable $\mu_a(t)$ and is only implicitly dependent of the parameter, t, as seen in Eq. B 9. Therefore, it is appropriate to model the stochastic processes, $a(\omega,t)$ and $z(\omega,t)$, and their mean square derivatives with a continuous function of $\mu_a(t)$ as the independent vairable in lieu of time, t. To this effect, we introduce a function of the average crack length, $\mu_a(t)$ as:

$$\tau(t) = \ell n\left(\frac{\mu_a(t)}{\mu_a(0)}\right) \quad \text{(B 13)}$$

Then *z* is a random variable given by the equation:

$$dz_\tau = \vartheta\, d\tau \quad \text{(B 14)}$$

where the Gaussian random variable $\vartheta \sim N(0,Q)$ is assumed to be independent of z_0. The physical interpretation of this is that after an inspection, the damage of a stressed component is represented by the mean $\mu_a(0)$ and variance $\sigma_a^2(0)$ of crack length. Subsequently, as the structural component is subjected to load cycles, the mean crack length, $\mu_a(t)$ is obtained via the deterministic model of crack growth; while $\sigma_a^2(t)$ and $\tau(t)$ are obtained from Eqs. (B 10) and (B 13), respectively. The impact of mechanical load cycles on the uncertainty of the crack growth behavior is realized by the variance Q of the random variable ϑ. This variance of crack length is then, purely a result of the uncertainty in the crack growth process and is independent of the initial uncertainty, $\sigma_a^2(0)$, which is dependent on the crack length measurement noise. The variance of crack length as a function of time after the inspection is then the sum of the variance due to the inspection uncertainty and the variance due to uncertainty in the crack growth process. For constant amplitude cyclic stresses, Q remains constant; however, for variable amplitude loading (which has not yet been experimentally verified and is therefore not included in this proposal), Q must vary with load and the random variable ϑ becomes a stochastic process.

B.3 Weighted Least Squares Estimation of Fatigue Crack Size

By using the LDCL stochastic model developed in section B 2, the stochastic differential equation that was solved in section B 1 by an extended Kalman filter is replaced by a static stochastic model. This means that a static least squares estimator can be used, thus saving computational effort over the Kalman filter. The weighted least squares estimator finds a weighted average, where the weight of each term in the average is reduced by its variance. If there are N measurements at time t_k, the measurement equations are given by:

$$Z_i = a(t_k) + v_i(t_k) \qquad i \in (1, N) \tag{B 15}$$

where $a(t_k)$ is the crack length; $v_i(t_k)$ is the noise associated with the measurement; by assumption $E[v_i] = 0$; $E[v_i^2] = \sigma_i^2$; $E[v_i v_j] = 0$ for $i \neq j$

Since the measurements and the crack length are scalars and the errors in each term are assumed to be independent, the crack length estimate is given by (Stark and Woods,1994):

$$\hat{a}(t_k) = \frac{\mu(t_k)/\sigma_a^2(t_k^-) + Z_1(t_k)/\sigma_{z_2}^2 + Z_{2(t_k)}/\sigma_{z_2}^2 + \ldots + Z_N(t_k)/\sigma_{z_n}^2}{(1/\sigma_a^2(t_k^-) + 1/\sigma_{z_1}^2 + 1/\sigma_{z_2}^2 + \ldots + 1/\sigma_{z_n}^2)} \tag{B 16}$$

Where μ is the estimate from the deterministic model of the crack length a at time t_i and the Z_j are the measurements (scaled to units of crack length). The estimated covariance of the crack length after the measurement is given by:

$$\sigma_a^2(t_k^+) = 1/(1/\sigma_a^2(t_k^-) + 1/\sigma_{z_1}^2 + 1/\sigma_{z_2}^2 + \ldots + 1/\sigma_{z_n}^2) \tag{B 17}$$

The estimator works as follows: The initial crack length is given by B 16, with μ_a and σ_a set to zero, after an initial measurement. The covariance is calculated from B 17 with the σ_a term on the right hand side of the equation set to zero. At the next measurement, μ_a is calculated from the deterministic model, and σ_a is calculated as shown in eqn. B 10/B 13. Then the new estimate is produced from B 16 and B 17. One of the advantages of this estimator structure is that it can be used with any of the measurements missing,

simply by deleting the terms in equations B 16 and B 17 that are associated with the missing measurements.

References

Anderson, T. L.,1995, *Fracture Mechanics, Fundamentals and Applications*, CRC Press, Boca Raton

Balas, G. J., Doyle, J. C., Glover, K., Packard, A. and Smith, R., 1993, *μ-Analysis and Synthesis Toolbox for use with MATLAB*, The Math Works Inc., Natick, MA

Bannantine, J. A., Comer, J. J. and Handrock, J. L., 1990, *Fundamentals of Metal Fatigue Analysis*, Prentice Hall, Englewood Cliffs, New Jersey.

Bogdonoff, J. L. and Kozin, F., 1985, *Probabilistic Models of Cumulative Damage,* Wiley Interscience, New York.

Bolotin, V. V., 1989, *Prediction of Service Life for Machines and Structures*, ASME.

Chang, J.B. and Engle, R.M., "Improved Damage Tolerance Analysis Methodology", Journal of Aircraft, Vol. 21, No. 9, September 1984.)

Connolly, M. P., "the Measurement of Regular and Irregular Surface Cracks Using the Alternating Current Potential Difference Technique," *Special Applications and Advanced Techniques for Crack Size Determination*, ASTM STP 1251 J. J. Ruschau and J. K. Donald, Eds., American Society for Testing and Materials, Philadelphia, 1995, pp. 3-16.

De Belleval, J.F. and Gherbezza, J.M., 1994, "Compensation of Ultrasonic Transducers Response By Adapting Excitation Signals, Application To Defects Evalustion", X.P.V. Malague (ed.), *Advances in Signal Processing for Nondestructive Evaluation of Materials*, 31-42, Kluwer Academic Publishers.]

Elber, W., 1971, in *Damage Tolerance in Aircraft Structures, ASTM STP 486*, American Society for Testing and Materials, pp. 230-242.

Enneking, T. J., 1991, *On the Stochastic Fatigue Crack Growth Problem*, Ph.D. Dissertation, Department of Civil Engineering, University of Notre Dame, South Bend, Indiana.

Ghonem, H. and Dore, S., 1987, "Experimental Study of the Constant Probability Crack Growth Curves under Constant Amplitude Loading," *Engineering Fracture Mechanics*, Vol. 27, pp. 1-25.

Hertzberg, R. W., 1989, *Deformation and Fracture Mechanics of Engineering Materials*, John Wiley & Sons, Inc., New York.

Ibrahim, F. K., Thompson, J. C. and Topper, T. H., 1986, "A Study of the Effect of Mechanical Variables on Fatigue Crack Closure and Propagation," *International Journal of Fatigue*, Vol. 8, No. 3, pp. 157-170.

Jablonski, D.A., "Measurement of Muliple-Site Cracking in Simulated Aircraft Panels Using AC Potential Drop," *Special Applications and Advanced Techniques for Crack Size Determination, ASTM STP 1251*, J.J. Ruschau and J.K. Donald, Eds., American Society for Testing and Materials, Philadelphia, 1995, pp. 33-50.

Kollár, I., 1994, *Frequency Domain System Identification Toolbox*, The Math Works Inc., Natick, MA

Langenberg K. J., Fillinger, P., Marklein, R., Zanger, P., Mayer, K., and Kreuttier, T., “Inverse Methods and Imaging,” *Evaluation of Materials and Structures by Quantitative Ultrasonics* ,J.D. Achenbach, Ed, Springer-Verlang, New York, 1993, pp. 317-398.

Ljung, L., 1999, *System Identification: Theory for the User*, Prentice Hall, Englewood Cliffs, New Jersey.

Lorenzo, C. F. and Merrill, W. C., 1991, "Life Extending Control: A Concept Paper," *Proceedings of 1991 American Control Conference*, Boston, MA, pp. 1080-1095.

McMillan, J. C. and Pelloux, R. M. N., 1967, “Fatigue Crack Propagation Under Program and Random Loads,” Fatigue Crack Propagation, *ASTM STP 415*, pp. 505-532

MIL-A-83444, “Airplane Damage Tolerance Requirements," 2 July 1974.

Manson, S. S. and Halford, G. R., 1981, "Practical Implementation of the Double Linear Damage Rule and Damage Curve Approach for Treating Cumulative Fatigue Damage," *International Journal of Fatigue*, Vol. 17, No. 2, pp. 169-192.

Mattingly, J. D., Heiser, W. H., Daley, D. H.,1987, *Aircraft Engine Design,* American Institute of Aeronautics and Astronautics, Inc, New York.

Maybeck, P. S., 1979, *Stochastic Models, Estimation and Control*, Volume 1, Academic Press, San Diego.

Newman, Jr., J. C., 1983, "A Crack-Closure Model for Predicting Fatigue Crack Growth under Aircraft Loading," *Methods and Models for Predicting Fatigue Crack Growth under Random Loading, ASTM STP 748*, pp. 53-84.

Newman, Jr., J. C., Swain, M. H. and Phillips, E. P., (Eds. R. 0. Ritchie and J. Lankford),.1986, "An Assessment of the Small-Crack Effect for 2024-T3 Aluminum Alloy," *Small Fatigue Cracks*, Proceedings of the Second Engineering Foundation International Conference/Workshop, Santa Barbara, California, pp. 427-452.

Newman, Jr., J.C., 1984, “A Crack Opening Stress Equation for Fatigue Crack Growth,” *International Journal of Fracture*, **24**, pp. R131-R135.

Newman, J.C., Jr., 1992, *FASTRAN-II — A Fatigue Crack Growth Structural Analysis Program*, NASA Technical Memorandum 104159, Langley Research Center, Hampton, VA.

Paris, P.C. and Erdogan, F., 1963, "A Critical Analysis of Crack Propagation Laws," *ASME Journal of Basic Engineering*, Vol. D85, pp. 528-534.

Patankar, R. and Ray, A., 1999, "Damage Mitigating Controller Design for Structural Durability," *IEEE Trans. on Control Systems Technology*, **7**, No. 5, pp. 606-612.

Patankar, R. and Ray, A., 2000, “State-Space Modeling of Fatigue Crack Growth in Ductile Alloys,” *Engineering Fracture Mechanics*, Vol. 66, pp. 129-151.

Porter, T.R., 1972, "Method of Analysis and Prediction for Variable Amplitude Fatigue Crack Growth," *Engineering Fracture Mechanics*, Vol. 4, pp. 717-736.

Ray, A., Wu, M-K., Carpino, M. and Lorenzo, C.F., 1994a, "Damage-Mitigating Control of Mechanical Systems: Part I - Conceptual Development and Model Formulation," *ASME Journal of Dynamic Systems, Measurement and Control*, Vol. 116, No. 3, September, pp. 437-447.

Ray, A., Wu, M-K., Carpino, M. and Lorenzo, C.F., 1994b, "Damage-Mitigating Control of Mechanical Systems: Part II - Formulation of an Optimal Policy and Simulation," *ASME Journal of Dynamic Systems, Measurement and Control*, Vol. 116, No. 3, September, pp. 448-455.

Ray, A., Dai, X., Wu, M-K., Carpino, M. and Lorenzo, C. F., 1994c, "Damage-Mitigating Control of a Reusable Rocket Engine," *AIAA Journal of Propulsion and Power,* Vol. 10, No. 2, March/April, pp. 225-234.

Ray, A., Wu, M-K., Carpino, M., and Lorenzo, C.F., 1994, “Damage-Mitigating Control of Mechanical Systems: Parts I and II,” *ASME Journal of Dynamic Systems, Measurement and Control*, Vol. 116, No. 3, pp. 437-455.

Resch, M. T. and Nelson, D. V., 1992, “an Ultrasonic Method for Measurement of Size and Opening Behaviour of Small Fatigue Cracks,” Small-Crack Test Methods, ASTM STP 1149, J.M. Larsen and J.E. Allison, Eds., American Society for Testing and Materials, Philadelphia, pp. 169-196.

Schijve, J., 1976, "Observations on the Prediction of Fatigue Crack Growth Propagation Under Variable-Amplitude Loading," *Fatigue Crack Growth Under Spectrum Loads*, ASTM STP 595, pp. 3-23.

Sobczyk, K. and Spencer, Jr., B. F., 1992, *Random Fatigue: Data to Theory*, Academic Press, Boston, MA.

Spencer, Jr., B. F., and Tang, J., 1988, "A Markov Process Model for Fatigue Crack Growth," *ASCE Journal of Engineering Mechanics*, Vol. 114, No. 12, pp. 2134-2157.

Spencer, Jr., B. F., Tang, J. and Artley, M. E., 1989, "A Stochastic Approach to Modeling Fatigue Crack Growth," *The AIAA Journal*, Vol. 27, No. 11, pp. 1628-1635.

Stark, H and Woods, J. W., 1994, *Probability, Random Processes, and Estimation Theory for Engineers*, 2nd Edition, Prentice Hall, Englewood Cliffs, New Jersey.

Suresh, S., 1991, *Fatigue of Materials*, Cambridge University Press, Cambridge, UK.

Szilard, J.,1982, *Ultrasonic Testing, Non-conventionalTesting Techniques*, John Wiley and Sons, New York

Virkler, D. A., Hillberry, B. M. and Goel, P. K., 1979, "The Statistical Nature of Fatigue Crack Propagation," *ASME Journal of Engineering Materials and Technology* , Vol. 101, No. 2, April, pp. 148-153.

Vita

Eric Keller was born in Iowa City, Iowa on August 13, 1958. He received a Bachelor of Science degree in Mechanical Engineering from Virginia Polytechnic Institute and State University in 1982. He joined the United States Air Force and was commissioned as a 2nd Lieutenant in 1983. He received a Master of Science degree in Aeronautical Engineering in 1985. He received an honorable discharge in 1994 as a Captain in the Regular Air Force, and began graduate study at The Pennsylvania State University. He developed a laboratory focusing on advanced techniques for real-time sensing of fatigue damage in ductile alloys.